

KINEMATIC AND DYNAMIC MODELLING OF GRINDING PROCESSES

by

MERT GÜRTAN

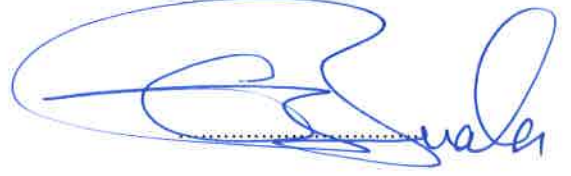
Submitted to the Graduate School of Engineering and Natural Sciences  
in partial fulfillment of  
the requirements for the degree of  
Master of Science

Sabancı University  
December 2017

KINEMATIC AND DYNAMIC MODELLING OF GRINDING PROCESSES

APPROVED BY:

Prof. Dr. Erhan Budak  
(Thesis Supervisor)



Asst. Prof. Dr. Bekir Bediz



Asst. Prof. Dr. Umut Karagüzel



DATE OF APPROVAL:

10.01.2018

© Mert Gürtan 2017

All Rights Reserved

## ABSTRACT

The use of abrasive tools in grinding and similar manufacturing processes continues to increase in the production of high surface quality or difficult to process materials used in especially aviation, automotive and biomedical industry. The complicated geometric structures of the abrasives used in these processes show significant differences with the tools in other machining processes. Instability in material removal operations has been one of the critical obstacles in manufacturing, hindering productivity as well as resulting in unfavorable workpiece quality. Abrasive processes are often associated with finishing operations, aimed to give workpiece a final geometry and surface condition which makes chatter even more critical in grinding. For these reasons, it is quite time-consuming, costly, and in some cases impossible to achieve the desired quality and performance with conventional trial and error methods in abrasive processes. Process models based on analytical and experimental methods constitute the aim and goal of this thesis as they can be used effectively in the analysis of these processes and in selecting the most appropriate process conditions to increase the performance of abrasive processes. In this study, a new simulation method named geometric-kinematic model has been developed for grinding. The geometric-kinematic model provides the prediction of grinding forces and surface roughness of the workpiece by simulating the micro-interactions of the abrasive particles and the workpiece surface. Using the milling analogy and the normal distribution of the individual grits on the wheel surface, determination of active grits hence the chip thickness calculation per grit is also possible. A time-domain simulation is constructed employing the regenerative effect by utilizing the dynamic chip thickness calculation. The stability regions are determined through time domain simulations and analytical model predictions. The simulation results are compared and verified by experimental data.

**Keywords:** Surface grinding, kinematic force model, stability model

## ÖZET

Taşıma ve benzeri üretim süreçlerinde aşındırıcı malzemelerin kullanımı, özellikle havacılık, otomotiv ve biyomedikal endüstrisinde gerekli olan yüksek yüzey kalitesi veya işlenmesi zor malzemeler üretiminde artmaya devam etmektedir. Bu süreçlerde kullanılan aşındırıcı takımların karmaşık geometrik yapıları, diğer üretim yöntemlerine göre büyük farklılık göstermektedirler. Talaş kaldırma operasyonlarındaki kararsızlık, üretim hacmine etki eden kritik engellerden birisidir ve elverişsiz iş parçası kalitesine neden olur. Taşıma işlemleri genelde son yüzey oluşturma işlemleriyle ilişkilendirilir ve son yüzey oluşturma işleminde iş parçası üzerinde gerçekleşecek takım tırmalası kötü bir yüzey pürüzlülüğüne neden olacaktır. Bu nedenlerden ötürü, taşıma operasyonlarında geleneksel deneme yanılma yöntemleriyle istenilen kalite ve performans elde edilmesi oldukça zaman alıcı, masraflıdır hatta bazı durumlarda mümkün değildir. Bu tezin amacı ve hedefi, analitik ve deneysel yöntemlere dayanan süreç modelleri oluşturup, bu süreçlerin analizinde etkili bir şekilde kullanılabilme ve aşındırıcı operasyonların performansını artırmak için en uygun süreç parametrelerinin seçilip kullanılmasıdır. Bu çalışmada taşıma için geometrik-kinematik model adlı yeni bir simülasyon yöntemi geliştirilmiştir. Geometrik kinematik model, taşıma taşı üzerindeki aşındırıcı parçacıklarının ve iş parçası yüzeyinin mikro etkileşimlerini simüle ederek taşıma kuvvetlerinin ve iş parçasının yüzey pürüzlülüğünün tahminini sağlar. Freze analogisi ve taşıma taşı yüzeyinde tek tek aşındırıcı parçacıkların normal dağılımı kullanarak aktif parçaların belirlenmesi, dolayısıyla aşındırıcı başına talaş kalınlığı hesaplanması da mümkündür. Dinamik talaş kalınlığı hesaplaması ve rejeneratif etki kullanılarak bir zaman kümesi simülasyonu oluşturulmuştur. Kararlılık bölgeleri, zaman kümesi simülasyonları ve analitik model tahminleri aracılığıyla belirlenir. Simülasyon sonuçları deney verileri ile karşılaştırılarak doğrulanır.

**Anahtar Kelimeler:** Satın taşıma, kinematik kuvvet modeli, kararlılık modeli

## ACKNOWLEDGEMENTS

I would like to offer my sincere gratitude to the thesis supervisor Prof. Dr. Erhan Budak for guiding my way for completion of this thesis with his immense knowledge and patience. He made this research possible by not only enlightening me with his skills and experiences, but also by broadening my way of seeing and understanding the life.

I would also like to thank the members of the committee Assistant Prof. Bekir Bediz and Assistant Prof. Umut Karagüzel for their guidance.

A great appreciation would go to the members of the Maxima R&D: Dr. Emre Özlü, Muharrem Sedat Erberdi, Veli Nakşiler, Esmâ Baytok, Anıl Sonugür, Ahmet Ergen, Tayfun Kalender and Dilara Albayrak. Their help for this research is very well received.

I owe a lot of gratitude to the members of the MRL. First of all, my grinding project mates Batuhan Yastıkçı, Mert Kocaefe and Hamid Jamshidi have helped and guided me intensely throughout my master study. I am deeply thankful to Batuhan for being a really good game mate, to Mert for being an excellent gym mate and Hamid for being a superb experiment mate. I would also thank to my other class mates: Faraz Tehranizadeh, Zahra Barzegar, Milad Azvar, Amin Bagherzadeh, Esra Yüksel, Muhammed Hassan Yaqoub, Kaveh Rahimzadeh, Yaser Mohammadi, Cihan Özerener, Ekrem Can Unutmazlar, Samet Bilgen, Gözde Bulgurcu, Turgut Köksal Yalçın, Mehmet Albayrak and Yiğit Özcan. Süleyman Tutkun and Ertuğrul Sadıkoğlu's help for the technical issues I have had, is deeply acknowledged.

Last but not the least, I am most thankful to supports of my family, Hasene & Murat Gürtan and Damla & Kemal Çiftçi. They had the most patience and were with me the whole time from start to the present. Therefore, I dedicate my study to them.

## TABLE OF CONTENTS

1	INTRODUCTION .....	1
1.1	Literature Survey on the Mechanics of Grinding.....	2
1.2	Literature Survey on the Dynamics of Grinding.....	5
1.3	Objective & Scope .....	8
1.4	Lab equipment.....	9
1.4.1	Grinding CNC Machine .....	10
1.4.2	$\mu$ surf Explorer Nanofocus .....	11
1.4.3	Kistler Dynamometer.....	13
1.4.4	Talysurf Surface Profilometer.....	13
1.5	Layout of the Thesis.....	14
2	MEASUREMENT AND MODELLING OF ABRASIVE TOOLS.....	15
2.1	C Number Identification.....	19
2.2	Individual Grit Measurement .....	20
2.3	Virtual Construction of Wheel Surface .....	22
2.4	Measurement Results .....	24
2.5	Summary .....	25
3	KINEMATIC MODEL OF ABRASIVE PROCESSES.....	26
3.1	The Geometric-Kinematic Model .....	28
3.1.1	Electroplated CBN wheel properties .....	28
3.1.2	Determination of Active grits .....	31
3.2	Surface Roughness in perpendicular to cutting direction.....	36
3.3	Grinding Force .....	39
3.3.1	Undeformed Chip Thickness .....	39
3.3.2	Mechanistic Force Model .....	40
3.3.3	Thermomechanical Force Model .....	41

3.4	Results .....	44
3.4.1	Active grits.....	44
3.4.2	Grinding Force and surface roughness .....	48
3.5	Summary .....	50
4	DYNAMIC FORCE MODEL FOR ABRASIVE PROCESSES .....	52
4.1	Dynamic Chip thickness and Dynamic Forces .....	52
4.2	Vibration and surface roughness in the cutting direction.....	56
4.3	Time domain Simulation.....	57
4.4	Experimental Procedure .....	62
4.5	Dynamic Force Results .....	65
4.6	Surface Roughness Results .....	71
4.7	Summary .....	73
5	CHATTER STABILITY OF ABRASIVE PROCESSES .....	75
5.1	Frequency domain solution .....	76
5.2	Time domain solution.....	77
5.3	Stability diagrams.....	86
5.4	Experimental results.....	90
5.5	Summary .....	99
6	SUGGESTIONS FOR THE FUTURE RESEARCH .....	100
7	DISCUSSIONS AND CONCLUSIONS .....	101
8	REFERENCES .....	104

## LIST OF FIGURES

Figure 1: Grinding CNC Machine .....	10
Figure 2: Nanofocus.....	12
Figure 3: 20x measurement on Nanofocus .....	12
Figure 4: 50x lens capture.....	13
Figure 5: Grinding wheels for different applications.....	16
Figure 6: SEM picture of a CBN wheel surface I.....	17
Figure 7: SEM picture of a CBN wheel surface II.....	17
Figure 8: Measured grinding wheels. From left to right 1) 10mm B126 CBN 2) 5mm B64 CBN 3)30mm B150 CBN 4) 10mm B126 CBN dressed 5) 10mm B126 CBN worn 6) 20mm B120 Al <sub>2</sub> O <sub>3</sub> .....	19
Figure 9: C number identification a) tool #1 b) tool #3.....	20
Figure 10: Individual grit measurement with 50x lens a) 2D b) 3D.....	21
Figure 11: Identification of geometrical properties of individual grits from 2D side view a) dimensions b) edge radius.....	21
Figure 12: Identification of oblique angle of abrasive grit from 2D top view.....	22
Figure 13: Axial discretization of the wheel.....	23
Figure 14: Depiction of active grits (a) virtual wheel (b) real wheel surface.....	27
Figure 15: Height distribution of grit measurements.....	28
Figure 16: 20mm diameter B126 (gritsize) ElectroPlated CBN wheel .....	29
Figure 17: Measurement results of the presented wheel.....	30
Figure 18: SEM captures of a single grit .....	31
Figure 19: Kinematic trajectories of the grits .....	32
Figure 20: Trajectories on x-z plane .....	33
Figure 21: Depiction of case 1 or 2.....	34
Figure 22: Depiction of case iii.....	35
Figure 23: Flowchart of Active grit algorithm.....	35
Figure 24: Recreated wheel with active grits only.....	36
Figure 25: Trajectories for the surface roughness calculation .....	37
Figure 26: Last surface.....	37
Figure 27: Last surfaces of all the elements.....	38
Figure 28: 3D projection of last surfaces .....	38

Figure 29: Milling cutter with run-out .....	39
Figure 30: Flowchart for force calculation .....	44
Figure 31: Active grit number table .....	45
Figure 32: Active grit number for wheel 1 for varying depth of cut .....	47
Figure 33: Active grit number for varying feed rate and 5 wheels .....	47
Figure 34: Verification of force model: Depth of cut: 20 $\mu$ m. a) CBN wheel b) conventional wheel .....	49
Figure 35: Verification of the force model. Depth of cut: a)40 $\mu$ m b) 60 $\mu$ m. (CBN wheel)..	49
Figure 36: The effect of grit number on the forces .....	50
Figure 37: Y path profile.....	56
Figure 38: The dynamic grinding flowchart .....	58
Figure 39: The block diagram.....	59
Figure 40: The discretized wheel element .....	60
Figure 41: The active grits and delays .....	60
Figure 42: The shadow-element method visualization .....	61
Figure 43: The hammer test setup.....	62
Figure 44: The experiment setup .....	63
Figure 45: The measured forces of 40 $\mu$ m radial depth for varying feed rate .....	64
Figure 46: The laser sensor mounting.....	65
Figure 47: Dynamic forces and vibrations, 40000rpm, 0.125 mm/rev, 40 $\mu$ m radial depth (a) forces (b) vibration (c) vibration frequency .....	66
Figure 48: Comparison of the experimental force data. Wheel speed 40m/s, radial depth of cut 40 $\mu$ m, table speed: 5000mm/min.....	67
Figure 49: Comparison of measured and predicted force (Geometric-kinematic model) data for varying feed rate, wheel speed 40m/s, radial depth of cut 40 $\mu$ m.....	68
Figure 50: Comparison of measured and predicted force (Dynamic model) data for varying feed rate, wheel speed 40m/s, radial depth of cut 40 $\mu$ m.....	69
Figure 51: Dynamic forces when feedrate is 5000mm/min.....	70
Figure 52: Dynamic forces when feedrate is 7000mm/min.....	70
Figure 53: The experimental setup .....	71
Figure 54: Model and experimental results of the surface roughness for wheel 1 at different feed rates. ....	72
Figure 55: Model and experimental results of the surface roughness for wheel 2 at different feed rates. ....	72

Figure 55: A sample dynamic grinding output (a) force (b) tool tip vibration (c) vibration spectrum.....	78
Figure 56: 40000 rpm, 5 mm depth, 5000 mm feed (a) force (b) tool tip vibration (c) vibration spectrum.....	79
Figure 57: 40000 rpm, 7 mm depth, 5000 mm feed (a) force (b) tool tip vibration (c) vibration frequency.....	80
Figure 58: 40000 rpm, 7.7 mm depth, 5000 mm feed (a) force (b) tool tip vibration (c) vibration spectrum. ....	81
Figure 59: 40000 rpm, 10 mm depth, 5000 mm feed (a) force (b) tool tip vibration (c) vibration spectrum. ....	82
Figure 60: 40000 rpm, 5 mm depth, 5000 mm feed (a) tool tip vibration (b) vibration spectrum.....	83
Figure 61: Stable dynamic forces, depth: 5mm, speed: 40000 rpm.....	84
Figure 62: Unstable grinding. Depth: 5mm, Spindle speed: 35000rpm (a) tool tip vibration (b) vibration spectrum .....	85
Figure 63: Unstable grinding forces. Depth: 5mm. Spindle Speed: 35000 rpm.....	85
Figure 64: Stability diagram for 5000mm/min feed rate .....	86
Figure 65: Stability diagrams for different feedrates .....	87
Figure 66: Stability charts with respect to radial depth of cut for different tools and feeds....	89
Figure 67: Force measurements of chatter investigation test.....	91
Figure 68: Comparison of the force measurement of the stable (a) and unstable (b) case .....	92
Figure 69: Comparison of the sound measurement of the stable (a) and unstable (b) case.....	92
Figure 70: Comparison of surface of the workpiece of the stable (a) and unstable (b) case ...	93
Figure 71: Surface roughness measurement of the workpiece .....	93
Figure 72: Comparison of surface profile of the workpiece of the stable (a) and unstable (b) case.....	94
Figure 73: Condition of the wheel after the last operation .....	95
Figure 74: Model and experiment comparison .....	97
Figure 75: The chatter marks on the workpiece.....	97
Figure 76: Detection of chatter sound.....	98

## LIST OF TABLES

Table 1: Grinding wheel specifications .....	18
Table 2: List of wheel measurement results .....	24
Table 3: Specifications for the presented wheel in Figure 16.....	29
Table 4: Constants of Johnson-Cook equation for Inconel 718.....	42
Table 5: Wheel specifications for the active grit calculations .....	46
Table 6: Modal parameters of the wheel.....	62
Table 7: Process parameters for different feed rate conditions.....	87
Table 8: Process parameters for different feed rate and wheel conditions .....	89
Table 9: Modal parameters of the 21mm overhang tool.....	96

## 1 INTRODUCTION

Grinding is one of the many manufacturing methods and it can be considered as the oldest one. The first grinding operations in the world was done in the early ages of the society [1]. After mankind started to make tools they realized they needed to sharpen their tools to assure the durability and continue the usage without failure. First attempts were sharpening the tools by rubbing them with stones. Since then grinding is used widely around the world.

Grinding is included in abrasive processes under machining operations. Like other machining operations it includes material removal. This material removal cannot be considered as cutting and regarded as abrasive operations. Abrasive operations basically mean in the medium of contact of two materials, the harder material removes particles from the surface of the softer material. In the world, 20-25% of all expenses regarding the machining operations are coming from grinding [2]. The material removal is done with abrasive particles. These abrasive particles are bonded in various ways to the grinding wheel [3]. Grinding wheels come in different types and shapes. The type of abrasives is a key factor which includes aluminum oxide, SiC, CBN and diamond grits [4].

Abrasive technology is generally used in finishing operations. The aim is to give the workpiece the final geometry and surface profile. Mostly after all production steps are completed, the materials are ground and then sent to inspection. There are some other cases in which the grinding is used. If the workpiece material is comparably soft and easy to machine, a production engineer will most likely choose the turning or milling operations as roughing and primary shaping step but if the workpiece is a hard to machine material such as Ti, Ni or Cr alloys [5], which are mostly used in aerospace industry, the engineer would choose grinding as roughing operation. Abrasive operations are known for their increased performance on hard to machine materials [6]. First, a direct cutting method is not used in grinding and usually the depths of cut are low. This enables the abrasive wheel to form particles of the workpiece to remove them. Moreover, in grinding the cutting speeds are generally high and the heat can be absorbed by the wheel more comparing to standard cutting operations especially when

CBN wheels are used [7]. Furthermore, the grinding wheel can be more durable and the tool life is increased [8].

## **1.1 Literature Survey on the Mechanics of Grinding**

As for other cutting operations, empirical and analytic models have been used in modeling of grinding. Until 1980s the models mostly relied on linear regressions and empirical-physical approaches [9]. Empirical models rely on equations which consist of many grinding parameters such as depth of cut, feed rate, spindle speed, workpiece velocity etc. The important parameters are identified or calibrated after doing many tests on specific conditions. These equations are used to predict process forces, surface roughness, temperature, wear and vibrations [10]. The advantage of empirical models is that they are easy to implement, can be considered shop floor friendly and sometimes practical if the production engineer will consider only a few operations for a considerable amount of time. Although these models are mostly very accurate, generation of them is very time consuming and their modularity is very low. In case of any changes such as. change of tool, workpiece or any process parameter, the model will most probably be useless new sets of experiments will have to be conducted.

Grinding process is very hard to model analytically due to its stochastic nature [11]. The grits on the wheel come in random shapes and sizes which means that the cutting edge is not defined. In reality, everything is in a constant state of change in grinding as during the operation the wear may become so rapid that the process parameters may change even in the first passes of grinding [12]. However, through some simplifications and assumptions one can model the grinding process analytically as can be found in the keynote paper by Tönshoff et al. [13].

The analytical modelling initially requires a definition of geometric properties on the contact surfaces of the grinding wheel and the workpiece. The identification process of cutting geometry relies on the measurements done on the grinding wheel before the grinding process. These measurements are crucial as unlike turning or milling, the abrasive grits on the grinding wheel don't have well defined cutting edges. The geometric properties of the wheel can be categorized into two, namely the macro and micro properties [14]. The macro properties mostly related to the unbalance and run-

out, clamping errors or excessive wear. The micro properties of the wheel on the other hand can be listed as density, distribution, shape etc. of the grits.

The measurements of the wheel regarding its macro properties can be done straightforwardly with tactile methods. In [15], a tungsten carbide tip coupled with an oscillating pin is applied on the grinding wheel surface. Any defects made on the surface can be successfully observed with this method if small forces and oscillations are applied. Buchholz [16] used pneumatic sensors to measure the macro features. The concept is the same as the method described in [15]. The pneumatic sensor is coupled with a pressure plate where constant air pressure is applied on the plate and motions are observed. Moreover, it is also possible to measure the macro structure with AE sensors [17]. These sensors provide a non-contact method with an increased sample rate. Again, the sensors need to be coupled with a single-point dresser tool.

The measurements on the wheel surface regarding the micro sense first tried with inductive wheel loading sensors [18]. This is a thermoelectrical method and requires very complex test setup. A winding, core and a stray field are used with a magnetic head. Magnetic head records the electrical activity on the surface of the wheel. Furthermore, the other way of identifying micro structure of the wheel is using light sensors. The first attempt was done by Piegert [19]. This is a scattered light-sensor and works with a signal processing module. Nowadays with the advancement of measurement technologies, the reflection and laser sensors are used to determine the grit properties on the wheel surface [14].

After the observations and identifications of basic grit properties, the next step is to create a wheel topography model to use it in the analytical process models.

Generally, the individual grits are carefully analyzed, and the geometric properties of the grits are identified. The results are to be used in the computer simulations of the grinding process [20,21]. The surface of the grinding wheel is scanned, and the geometric properties are determined for grit density, height, width, rake angle, oblique angle, edge radius and distance between grits. A straightforward way is to model the grits is to assume that they are in a simple geometrical shape such as a sphere, a cone or sometimes more complex shapes such as cuboids or tetrahedrals [22,24]. The other way, which is computationally more expensive, is to model each single grit in the simulation so that each geometric property stored in arrays of the data rather than

applying one general shape. The identification of all grits on the wheel surface is a tiresome challenge, but one can simply model the grits using random distribution that is obtained from the measurements of smaller set of grits. The selection of random distribution is discussed and applied in the literature [25,28].

After the wheel topography is modeled, observing the kinematics of the grinding process is one of the most effective methods of modelling the chip removal mechanism. In the literature there are many works about the grinding kinematics. McDonald et al. [29] developed a computationally cheap method which involves determining peak surface values of the grits. The data is gathered through 3D measurements of the wheel surface. The active grits are also calculated through the kinematic simulations of the grits with the interaction on the workpiece surface. Barrenetxea et al. [30] developed a model to predict the tribo-thermo-mechanical behavior of the grinding process. The idea was to apply the controlled kinematic chip removal through a time domain simulation method. The method of creating a standardization of geometrical shapes of the grits is applied in [31]. Some elemental grit shapes are chosen as cuboids, triangle prisms, triangular pyramid variants and dodecahedrons, and cutting edges are generated by slicing with planes on the predefined elemental grit shapes to represent variety of grits on the wheel surface. Orthogonal cross section of the trajectories of the grits on the workpiece is created to calculate the chip thickness in the process. Uhlmann et al. [32] proposed a variety of methods to model the grinding kinematics for different types of abrasive operations such as conventional surface grinding, oscillation surface grinding and tilt surface grinding.

Surface roughness is another key factor in grinding as it is generally used in finishing operations. The final geometry and dimensions are crucial factors in abrasive processes. In [33] a simplified predictive surface roughness model is developed in which the stochastic nature of the grinding is considered. The prediction is verified by using the found relationship between the roughness and chip thickness. In [34], the effect of process parameters on surface roughness is analyzed. The influence of grinding wheel parameters such as grain density, grain size or process parameters such as rotational speed, feed rate and depth of cut are analyzed on the grinding force. An optimization of input parameters is proposed for the increased workpiece surface roughness. Single-grit wheel experiments are conducted by Ma et al. [35] and showed that the grit-wise effect

on surface roughness is based on the two angles described in the paper as inclining and deflecting angles.

Grinding force is a key factor to determine the strategy for the process. Force can predict if the operation can be done under the machine capabilities. It can lead to prediction of surface roughness, temperature, vibrations, wear etc. Empirical force models are applied on the literature [36,37]. These early empirical models consist of mathematical relations between input and output parameters. This means that the grinding force is expressed with respect to the cutting conditions such as grinding depth, spindle speed, feed rate with calibrations constants. Even though these empirical models can predict grinding forces accurately, they rely on high number of time consuming tests. Malkin [38] proposed a model consisting of specific energy constant which depends on chip formation, ploughing and sliding forces. Single grit models are proposed to closely study the grit formation and material properties of the workpiece. This way the force can be modeled with respect to strain and strain rate hardening of the workpiece material [39]. An analytical model was presented in [40] to predict the surface roughness and force by using Johnson-Cook material and dual zone contact models.

## **1.2 Literature Survey on the Dynamics of Grinding**

Instability in material removal operations has been one of the critical obstacles in manufacturing, hindering productivity as well as resulting in unfavorable workpiece quality. Abrasive processes are often associated with finishing operations, aimed to give workpiece a final geometry and surface condition which makes chatter even more critical in grinding.

As a process related self- excitations are one of the significant problems in grinding operations because the geometrical accuracy and the surface finish are the crucial anticipations of the process [41], several models have been developed to cope with this problem.

The vibration phenomenon of the grinding has been carefully investigated and distinguished into three categories; self-excited vibrations due to workpiece surface

regeneration, wheel surface regeneration and forced vibrations. Even though the contribution of the wheel regeneration can be considerable on conventional wheels, majority of the vibration originate from the workpiece surface regeneration since the wear is relatively negligible on CBN wheels [42].

A time-domain model for the surface grinding is presented in [43] whereas dynamic simulation is constructed to see the workpiece-wheel interaction in an enhanced way. The workpiece is discretized into elements by using the z-buffer approach. This approach provides more advanced way to observe the volume engaged by the wheel and thus modelling the equivalent chip thickness removed from the workpiece. By pairing this dynamic material engagement mechanism with a specific-energy based force model, the time-domain simulations are constructed with a Simulink model.

Additional time-domain dynamic model is introduced in [44]. The work focuses on the simulation of the cylindrical plunge grinding governed by common grinding parameters. A predictive model for chatter boundaries is developed together with the calculation of the growth rates. Some crucial effects are considered, mostly non-linear attributes such as distributed forces along the contact length, tool and workpiece vibration and the delay between the consecutive time discretization. The simulation program is able to model the dynamic forces, vibrations, stability regions and the surface profiles of the workpiece.

The effect of the stochastic nature of the grinding on the dynamic response of the process is discussed in [45] where excitation is calculated by distributed individual grits. The emphasis is put on the grinding contact especially the distribution of grits and the unbalance of the wheel. It is presented that the time domain simulations are essential for modelling the nonlinearities in grinding as the operation itself is considered highly complicated

The employment of milling analogy while modeling grinding operations is used carefully in [40] where a surface roughness and thermo-mechanical force models are developed. Instead of a cutter with defined geometry, numerous grits are created with randomly distributed shapes. Each grit is treated separately, all the information is stored in an array and the theory and formulations are repeated for each grit. Applying the

Johnson-Cook Material model and dual zone contact model presented in [46] the grinding forces can be predicted with low discrepancies relative to the experimental outputs.

It is denoted in [42], that the types of vibrations in the grinding process can be categorized into two: forced vibration and self-excited vibration. The main cause for the forced vibrations is the unbalance of the grinding wheels. In such cases the source can be hydraulic devices or any other external source as well. In this type of vibrations, the source can easily be located through frequency measurement. It is useful to mention that the gyroscopically induced self-excited vibrations are also studied in the literature [47]. However, the self-excited vibrations are mainly due to the regenerative chatter in. The regenerative effect in abrasive processes is similar to other cutting processes: During the cut, as a result of the phase between the vibration waves in the successive passes the chip thickness will be varying. The phase shift between these waves will determine the stability of the process based on the chip thickness variation.

However, in grinding processes the source of regeneration mechanism is based on two effects. The regeneration may be effective on either the wheel or the workpiece surface [42]. This part makes the stability analysis of the grinding more complex compared to cutting processes. The regenerative effect on the workpiece surface is related to the surface quality and the effect on the wheel is related to the wear resistance. The wheel regeneration propagates slower than the workpiece regeneration. The tool regeneration can be seen even in the dressing process. These two regenerations can be modeled with double delay systems.

Altintas and Weck [48] mentions Inasaki's model [42] by applying "n" intersection areas on the surface of the workpiece rather than just one. The paper investigates the limiting phase criterion which is derived from the Nyquist stability criterion. It is stated that when the phase of the transfer function goes below the limiting phase curve the system will have the means to start a regenerative chatter. If the phase curve cuts the limit curve in the first section, there is the risk of workpiece induced chatter. If the intersection occurs in the second section of the limit curve only, the chatter is caused by the side of the wheel.

Double-delay systems are developed to investigate the wear on the wheel and the workpiece further [49]. The dynamic model includes the two inherent delayed force fluctuations caused by the both surfaces due to regeneration mechanism of the both surfaces. The inspection of the double regenerative grinding process is done by handling the differential equations written for both the undulations due to the wheel surface and the workpiece surface. After the development of the model, a sensitivity analysis is proposed to detect the chatter of the doubly inherent structure. With this sensitivity analysis the change of parameters in an optimal way is proposed to cope with the instability in grinding operations.

In transverse grinding, the wheel moves along a slender workpiece introducing unique grinding dynamics. The work presented in [50] offers a new dynamic modelling for this unique interaction in grinding. The plunge grinding operations are relatively less complex as they contain one region of contact. On the other hand, the transverse dynamics must be analyzed in two different contact regions.

### **1.3 Objective & Scope**

In this work, the main aim of the research is to increase the performance of grinding operations by use of mathematical models, develop measurement and monitoring methods and select the best strategy for grinding, concerning the surface roughness, maximum MRR and product quality.

The scope of this thesis is to develop measurement methods for grinding tools, models to mimic the grinding operation down to particle level, model the process forces both for the static and dynamic case and speculate chatter free grinding conditions all which can be achieved by implementing analytical models.

Abrasive machining has mostly been used for finishing operations, but since the aviation industry brought the requirement of using difficult to cut materials, grinding came to use for roughing operations due to its increased performance on these types of materials. The complicated geometric structures of the abrasives used in these processes show significant differences from the other machining processes. For these reasons, it is quite time-consuming and expensive to sustain a decent result and

performance with empirical modelling methods in grinding processes. Process models based on analytical and experimental methods constitute the aim and goal of this project as they can be used effectively in the analysis of these processes and in selecting the most appropriate process conditions. Within the scope of the thesis, abrasive grit geometry, grinding kinematics, forces and vibrations were studied in detail by experimental and analytical methods and process models were developed. With this approach, the required number of experiments can be reduced to the lowest and highly accurate estimations can be made. In addition, developed and experimentally validated process models were used to determine the process conditions required to achieve the desired quality at the lowest possible time and cost, and applications on industrial components were demonstrated.

In order to achieve the described aims of the thesis, a measurement method and procedure for the abrasive grits has been developed. Using the measurements, the abrasive wheel topography has been modeled. Applying milling analogy and the geometrical random distribution of the grits on the grinding wheel, the simulation can predict the dynamic forces and vibrations. A geometric-kinematic model is developed in order to predict the grit trajectories during the grinding process. The active grits are calculated and the chip thickness per active grit is computed with the trajectory simulation of the wheel. The dynamic model is created with the inclusion of the regenerative effect of the workpiece surface. The aim of this model is to model the dynamic behavior of the surface grinding and predict the region of grinding parameters which cause instability in the closed loop time domain system. Applying milling cutter analogy in grinding allows the use of the dynamic milling equations presented in [51,52]. These models will be used to plan and schedule the best available performance of grinding operations based on the required process conditions.

#### **1.4 Lab equipment**

In this subtitle, the lab equipment that is used during this thesis is presented.

### 1.4.1 Grinding CNC Machine

The grinding CNC machine used in the experiments is Chevalier Smart B818 CNC Profile & Forming Grinding CNC machine. %5 oil based coolants are used in the experiments. The machine is shown in Figure 1.



Figure 1: Grinding CNC Machine

The machine is a 3 axis CNC capable of moving in x, y and z axes. It is sufficient for academic use and tests where mass production is not the main concern. The dynamometer couple is placed on the magnetic bed for force measurements during grinding tests. A couple of fixtures are produced in order to enable the use of different shaped of workpieces to be clamped on the dynamometer. There are 2 spindles on the machine with low and high-speed capabilities. The high-speed spindle can reach 40000 rpm. Where the low speed one has the maximum speed of 8000 rpm. The bearings inside the spindle will lose their efficiency and there is a chance to break when the spindle is used below the minimum speed. Furthermore, the spindle will lose its torque and power efficiency as the speed gets slower. It is advised that the speed should be chosen between the 70% of its max speed to 100% of its maximum speed as the torque and power curves gets low in the lower speeds. Since it is high speed spindle, accordingly smaller grinding wheels should be used. For conventional wheels at full rpm it is recommended to use maximum 20mm diameter wheels and for CBN wheels

the wheel diameter can go up to maximum of 30mm diameter to satisfy the required grinding speed. For larger tools it is recommended to decrease the spindle speed rather than 40k to maintain a cutting speed of around 35m/s.

The machine has a dresser unit installed next to the magnetic table and it is ready to be used if a dresser wheel is purchased. It is noticed during the experiments that the dresser unit creates unpredictable noise signals even when it is not running. These noises were observed on the thermocouple measurements as thermocouples are highly sensitive to magnetic current and the temperature measurement was not very successful. Due to these problems, the dresser unit was unplugged from the PLC board of the machine during this study and thus not used in the experiments.

#### **1.4.2 $\mu$ surf Explorer Nanofocus**

Nanofocus is a light sourced microscope which is used in measuring of the grinding wheels. There are a number of lenses available for the measurement of individual grits or multiple of them. The wheel measurement is the fundamental part of modelling abrasive operations as the grinding mechanism is quite complex compared to other machining operations. The measurements in nanofocus is done by light fringes. The discretization is done along z axis layer by layer such as the way the rapid prototyping works. The light reflections may be problematic on conventional grinding tools as generally the aluminum and SiC abrasive grits may shine too much and introduce noise to the measurement. A coating procedure may be applied to increase the measurement quality in that case. On the other hand, measurements done on CBN tools can be conducted easily. The Nanofocus comes with a software which enables 3D scanning of the grits. The device is shown in Figure 2.



Figure 2: Nanofocus

It is recommended to use 2 types of lenses on grinding wheels, namely 20x and 50x lenses. The 20x lens can cover an area of approximately  $0.64\text{mm}^2$  which will probably include around 30 abrasive grits. where a sample picture is shown in Figure 3. This lens is used to count the grits and determine the grit density; one of the key elements in process modeling. Red regions indicate the light scan.

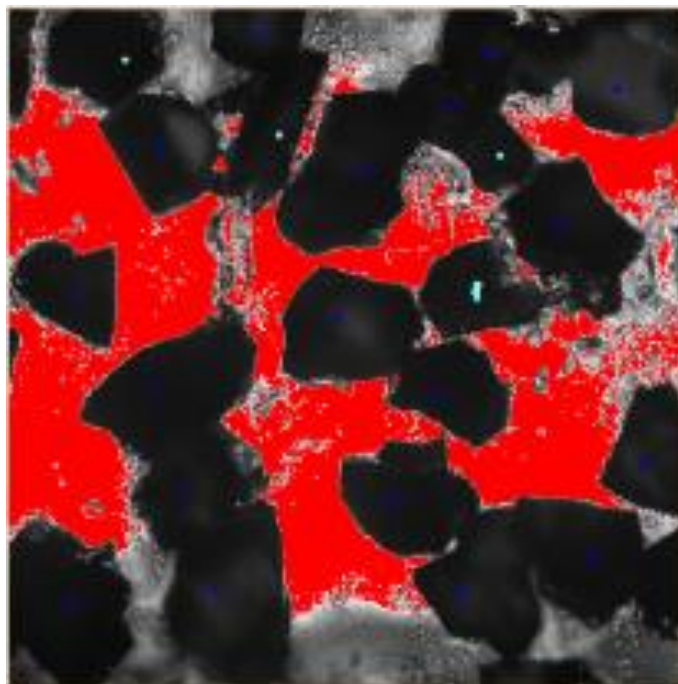


Figure 3: 20x measurement on Nanofocus

The 50x lens, on the other hand, provides just one grit per one scan most of the time. However, this enables a closer look to the abrasive grit offering identification of cutting edge of the grits and some certain process inputs such as oblique angle, rake angle, edge radius etc. A sample of the 50x lens scan is shown in Figure 4.

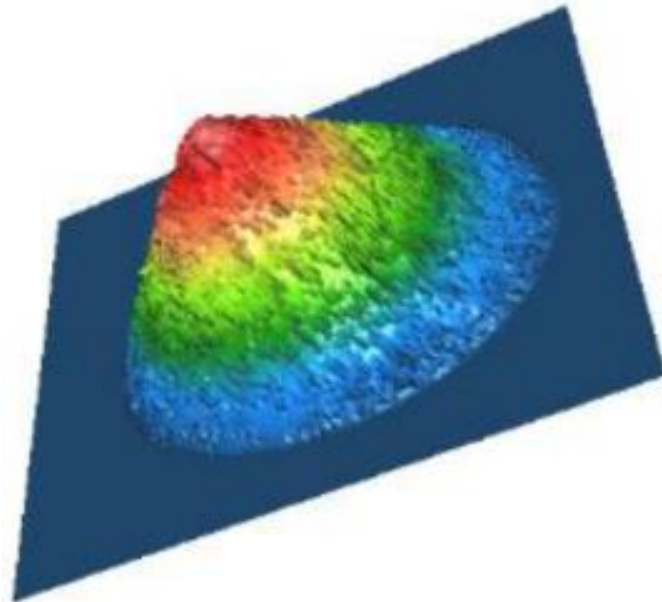


Figure 4: 50x lens capture

#### **1.4.3 Kistler Dynamometer**

A 3-axis Kistler 9129AA table type dynamometer is used in the experiments. The focus is given on the forces of z and x axes. Although the forces in the y-direction exist, they are mostly neglected in grinding operations as they are negligibly low.

#### **1.4.4 Talysurf Surface Profilometer**

For surface roughness measurements on the workpiece, a Talysurf surface profilometer was used. The device has a diamond probe  $2\mu$  and provides a sufficient measuring sensitivity for grinding operations. Although the accuracy is quite high with this device,

it lacks mobility and when a surface roughness measurement is needed, the workpiece is dismantled and carried to the measurement room and mounted again.

## **1.5 Layout of the Thesis**

The organization of the thesis is given as follows:

Chapter 2 is about Measurement and Modelling of Abrasive Tools. The steps are given:

- “C” number calculation, where the grit number per  $\text{mm}^2$  is calculated
- Individual grit observation, where the geometric properties of the grits are identified.
- Axial discretization of the wheel & Wheel creation, where the wheel is modeled with normal distribution.

Chapter 3 is about the Kinematic Model of Abrasive Processes. The steps are given:

- Calculation and printing of the kinematic trajectories of the grits.
- Identification of active grits using the intersections of the grits.
- Surface roughness in perpendicular to cutting direction and force prediction is completed using the geometric and kinematic model

Chapter 4 is about Dynamic Force Model of Abrasive Processes. The steps are given:

- Calculation of dynamic chip thickness and dynamic forces using the geometric and kinematic model.
- Vibration and surface roughness in cutting direction prediction using the dynamic model.
- Time domain simulations.

Chapter 5 is about Stability of Abrasive Processes. The steps are given:

- Stability prediction using time domain simulations and analytic methods.
- Verification of the proposed models with the experiments
- Stability conditions under varying wheel parameters.

Chapter 6 is about Discussion, Conclusion and Suggestions for Future Research

## 2 MEASUREMENT AND MODELLING OF ABRASIVE TOOLS

The most fundamental difference between grinding and other cutting operations regarding the material removal is the uncertainty and random nature of abrasive process chip formation. In grinding, the cutting edges are undefined whereas the geometrical properties of turning and milling tools can easily be obtained.

This chapter is about determining the geometric properties of abrasive particles to be used in simulations and experiments. Determination of these geometric features before applying the analytic models is one of the most important stages of grinding process modeling. The geometric values assigned to these measurements will be used for representing each particle. Information on the geometric properties of the tools in the industrial cutting operations is provided by the toolmakers, but this is not possible in grinding wheels and subsequent measurements are necessary.

Due to the manufacturing method of the grinding wheels the topography on the wheel surface will have random structure [41]. In measurements it is seen that the abrasive grits are randomly distributed over the surface of the wheel. This is a result of the way that the wheels are produced. First the abrasive particles are produced and gathered together. They are passed through a sieve to assure that the grits on the wheel have a certain dimensional range. The B number on the wheel represents the grit size which corresponds the size of the sieve that was used. After the sifting process, the abrasive grits are assembled on the grinding wheel. There two types of grinding wheels with respect to the type of assembly of the grits on the wheel; bonded and plated. The bonded types are the wheels that have multiple layers of abrasive grits on the surface of the tool on top of each other. The bond material provides the adhesion force between the layers of abrasive grits. Multiple layers of the abrasive grits provide dressing option for the grinding wheels when they are worn. The plated wheels are covered with single layer of abrasive grits and cheaper to produce comparing to the bonded ones as less overall material is needed. They are used without dressing due to existence of only single layer of abrasive grits. Thus, when the plated wheel is worn it is replaced.



Figure 5: Grinding wheels for different applications

It is also convenient to categorize the grinding wheels into two with respect to their abrasive grit materials. Grinding wheels which have Aluminum oxide or SiC abrasive grits are called conventional wheels whereas the wheels that have CBN or diamond particles are called super abrasive wheels. Super abrasive wheels are usually preferred for processing high alloy materials, such as nickel alloys, as they provide increased performance as a result of elevated hardness, thermal condition and abrasion resistance. Conventional wheels are cheaper and generally selected in low cost operations. Within the scope of this thesis, the overall focus is on CBN wheels whereas some applications of the conventional wheels are also presented.

To represent the surface of the grinding wheel and the randomness of the abrasive grits, electron microscope measurements were done on a CBN grinding wheel as shown in Figure 6 and Figure 7. As it can be seen, the distribution of the abrasive grits on the surface of the wheel is random and this results in a material removal with undefined cutting edges. Hence, proposing a modeling method for abrasive tools is crucial for process model development.

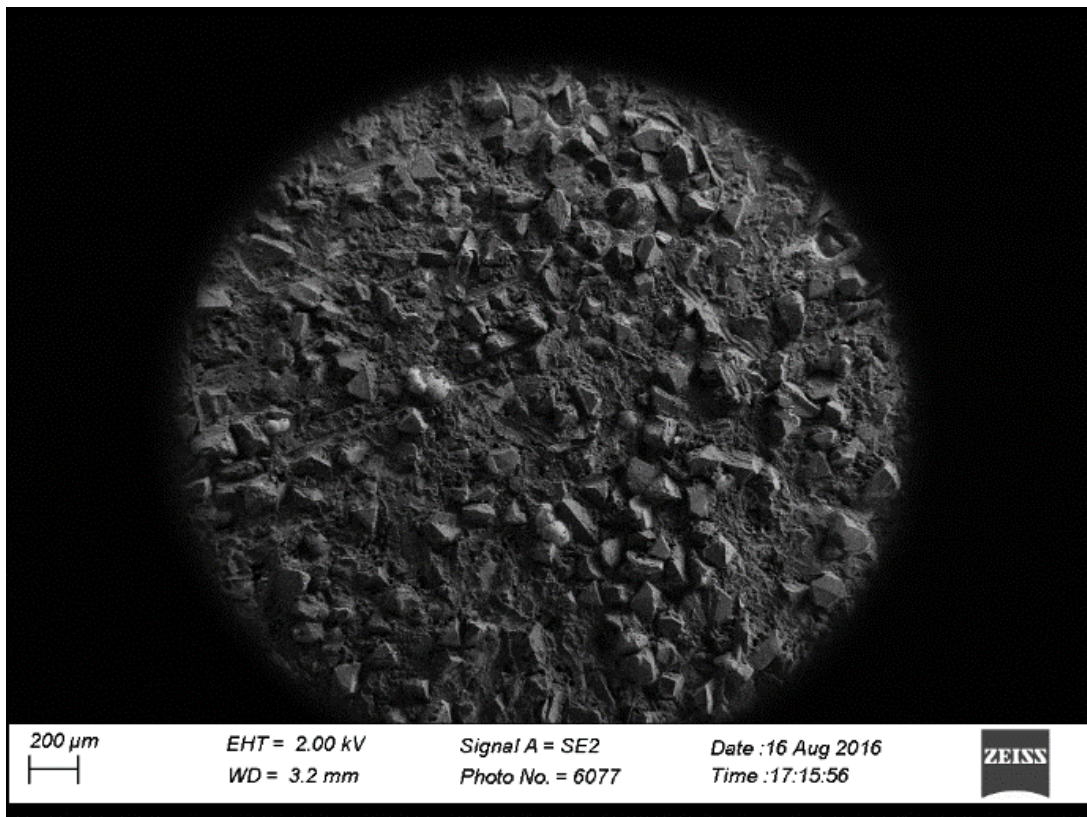


Figure 6: SEM picture of a CBN wheel surface I

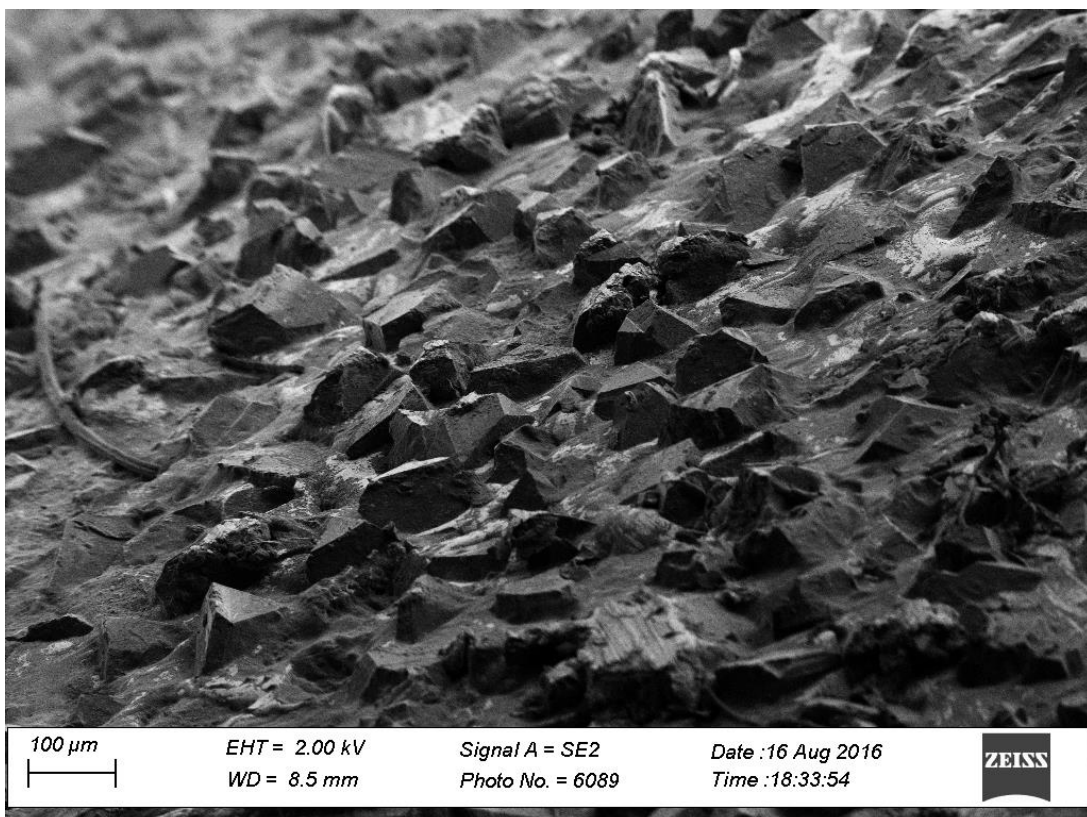


Figure 7: SEM picture of a CBN wheel surface II

Wheel no	1	2	3	4	5	6
Type	Mounted point					
Grit Material	CBN	CBN	CBN	CBN	CBN	Al <sub>2</sub> O <sub>3</sub>
Diameter (mm)	10	5	30	10	10	20
Grit size	B126	B64	B151	B126	B126	B120
Bond Type	Electroplated	Electroplated	Electroplated	Electroplated	Electroplated	Vitrified

Table 1: Grinding wheel specifications

As a result of the stochastic nature of the grinding wheels it is convenient to model the wheel using Gaussian distribution created from a sub set of data which are obtained through the measurements from the surface of the wheel. The fundamental information for process modelling is as follows:

- Number of abrasive grits per mm<sup>2</sup> (Analogous to teeth number in milling)
- Grit dimensions (height, width, width of cut)
- Process related geometric properties such as oblique angle, rake angle and edge radius ...etc.

In this chapter, a wheel model is proposed by using the fundamental information obtained from optical measurements. The grit data then processed and fit into a gaussian distribution thus creating the virtual wheel. The measurements are done on 6 different wheels and the specifications are given in Table 1. First 5 of the wheels are CBN and preferably have different number of grits sizes. 6<sup>th</sup> wheel is selected as a mounted point conventional wheel (Aluminum oxide). The wheels are shown in Figure 8, from the left to right the wheels numbers are 1,2,3,4,5 and 6 respectively. The measurement and modeling of the before mentioned wheels will be presented in the following sections to provide a database for future process modeling applications.



Figure 8: Measured grinding wheels. From left to right 1) 10mm B126 CBN 2) 5mm B64 CBN 3) 30mm B150 CBN 4) 10mm B126 CBN dressed 5) 10mm B126 CBN worn 6) 20mm B120 Al<sub>2</sub>O<sub>3</sub>

## 2.1 C Number Identification

C number is defined as the number of grits that reside on an area of 1mm<sup>2</sup> on the surface of the grinding wheel which is analogous to number of cutting teeth in milling. C number should be the initial parameter to be identified. C number of the wheel can be found by using the 20x lens on the  $\mu$ surf Nanofocus confocal microscope. Measurements were made at different points of the tool by scanning in the X and Y axes and determining the abrasive grits. In this method, the particles lying above a certain height of the Z axis are counted by using the microscope and confocal approach systems. When the confocal option is used, the highest points of the abrasive particles can be identified marked with red dots. Areas marked with red marks are perceived by the device as areas where the light reflects more, that is closer to the lens. Abrasive grits have been determined with this system, which is made at various points of the tool. The points are colored as blue.

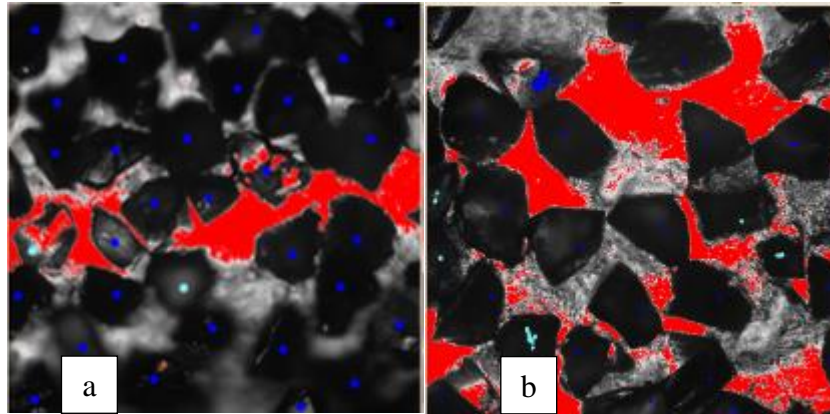


Figure 9: C number identification a) tool #1 b) tool #3

A sample measurement is given in Figure 9. As seen, the grits can be counted with nanofocus. The area of the measurement corresponds to  $0.64\text{mm}^2$  for the 20x lens. The numbers are found and then multiplied with a ratio to match the  $1\text{mm}^2$  area. The C number is used to identify the total number of grits on the whole surface of the grinding wheel.

## 2.2 Individual Grit Measurement

Individual grit measurements are necessary for the identification of process modeling related parameters such as oblique angle, rake angle and edge radius [1,11,12]. For this identification 50x lens in the Nanofocus is used to capture the 3D and 2D scanning of the individual grits. The software provided with this measurement device namely  $\mu\text{surf}$  analysis, provides an on-screen measurement tool on the scanning obtained from the microscope. The identification of the geometrical properties of all the grits on the grinding wheel is a very tiresome approach thus a normal distribution method [40] for creating the virtual wheel is used based on the mean and standard deviation of all measured geometric properties of the individual grits. The sample space for generation of Gaussian distribution is selected to be 50 measurements a little bit more than the magical number 30.. A 3D and 2D measurement sample of an individual grit is presented in Figure 10.

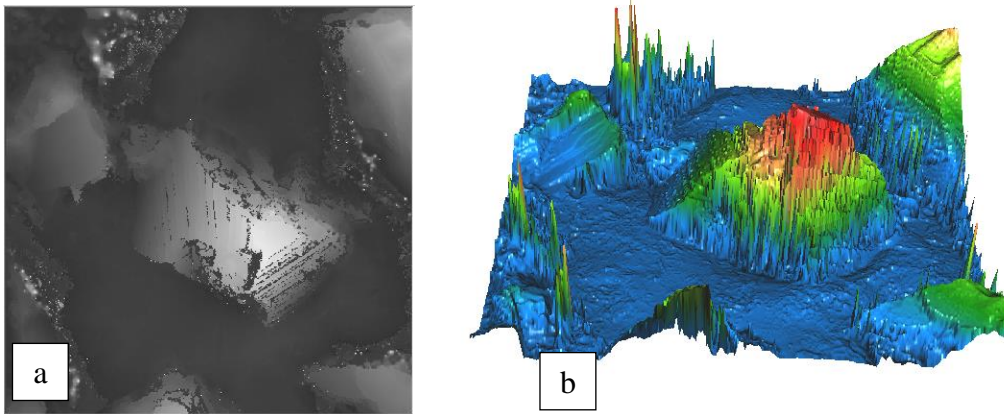


Figure 10: Individual grit measurement with 50x lens a) 2D b) 3D

The Nanofocus software can scan the profiles in x and y directions in the captured scan. The software can project the scans into top and side views. With this feature, the width, height and rake angle of the captured image are measured as follows. In Figure 11a, h1 represents the height, a2 represents the rake angle, and w0 represents the width of the particle. In Figure 11b, the profile of the rounding radius is set by a curve and its radius is measured. In Figure 11b, the radius of the curve is 5  $\mu\text{m}$ . The oblique angle measurement is done by using the same tool that is provided and is shown in Figure 12.

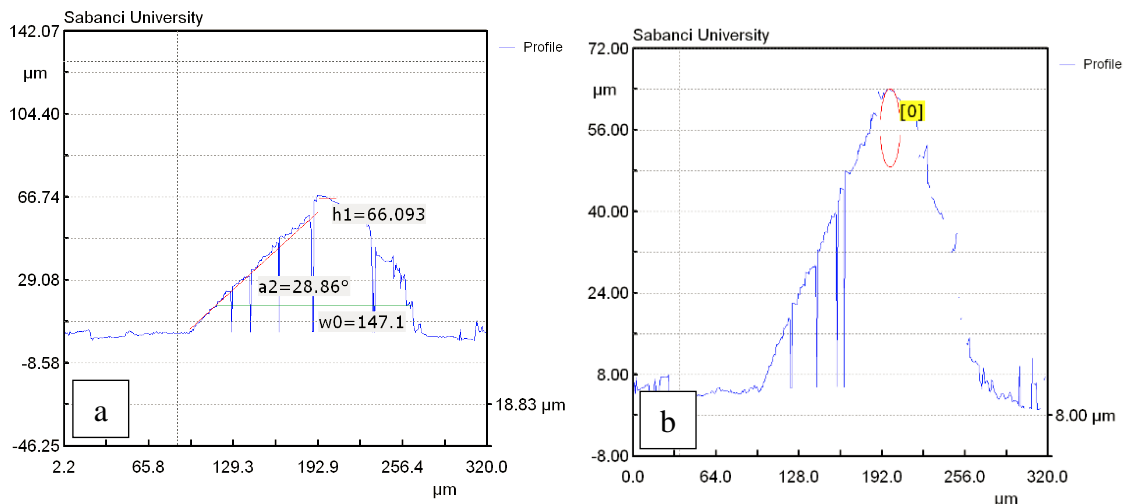


Figure 11: Identification of geometrical properties of individual grits from 2D side view  
a) dimensions b) edge radius

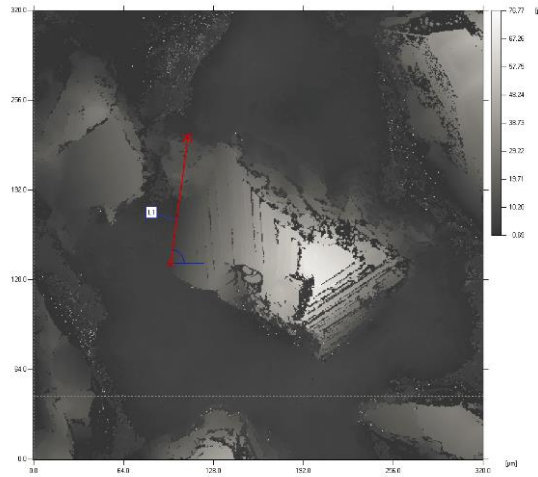


Figure 12: Identification of oblique angle of abrasive grit from 2D top view

However a circular fit does not provide an accurate measurement so later the edge radius scanning are done with SEM.

### 2.3 Virtual Construction of Wheel Surface

Regarding the stochastic nature of the grinding process and the difficulty in modeling the abrasive mechanism it's crucial that some assumptions must be considered. Essentially, the random values of geometrical properties of the grits are assumed to be Gaussian. It may be recognized as a solid assumption considering the production steps of the grinding wheels. Another vital assumption would be to presume the distance between all the adjacent grits along the perimeter of the grinding wheel surface are the same. This assumption is believed to be required to apply the milling analogy to the grinding technology. The adjacent distance is identified as an average term of the data obtained from measurements. Furthermore, it is also assumed that the grinding wheel is discretized into elements along the radial direction. Each element is identical, concentric and resembles a ring surrounding the circumference of the wheel. The width of each element is set to have an average value of grit width. Each element is considered to contain one grit and the whole part of it along the wheel width (or axial) direction whereas there may be many along the periphery. One may not find a grit that is divided and shared between two or more elements. The only geometric property of the grits that are randomly chosen will be the height and this will be the crucial factor in

this work. These assumptions are helpful during the modeling in terms of milling analogy. The illustration of the proposed wheel model is presented in Figure 13.

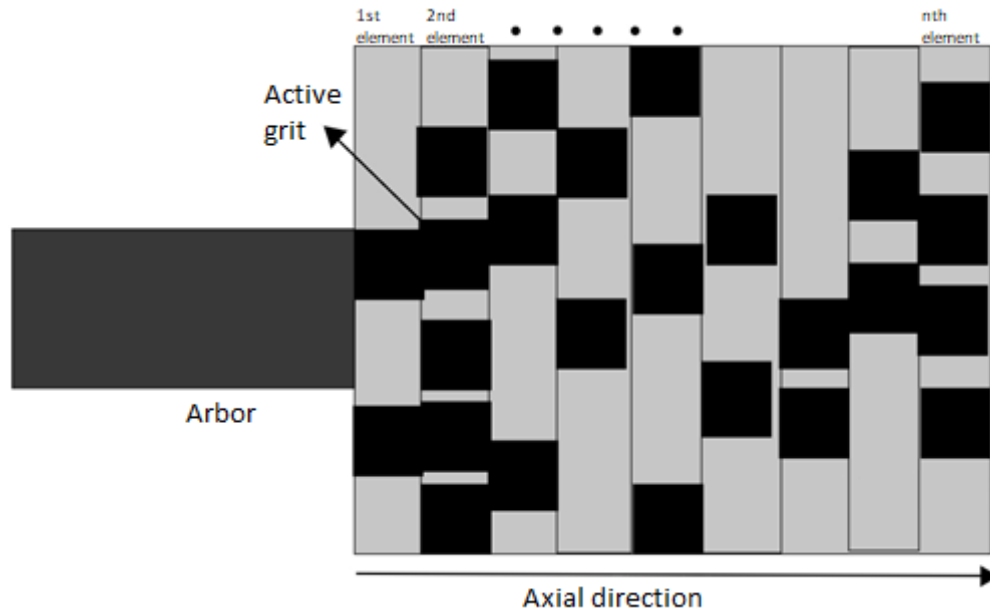


Figure 13: Axial discretization of the wheel

In this figure the grits that are marked with black do not represent all of the grits, instead they refer to the active grits which participate in grinding process. The determination of active grits will be discussed later in the thesis. The  $C$  number which refers to the number of grits per  $1\text{mm}^2$  area does not apply for active grits in the proposed model. It refers to the static number of grits. With the calculation of the mean and standard deviation values from the wheel inspections, a sample space created whose dimension matches the total number of grits along one element. The height amount of an individual grit is selected randomly from this sample space. The total dimension of this sample space is the distributed equivalent of  $c$  number over the area of single element. An imaginary wheel surface is created in this sense in which the model knows how many grits are distributed along the axial elements on the wheel and the geometric properties of them.

## 2.4 Measurement Results

The measurements of 6 different grinding wheels is conducted with the described method. The grit number per  $1\text{mm}^2$  area of grinding wheel is counted and then a number of individual grits on the measured. The geometric properties of the measured grits are identified with the beforementioned equipment and software. The results of the wheel measurements are presented in Table 2. Here the same naming convention that is in Table 1 is used.

Wheel no	1	2	3	4	5	6
Type	Mounted point					
Grit Material	CBN	CBN	CBN	CBN	CBN	$\text{Al}_2\text{O}_3$
Diameter (mm)	10	5	30	10	10	20
Grit size	B126	B64	B151	B126 dressed	B126 worn	B120
Bond Type	Electroplated	Electroplated	Electroplated	Electroplated	Electroplated	Vitrified
C number	33	97	23	33	31	34
Grit width ( $\mu\text{m}$ )	65	41	73	67	39	63
Edge radius ( $\mu\text{m}$ )	1.15	1	1.07	1	1.37	5
Mean and std. dev. Of grit height ( $\mu\text{m}$ )	46 & 18	30 & 11	88 & 17	37 & 8	25 & 0.2	63 & 14
Mean and std. dev. Of width of cut ( $\mu\text{m}$ )	18 & 6	9 & 4	23 & 11	17 & 7	16 & 7	20 & 6
Average rake angle (degrees)	-52	-51	-54	-53	-57	-45
Average oblique angle (degrees)	24	21	25	31	30	32

Table 2: List of wheel measurement results

## 2.5 Summary

In this chapter, a method for grinding wheel measurement and modeling is proposed. As a result of the stochastic nature of grinding tools, it is essential to develop a measurement method and to introduce wheel modeling based on the geometric data that is obtained through measurements. The measurements are used to identify the number of abrasive grits per unit area and the process related geometric dimensions. They are conducted by using a confocal light microscope. The number of abrasive grits are obtained by counting the peak points that are closer to the light source which are highlighted by red color with the instrument. The geometric properties of the individual grits are identified using the related software provided with the measurement device. The x and y profiles are measured from the 2D scans of the grits and the process related parameters are found. Moreover, the wheel model is presented by adding the individual grit data. The grinding wheel surface is discretized into elements along the axial direction. The elements resemble concentric rings of membrane around the periphery of the wheel. With respect to the number of abrasive grits per unit area, the grits are distributed along the discretized elements with each grit having the array of data of the geometric properties.

A set of measurements including 6 different grinding wheels is presented including 5 CBN wheels having different grit sizes and conditions and 1 conventional aluminum oxide wheel. A quick observation states that

- If the grit size is increases, C number decreases.
- The grid width is proportional to B number.
- Edge radii of CBN wheels is smaller than that of the conventional wheels
- The mean and standard deviation of height is getting lower if dressing is applied or the wheel is worn.
- C number may decrease due to wear because of the pull-out mechanism [12].

### 3 KINEMATIC MODEL OF ABRASIVE PROCESSES

Some models presented in the literature are insufficient to truly represent the mechanics of abrasive processes accurately. One crucial subject on this inadequacy is the determination of the active grits that participate in grinding. As a result of the stochastic nature of the grinding wheel structures, not all the abrasive grits are active during the process [38]. Throughout the experimental work for this thesis, it has been observed that the identification of the active grits around the grinding surface plays a significant role in the development of prediction of grinding force and workpiece surface roughness. This is significant especially when mounted point grinding wheels are used. In some of the works in the literature the active grit number is treated as a constant number [53] which is identified beforehand from tool measurements. During the studies [54], it was discovered that the percentage of active grits is not a static number, instead it highly depends on the grinding process conditions. In this work, a method to identify the active grit numbers is presented.

In Figure 14, a cross section of the grinding tool is depicted where grit number 1 is active and grit number 2 is passive. As it can be seen the abrasive grits on the surface of the wheel have different height profiles based on the mean and standard deviation of the values obtained from the measurements. This results in a situation where the taller grits compared to the others will indent more into the workpiece surface and the shorter grits will not even contact any material on their trajectory since the path is cleared by more dominant grits in the previous revolutions.

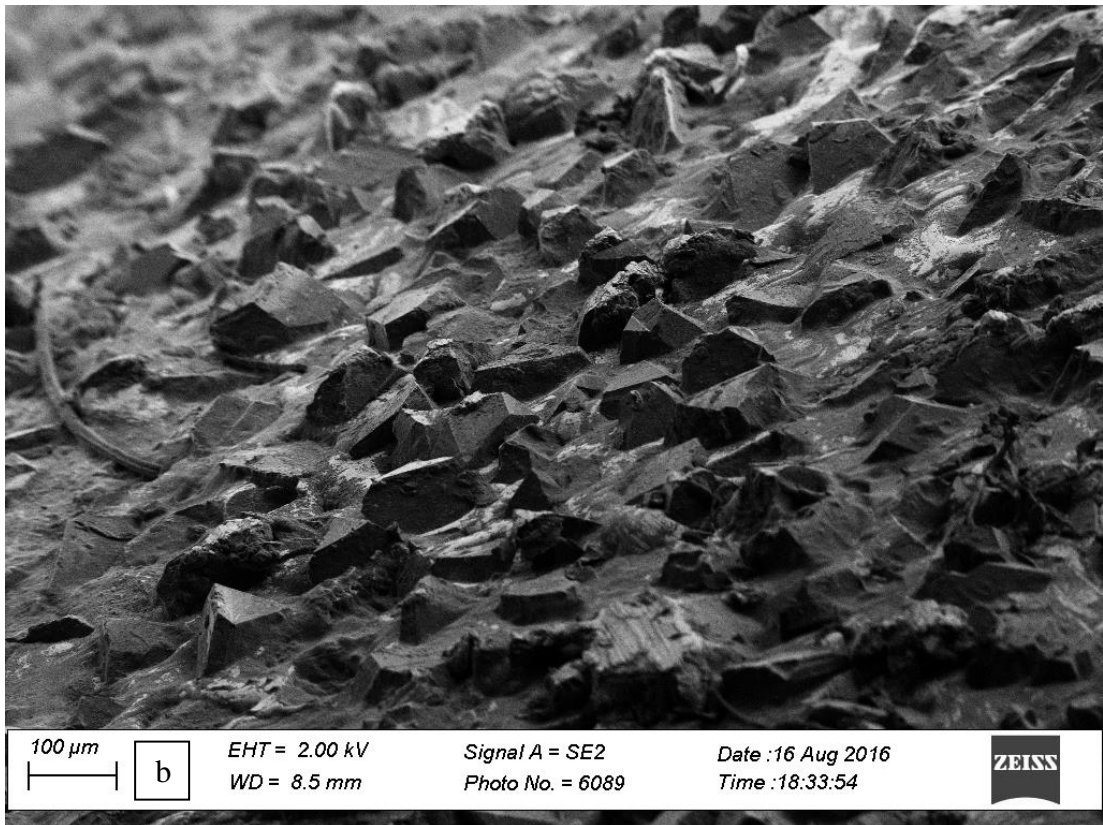
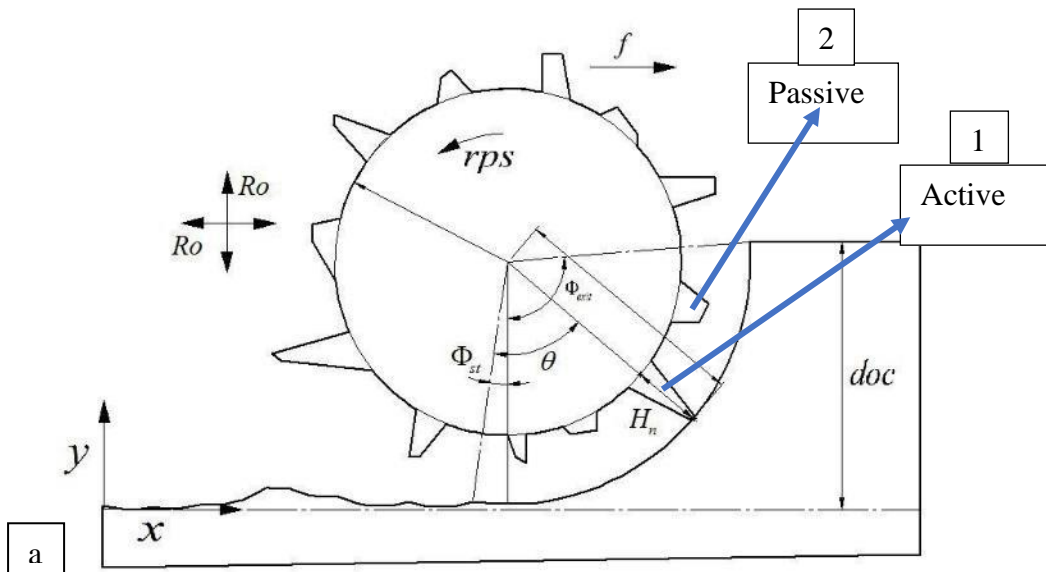


Figure 14: Depiction of active grits (a) virtual wheel (b) real wheel surface

When the algorithm for finding active grits completes the task, the active grits are determined and separated from the rest. For the static model, the virtual wheel is recreated by the active grits and the passive grits are disregarded. The details will be given in the following subsection.

### 3.1 The Geometric-Kinematic Model

Because of the stochastic nature of the grinding process, all grits on the wheel surface have a varying height profile. The identification of active grits is done through the comparison of grits in terms of their height profile.

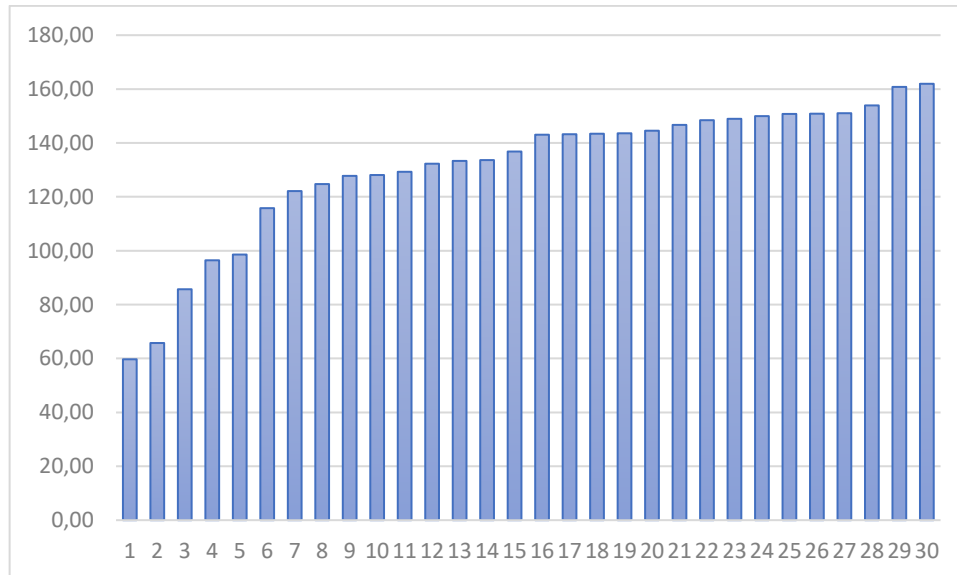


Figure 15: Height distribution of grit measurements

The effect of the workpiece velocity (feed) plays a crucial role on the number of active grits. For instance, imagine a hypothetical grinding operation carried out using a high enough feed velocity and very slow wheel rotational speed. For such a case regardless of the height distribution the number of active grits would be very high. Furthermore, the eccentricity of the grinding wheel will also affect the number of the active grits as it will change the height distribution. This thesis presents a model in which most of the grinding parameters are included in identifying the number of active grits. [55]

#### 3.1.1 Electroplated CBN wheel properties

Electroplated CBN tools are wheels that have a single layer of grits which are electroplated through a metallic bond. With these bonds and abrasive CBN grits, these wheels exhibit an enhanced quality of mechanical properties [41]. These abrasive grits

have increased toughness and hardness with a high thermal conductivity. These properties permit the use of electroplated CBN wheels in grinding of difficult-to-cut materials [3]. It is crucial to determine the mechanics of abrasive processes using CBN plated wheels which show significantly different characteristics compared to the conventional cutting processes.

The identification of the grit properties is essential for the geometric kinematic model. The geometry of the grits, the distance between them, the number of grits in a  $\text{mm}^2$  will be the important inputs to the model. The image of the CBN wheel that is used in the tests for force modelling is presented in Figure 16.



Figure 16: 20mm diameter B126 (grit size) ElectroPlated CBN wheel

The grinding CNC machine used on this work has a high-speed spindle and the experiments were carried out in the speed range of 36000-40000 rpm using smaller wheels. The results of the wheel measurements are given in Table 3. This wheel is different than the conventional wheels as the abrasive grits are CBN material the diameter is significantly low as the use of aluminum oxide wheels with diameters of 200-300 mm is more common.

Properties	Description
Diameter of the wheel	20 mm
Width of the wheel	10 mm
Arbor diameter	6 mm
Grit size	120 $\mu$

Table 3: Specifications for the presented wheel in Figure 16.

Some of the data about the wheel properties can be obtained from the manufacturer, but some properties that are specific to individual wheels cannot be found in the catalogs due to the stochastic nature of the abrasive tools [12]. Those are the individual grit properties such as height, grinding width, oblique and rake angles will influence the grinding mechanics. The grit measurements of the tool shown in Figure 16 are given in Figure 17. The chart illustrates the means and the standard deviations of the measurements together with the variation of the data. These measurements were done on the confocal microscope Nanofocus.

The Nanofocus device has its limits. As it works on a light scan procedure, some reflection errors on the wheel surface may cause deviations in the 3d model creation. If the measurement is aimed at a small viewpoint the values may reside within the noises. The edge radii of the grits will be quite small on grinding tools thus the measurements for edge radii on Nanofocus will not produce accurate results. Therefore, the edge radius measurement has been carried out on an electron microscope. In Figure 18, the images from the SEM machine are provided.

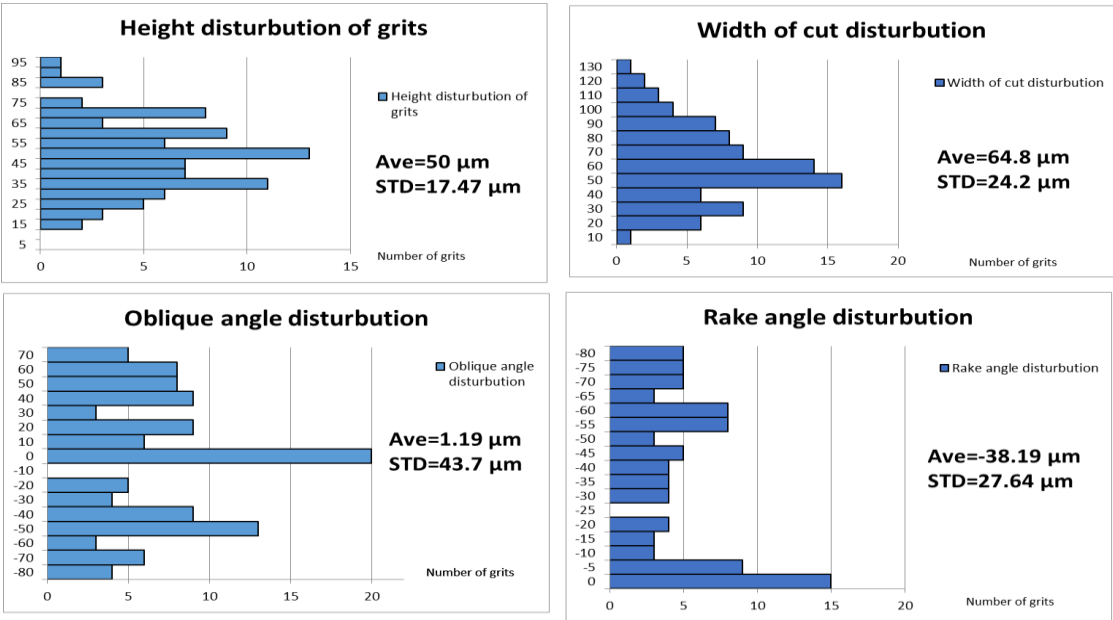


Figure 17: Measurement results of the presented wheel

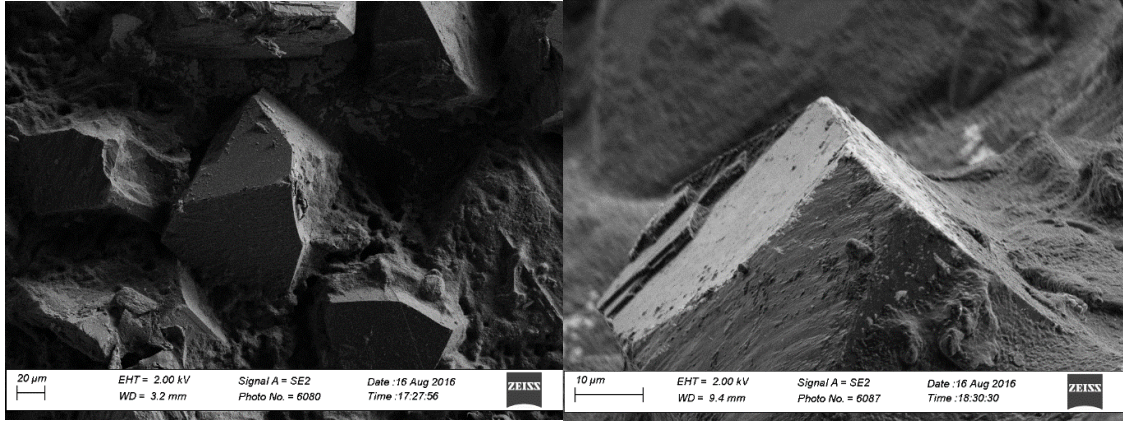


Figure 18: SEM captures of a single grit

It is believed that the measurements obtained from the SEM are more accurate than those of the Nanofocus. It is observed that the nose radius of some of the grits reside on nanoscale. Small edge (1 micrometer or lower) radii is a strong advantage of the CBN tools compared to the conventional wheels as low edge radius lead to less rubbing effect on the grinding zone [56]. This results in a grinding mechanism where while the chip removal is increased the rubbing effect is reduced yielding a more favorable situation regarding the decrease of process forces and temperatures.

### 3.1.2 Determination of Active grits

The principle for determining if one grit is active or not relies on the movement of the grits. The virtual wheel is moved and turned along the surface while the trajectories of the respectful grits are printed, and the intersections of these trajectories are carefully investigated.

The trajectory generation for each grit relies on its radial position. Due to their random heights, the grits will have different radii along the wheel. The model also considers the run-out amount of the wheel and adds it to the respective grit. The coordinates along the trajectory of the grit can be calculated as follows (1-3).

$$x_n = [R_n + R_o \cdot \cos(\theta)] \sin(\theta) + f \cdot t \quad (1)$$

$$y_n = [R_n + R_o \cdot \cos(\theta)](1 - \cos(\theta)) \quad (2)$$

$$R_n = r + H_n + R_o \cdot \cos((n - 1) \cdot 2\pi/N) \quad (3)$$

where  $R_n$  is the radius of the respective grit and  $R_o$  is the runout amount of the grinding wheel.  $H_n$  is the random grit height value,  $f$  is the feed,  $\theta$  is the immersion angle,  $t$  is the time and  $N$  is the number of grits on the element. The kinematic trajectories are calculated according to the formulae given above and they are printed in  $x$ ,  $y$  and  $z$  domain as shown in Figure 19.

When the measurements on the tool are completed and the virtual wheel is created with normal distribution, the simulation starts as the virtual wheel is turned on the surface of the workpiece. This is a real-time simulation and the trajectories for the active grits are created simultaneously step by step. The steps are discretized in terms of small angle increments and each grit has its respective start and end angles. The grits start to create print their trajectories as the corresponding approach angle is reached during the simulation. As the simulation starts, the first two grit trajectories are printed on the  $x$ - $z$  plane as shown in Figure 20. There are 3 cases for the interaction:

- i) There is no interaction and the second grit is shorter than the first one
- ii) There is no interaction and the second grit is taller than the first one
- iii) There is interaction

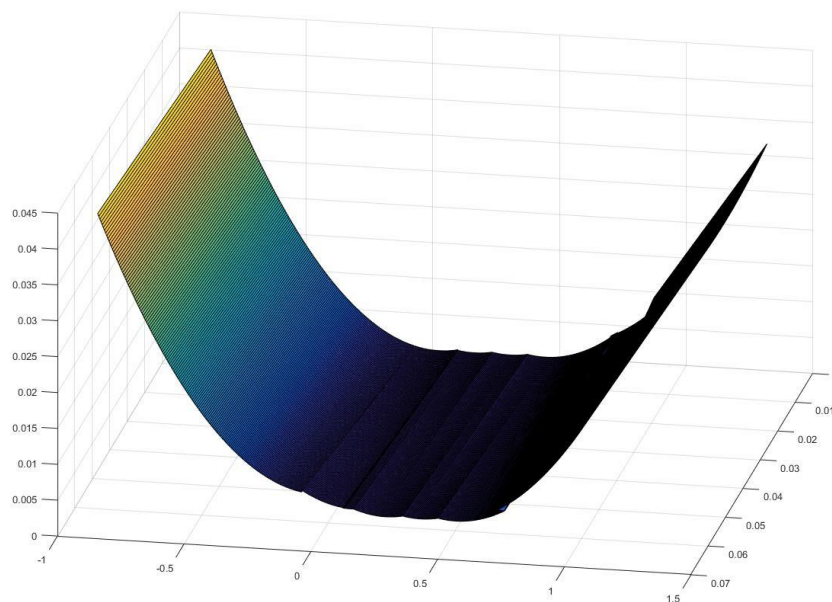


Figure 19: Kinematic trajectories of the grits (all units are in mm)

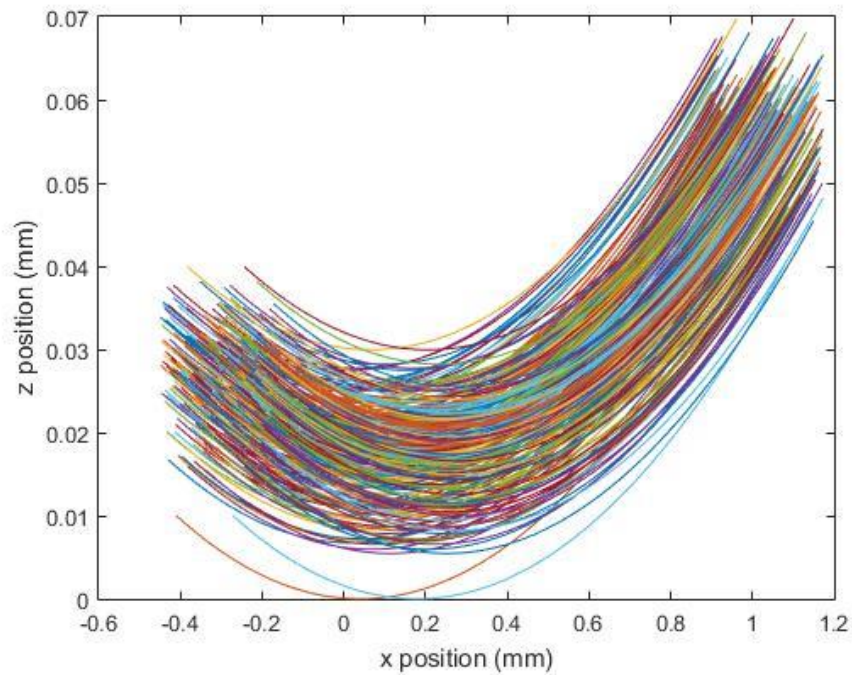


Figure 20: Trajectories on x-z plane

The first case implies that the first grit is dominant to the consecutive one. When the first grit has larger height than the second one it will remove some part of the workpiece material. When the second grit starts its trajectory movement it will not meet with the last surface of the workpiece that is defined by the previous grit. When this case is received in the algorithm it means that the first grit is flagged as active grit and the second grit is flagged as a passive grit.

The second case indicates that the second grit is dominant to the consecutive one. When the first grit starts its trajectory, it will meet with some of the workpiece material and will cut the workpiece. This doesn't guarantee that it is flagged as active because the algorithm waits for the second grit's response. The second grits will also meet with undeformed material on the surface. When the wheel completes its revolution, and comes to the same rotational orientation this time if the second grit isn't reflagged as passive, only then both of the grits are flagged as active. If the second grit is reflagged as passive in the previous program loops, then both grits are reflagged as passive. The trajectories for the depiction of first two cases are given in Figure 21.

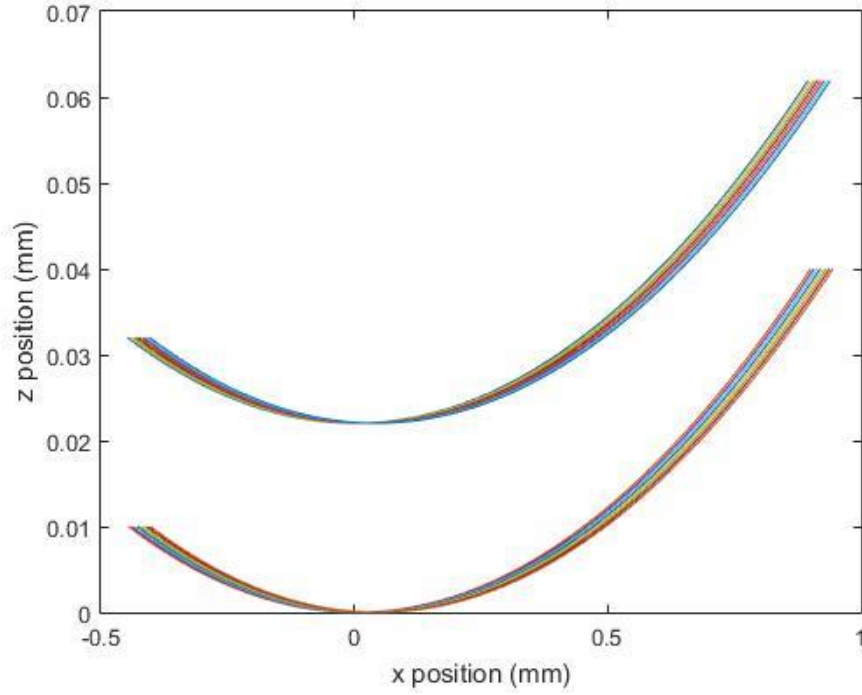


Figure 21: Depiction of case 1 or 2

The third case implies that the consecutive grits have similar heights. When there is a path interaction in the trajectory map. The second grit is flagged as active regardless of the situation of the first grit only if the second grit's trajectory creates a chip thickness that is larger than the minimum uncut chip thickness of the grit. The trajectories for the depiction of the third case is given in Figure 22. The critical chip thickness is defined as:

$$h_{cr} = r_t \cdot [1 - \cos(\alpha)] \quad (3)$$

where  $\alpha$  is stagnation angle which is taken as 55 degrees [57] and  $r_t$  is edge radius of the grit. Equation 9 has been used in this study as a criterion to update the path generated by active grits. If maximum chip thickness created by a particular grit is less than the critical chip thickness the path is not updated even though the grit is considered as an active one.

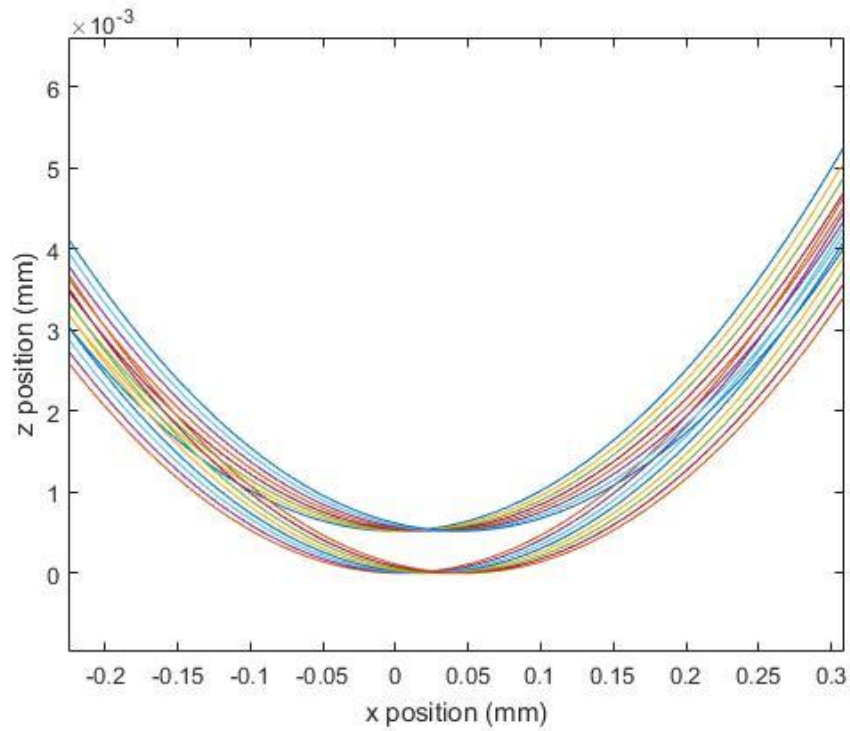


Figure 22: Depiction of case iii

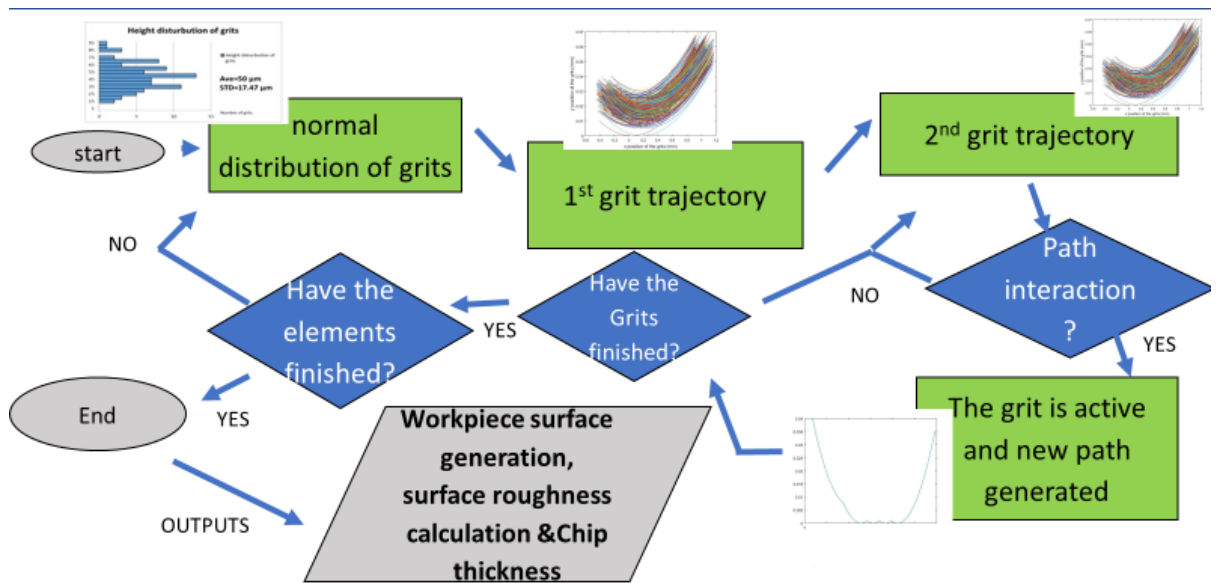


Figure 23: Flowchart of Active grit algorithm

When the trajectories of all the grits of the first element is completed and the active grits of the corresponding element is identified, the algorithm continues with the next element and with the same procedure until the elements are finished. When the elements are finished, the virtual wheel is recreated by omitting the passive grits. A demonstration of the virtual wheel is given in Figure 24.

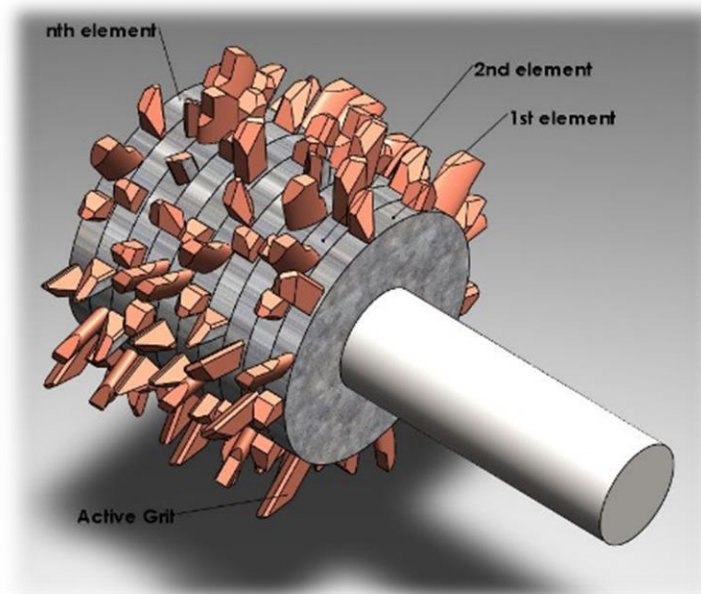


Figure 24: Recreated wheel with active grits only

### 3.2 Surface Roughness in perpendicular to cutting direction

Surface roughness prediction is one of the fundamental aims in process modelling of the abrasive operations since the general use of grinding operations is to give the final geometry and surface quality to the workpiece. The surface roughness of the workpiece perpendicular to cutting direction can be obtained utilizing the geometric-kinematic model developed for this thesis. The model inherently accumulates the data that is required for the surface roughness calculation and it can be calculated instantaneously as the simulation is being performed. Please recall that the geometric-kinematic model is able to print the kinematic trajectories of the abrasive grits as the wheel is being turned and fed to the workpiece from Figure 20. While the trajectories are created for the selected element, the intersection point is investigated again to find the last surface created on the workpiece surface. The trajectories for the half of the revolution of the wheel is presented in Figure 25.

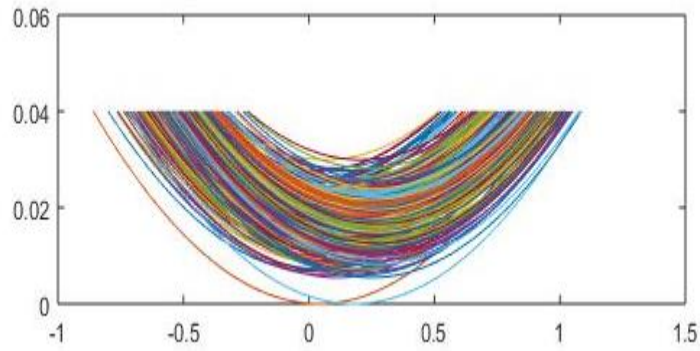


Figure 25: Trajectories for the surface roughness calculation

After the trajectories are printed the trajectories that belong to the passive grits are omitted. The trajectories of the active grits are investigated. The intersections of the consecutive active grits and the intersections between the workpiece surface is identified. The conjugate trajectory is found which has the contact over the workpiece. This trajectory indicated the last surface that is imprinted on the workpiece surface which is illustrated in Figure 26.

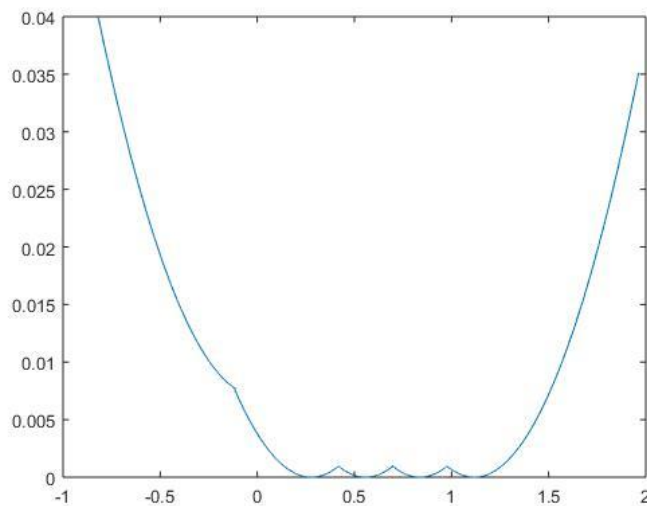


Figure 26: Last surface

The last surface on the workpiece has the information for the surface roughness in the cutting direction inherently and can be easily found the average values of the coordinate points on the trajectory. However, this information is a high underestimate of the

surface roughness as it only represents the feed marks on the surface due to difference in consecutive active grit heights. The effect of vibration is included which has the dominant effect on the surface roughness in cutting direction which will be covered in next chapter.

The surface roughness in the perpendicular to cutting direction can be found when last surfaces of the grits reside on the rest of the elements are printed such as in Figure 27.

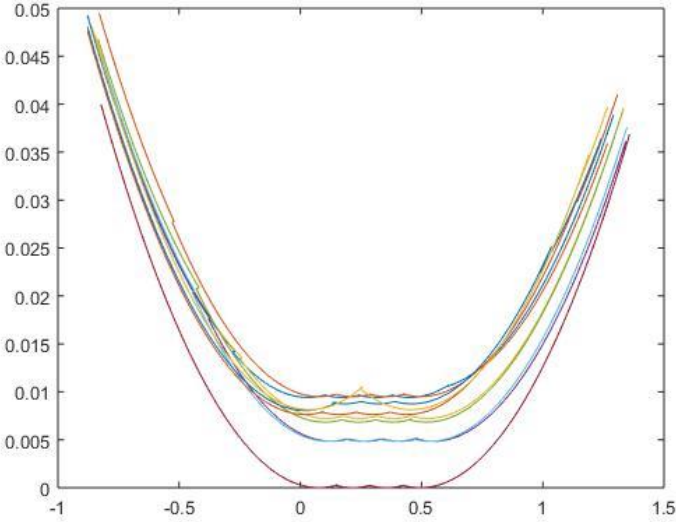


Figure 27: Last surfaces of all the elements

When all the last surfaces are created respective to each element, a basic 3Dprojection is applied to simulate the surface topography of the workpiece which is accurate in perpendicular to cutting direction. The surface is illustrated on Figure 28.

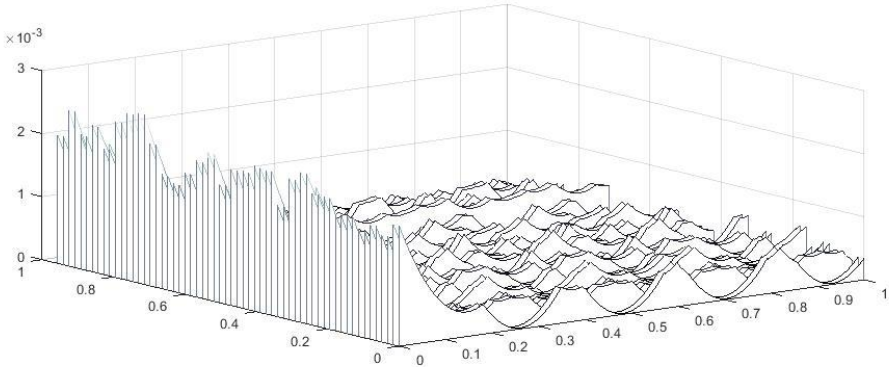


Figure 28: 3D projection of last surfaces

The Ra value therefore can be calculated as the average height values of the last surface coordinates along the axial direction divided by the element number.

### 3.3 Grinding Force

Since the milling analogy is used to simulate the wheel topography, the grinding force can be calculated after the resultant chip thickness is identified. The chip thickness in grinding is generally very low (in the magnitude of microns, sometimes lower) and there are a number of ways to predict it [1]. Apart from the empirical ways to calculate the chip thickness, the geometric-kinematic model can also be used to determine the resultant chip thickness during the grinding operation.

#### 3.3.1 Undeformed Chip Thickness

Just like the surface roughness the trajectories of the consecutive active grits and the intersections have the inherent data for the chip thickness calculation. If the milling analogy is applied again, having active grits which have different height distribution means the model is now analogous to milling cutter with run-out problem. The milling cutter with runout can be treated as it has different height values for each cutting flute. The milling cutter with run-out is simulated in Figure 29.

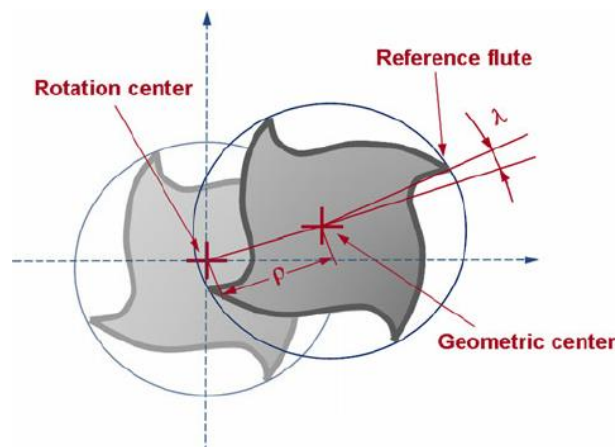


Figure 29: Milling cutter with run-out

The instantaneous chip thickness can be calculated as the geometric-kinematic simulation is being carried out. The chip thickness is the difference between the radial differences of the consecutive active grits in addition to the feed per active grit. The formula for the calculation is given in equations (4-5):

$$h_{i,j} = R_n - R_m + (n - m) \cdot f_t \sin(\theta_{i,j}) \quad 0 < \theta_{i,j} < \theta_{exit,i,j} \quad (4)$$

$$h_{max} = R_n - R_m + (n - m) \cdot f_t \sin(\theta_{exit,i,j}) \quad (5)$$

where  $h$  is the undeformed chip thickness per grit, with the indices  $i$  and  $j$  represent the  $i$ 'th active grit on the  $j$ 'th element. Indices  $n$  and  $m$  represent the consecutive positions of the active grits along with the circumference of the wheel. Angle  $\theta$  represents the immersion angle of the current grit. Finally,  $f_t$  indicates the feed rate. The calculation of the grinding force is a straightforward multiplication of the calculated undeformed chip area with the cutting force coefficients.

### 3.3.2 Mechanistic Force Model

Since the milling analogy is employed, the methods to predict the force can be categorized in two ways. The force can be computed using mechanistic or analytical approaches. The mechanistic force model requires applications of a number of tests in order to calibrate the force coefficients.

Assuming grinding wheel acts similar to a milling tool where each grain removes material from the workpiece, the milling analogy can be applied for grinding process. Axial force can be neglected here because the random distribution of the oblique angles (can change between positive and negative values) results in a very small force on the dynamometer [12]. Force components can be projected in  $x$  (cutting direction) and  $y$  (normal direction) directions as given in eq.1 where  $F_t$  and  $F_n$  are tangential and normal forces and  $\varphi$  is instantaneous immersion angles:(Minus/plus signs are for up/down grinding, respectively):

$$F_x = -F_t \cos(\varphi) \mp F_n \sin(\varphi) \quad (6)$$

$$F_y = F_t \sin(\varphi) \mp F_n \cos(\varphi) \quad (7)$$

Analytically derived average cutting forces can be obtained as it can be seen in formulae (8-9) (detailed calculation can be found in [58]):

$$\bar{F}_x = \left\{ \frac{Nfa}{8\pi} [K_{tc} \cos(2\varphi) - K_{nc}(2\varphi - \sin(2\varphi))] \right\}_{\varphi_{st}}^{\varphi_{ex}} \quad (8)$$

$$\bar{F}_y = \left\{ \frac{Nfa}{8\pi} [K_{tc}(2\varphi - \sin(2\varphi)) + K_{nc} \cos(2\varphi)] \right\}_{\varphi_{st}}^{\varphi_{ex}} \quad (9)$$

$K_{tc}$  and  $K_{nc}$  are the cutting force coefficients in tangential and normal directions, respectively,  $a$  is axial depth of cut,  $N$  is number of active grits which are defined around any line on the wheel periphery which participate in chip formation process which are the output of the geometric-kinematic model.  $f$  is feed per revolution per active grit.

In mechanistic approach in order to obtain force coefficients, instead of calculation of cutting variables such as shear angle, shear stress etc., a set of grinding tests are conducted at same wheel speed, axial and radial depth of cut but different feed rates. Results are used to identify force coefficients from Eq. 2. So, the coefficients are obtained experimentally [58]. Once the force coefficients are known, it is possible to predict grinding forces at any arbitrary condition in the range of experimental data.

### 3.3.3 Thermomechanical Force Model

In addition to mechanistic approach, force coefficients can be calculated analytically using mechanics of oblique cutting [58]. Analytical expressions for force coefficients are given below (10-11).

$$K_{tc} = \frac{\tau_s}{\sin \varphi_n} \frac{\cos(\beta_n - \alpha_n) + \tan i \tan \eta \sin \beta_n}{\sqrt{\cos^2(\varphi_n + \beta_n - \alpha_n) + \tan^2 \eta \sin^2 \beta_n}} \quad (10)$$

$$K_{nc} = \frac{\tau_s}{\sin \varphi_n \cos i} \frac{\sin(\beta_n - \alpha_n)}{\sqrt{\cos^2(\varphi_n + \beta_n - \alpha_n) + \tan^2 \eta \sin^2 \beta_n}} \quad (11)$$

where  $\tau_s$  is shear stress,  $\varphi_n$  is shear angle,  $\beta_n$  is friction angle,  $\alpha_n$  is rake angle,  $\eta$  is chip flow angle and  $i$  is oblique angle. In order to obtain force coefficients, three important variables i.e. shear stress ( $\tau_s$ ), shear angle ( $\varphi_n$ ) and friction angle ( $\beta_n$ ) should be known. Chip flow angle ( $\eta$ ) can be taken as equal to oblique angle ( $i$ ) based on Stabler's empirical rule. Oblique and rake angles are obtained by investigation of grit

properties which will be described in the next section. In this study, shear stress was obtained by using Johnson-Cook model [40]:

$$\tau = \frac{1}{\sqrt{3}} \left[ A + B \left( \frac{\gamma}{\sqrt{3}} \right)^n \right] \left[ 1 + C \ln \left( \frac{\dot{\gamma}}{\dot{\gamma}_0} \right) \right] \left[ 1 - \left( \frac{T - T_r}{T_m - T_r} \right)^m \right] \quad (12)$$

The Johnson-Cook equation constants is given in [59].

A (Mpa)	B	C	m	n
1485	904	0.015	1.689	0.77

Table 4: Constants of Johnson-Cook equation for Inconel 718.

The shear strain and the strain rate are given [58]:

$$\gamma = \frac{\cos(\alpha_n)}{\sin(\varphi_n) \cos(\varphi_n - \alpha_n)} \quad (13)$$

$$\dot{\gamma} = \frac{V \cos(\alpha_n)}{d \cos(\varphi_n - \alpha_n)} \quad (14)$$

where  $V$  is cutting speed and  $d$  is the shear zone thickness which can be approximated to 0.15 of shear plane length ( $l$ ) where [58]

$$l = \frac{h}{\sin(\varphi_n)} \quad (15)$$

where  $h$  is the uncut chip thickness that is calculated through the geometric-kinematic model.  $d$  was approximated as 1 micron in this study. During the analysis, it has been observed that thickness of shear plane did not affect the shear stress significantly. This fact was also reported in [46].

Friction angle and the shear angle (using the minimum energy principle) can be approximated as [58]

$$\beta_n = \tan^{-1} \frac{F_y}{F_x} + \alpha_n \quad (16)$$

$$\varphi_n = \frac{\pi}{4} - \frac{(\beta_n - \alpha_n)}{2} \quad (17)$$

A few grinding tests were done at different feed rates to identify the friction angle using equation (13) after subtracting the ploughing forces. It varied from 32.5 to 35.3 degree an average value of 33.9 degree was used here. Details can be found in [40].

The temperature in the shear zone can be calculated iteratively as the force is calculated. The detailed calculation can be found in [1].

A straightforward approach to identify the shear stress, friction and shear angles is using orthogonal database in which those values are defined experimentally for each pair of workpiece-tool at corresponding rake angle. Due to varying and high negative rake angle of the grain and very small undeformed chip thickness in grinding process, it is difficult and time consuming to conduct orthogonal cutting tests. Accordingly, in this work equations (12) to (17) was used instead. The total average force is obtained by summing up the force for all active grits.

Even though the mechanistic model can predict the grinding force accurately, it requires a set of experiments to be conducted for identification of the grinding force coefficients and calibrations are needed for various feed, speed, depth and grit parameters. The thermomechanical model on the other hand, can predict the grinding force with slightly poorer discrepancy while being applicable to wider range as no calibration is needed for varying process and wheel parameters. Direct analytical relationships can be developed between the inputs and outputs of the grinding process.

The flowchart for grinding force calculation is presented in Figure 30. As it can be seen, the first step for predicting the grinding force is optical measurements done on the grinding tools. Where the geometric properties of the abrasive grits can be identified for a substantial number of samples. Then the normal distribution is applied to the geometric properties to create a broader sample space in order to mimic the wheel topography. After the wheel is modeled, the kinematic trajectories of the grits are printed using the geometric-kinematic model. The geometric-kinematic model allows the prediction of;

- i) The number of active grits
- ii) Surface roughness in perpendicular to cutting direction
- iii) Instantaneous uncut chip thickness

By using the newly found uncut chip thickness the simulation can predict the force either directly by mechanistically identified grinding force coefficients or through the material model using the thermo-mechanical force calculation.

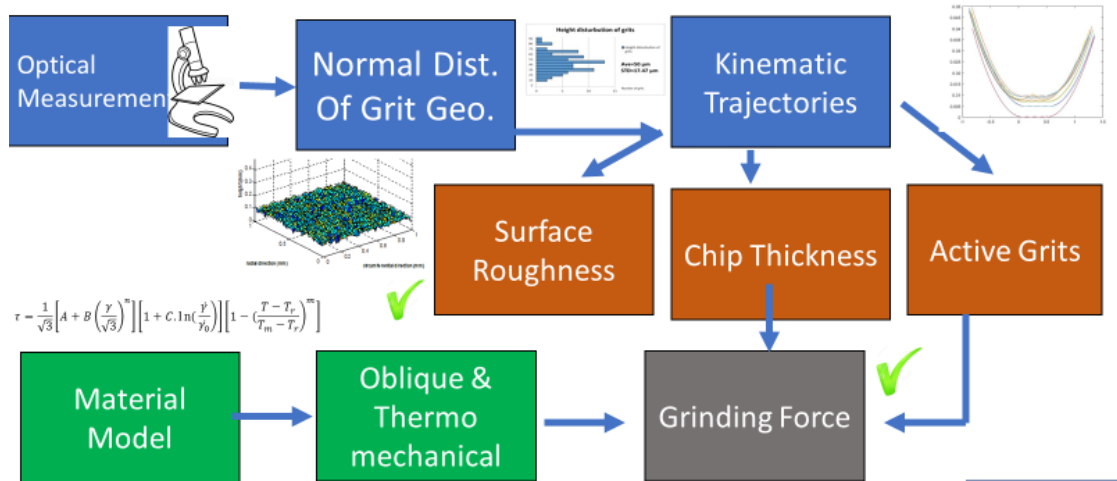


Figure 30: Flowchart for force calculation

### 3.4 Results

In this section of the chapter, the results obtained for the active grits, surface roughness and grinding force are presented. For calculation of active grits, the experimental verification can be a challenging task which will be covered later, however the experimental verification for the workpiece surface roughness and grinding force is compared with the outputs from the simulations and the models are verified.

#### 3.4.1 Active grits

First of all, large number of simulations are done in order to have a database of active grit numbers for different cutting conditions. This is the most crucial as it will be the key parameter for assigning the tooth number (milling analogy) and determining an average value for feed per tooth.

The algorithm for determining the number of active grits is a randomized problem. In the beginning of the simulation/computation a large amount of sample space is created from a smaller amount determined by the optical measurements. In this method, Gaussian distribution model is used (mean, std. Deviation values determine the larger sample space). [1,11,12]

This means that when the simulation is run, a new larger sample space is created from scratch based on the smaller sample space input. Although this will result in a different grinding wheel model in each run, the idea in this model is that if one includes sufficient number of elements for the wheel input, all program outputs such as grinding force, active grit number ...etc. will converge around an average value [1], [11], [12]. (The reason being in the Gaussian distribution, the values closer to the average will have higher probabilities). Having enough amount of sample space is generally possible since in the scope of this thesis, axial depth of cuts between 7-10mm are used. The simulation results are given for 40k rpm in Figure 31.

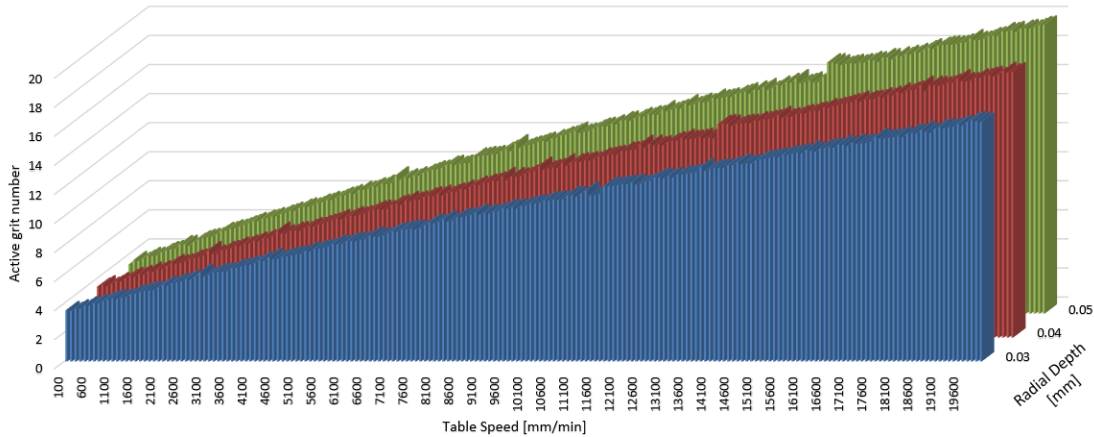


Figure 31: Active grit number table

The active grit simulation results shown in Figure 31 belong to the wheel presented in Figure 16.

It is observed that the active grit number increase with the table speed is linear, and it increases with the radial depth as well. However, through a larger set of simulations it is realized that the number of active grits directly depend on feed per revolution and the effect of radial depth of cut is small compared to the effect of the feed per revolution. A number of simulations were also carried out for the wheels given in Table 5. A first glance shows that the radial depth of cut increase in the process does not increase the active grits very much, not much as the effect of the feed per revolution at least. This situation is shown in Figure 32 for the depth of cuts between 35 $\mu$ m and 200 $\mu$ m (this region stands in the experiments range for the scope of this thesis). It can be seen that

Wheel 1's number of active grits doesn't have a major change when the radial depth of cut is increased. It is worth to mention that the numbers of active grits are not integer as average values are calculated from larger simulations.

Wheel no	1	2	3	4	5
Type	Mounted point				
Grit Material	CBN	CBN	CBN	CBN	CBN
Diameter (mm)	10	5	30	10	10
Grit size	B126	B64	B151	B126	B126
Bond Type	Electroplated	Electroplated	Electroplated	Electroplated	Electroplated
Condition	Fresh	Fresh	Fresh	Dressed	Worn
C number	33	97	23	33	31
Grit width ( $\mu\text{m}$ )	65	41	73	67	39
Edge radius ( $\mu\text{m}$ )	1.15	1	1.07	1	1.37
Mean and std. dev. Of grit height ( $\mu\text{m}$ )	46 & 18	30 & 11	88 & 17	37 & 8	25 & 0.2
Mean and std. dev. Of width of cut ( $\mu\text{m}$ )	18 & 6	9 & 4	23 & 11	17 & 7	16 & 7
Average rake angle (degrees)	-52	-51	-54	-53	-57
Average oblique angle (degrees)	24	21	25	31	30

Table 5: Wheel specifications for the active grit calculations

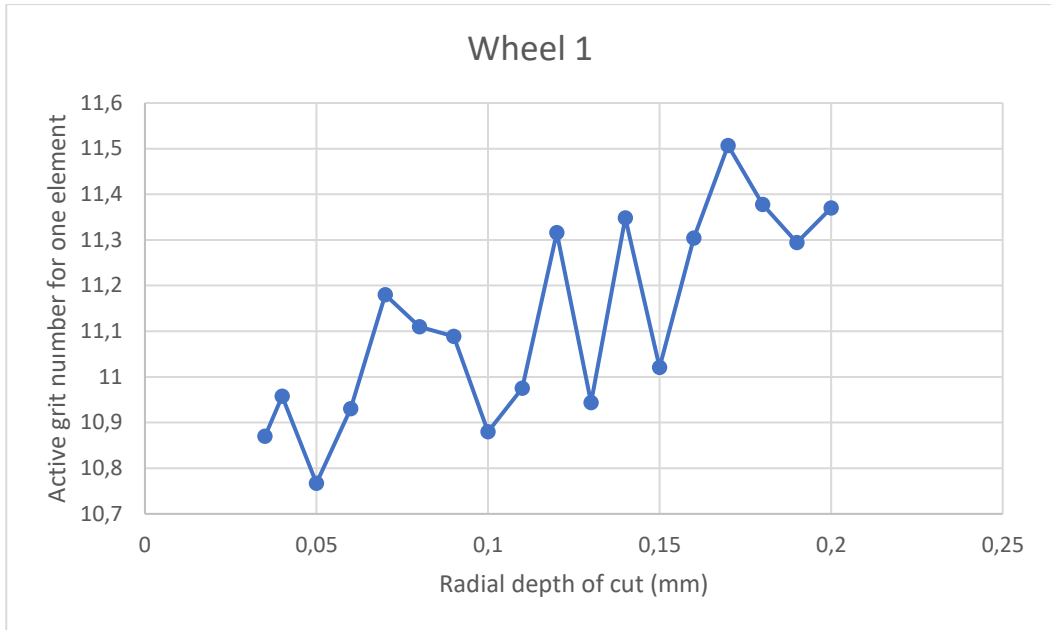


Figure 32: Active grit number for wheel 1 for varying depth of cut

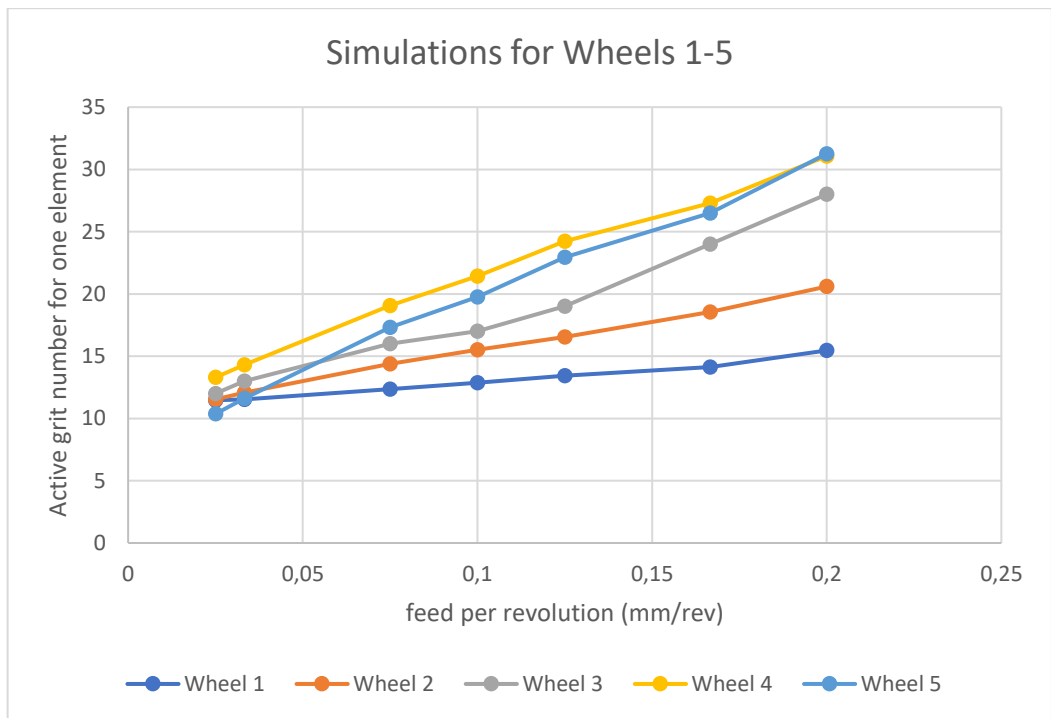


Figure 33: Active grit number for varying feed rate and 5 wheels

The active grit simulations for all of the 5 wheels are given in Figure 33. As it can be seen, the effects of wheel condition, diameter and grit size is presented. In terms of wheel condition, the Wheels 1,4 and 5 are fresh, dressed and worn wheels in a consecutive order. The active grit number is increased as the wheel is dressed or worn because of the decrease in the standard deviation of the height values of the grits. The active grits on Wheel 2 is larger than the ones on Wheel 1 because the grit size is lower on Wheel 2 as the grit size is B64. When the overall grit size is decreased, the number of active and passive grits in  $1\text{mm}^2$  is increased as more grits may now fit in the unit square. Furthermore, Wheel 3 has a diameter of 30mm and even though the grits size is big and the grit per  $1\text{mm}^2$  is low, the surface area of the wheel much higher which results in a higher number of active grits for Wheel 3 comparing to Wheel 1. The most active grits then will be on dressed and worn wheels as their standard deviation is significantly low comparing to other wheels.

### **3.4.2 Grinding Force and surface roughness**

The verification experiments of force and surface roughness were done with the 20mm Electroplated CBN tool grit size: B126 which was shown in Figure 16, together with a conventional wheel of the same grit size and diameter. The experiments were done for the following process parameters:

Feed rates ( $\mu\text{m}/\text{rev}$ ): 2.5, 5, 7.5, 10.

Radial depths of cut ( $\mu\text{m}$ ): 20, 40, 60.

Axial depth of cut: 9mm

Grinding speed: 40m/s.

Wheels: CBN B126 20mm and Conventional B120 20mm.

The comparison of the model outputs and the experiments are given in the following figures (Figure 34 and Figure 35). As it can be seen, the forces tend to increase linearly while the feed rate is increased. The prediction accuracy of the mechanistic force model is better compared to that of the analytical model but since it requires more time and

energy, the thermo-mechanical force model is more favorable with the fact that it is also sufficient for force prediction.

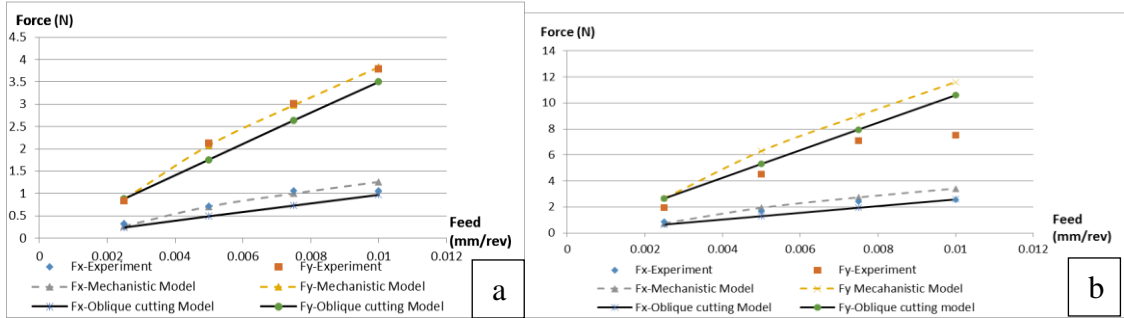


Figure 34: Verification of force model: Depth of cut: 20 $\mu$ m. a) CBN wheel b) conventional wheel

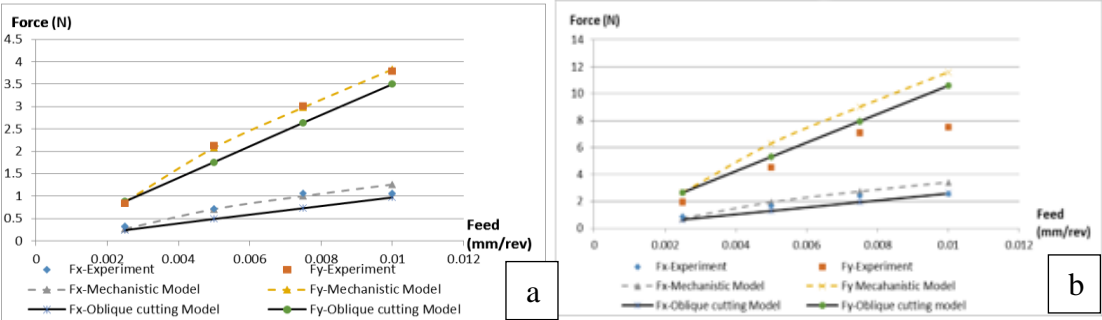


Figure 35: Verification of the force model. Depth of cut: a)40  $\mu$ m b) 60  $\mu$ m. (CBN wheel)

Another point is that the forces with the conventional wheel is high comparing to the CBN wheel. This is the reason that the conventional wheels are dressed before use making the height distribution with smaller deviation which increases the number of active grits. The increased number of active grits means more contact and increased edge forces. The ploughing forces are also increased with the conventional wheel due to the fact that the edge radii of the grits of the conventional wheel are approximately 5 times higher than that of the CBN wheel, thus creating more contact.

The phenomena of increased force with the number of active grits is also verified in Figure 36. As it can be seen, when the grit number per  $\text{mm}^2$  increases in a wheel which has lower standard height deviation, the forces tend to increase. The reason is that with

low standard height deviation the active number of grits will increase and will result in more contact with the workpiece. The wheel with higher standard height deviation of grits will not experience this effect since with the increased static number of grits the active grit number will not change significantly.

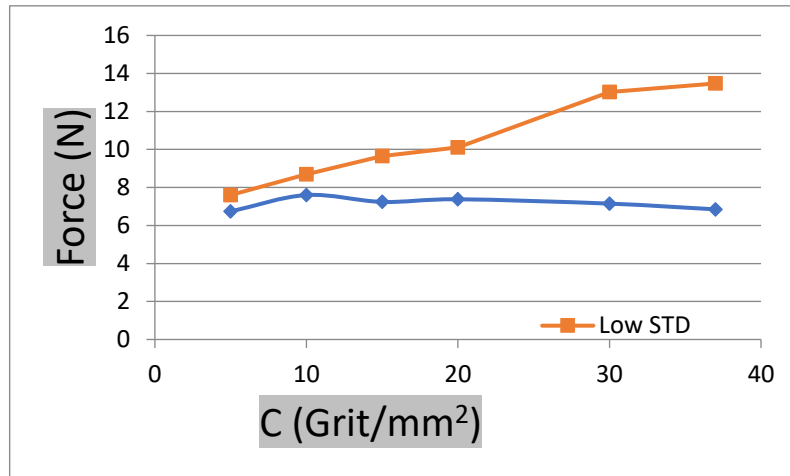


Figure 36: The effect of grit number on the forces

### 3.5 Summary

As one of the most complicated subtractive processes in the industry in terms of modelling and prediction, grinding process has stochastic nature and the first step of modelling grinding starts from coping with the effect of randomness of the process. The initial approach is to determine the wheel parameters such as the geometric data and the distribution of the grits on the surface of the grinding wheel. In this thesis a method for virtual wheel generation is developed by utilizing optical measurement methods to identify the geometric properties of the individual grits [1] and then applying random distribution to create a sample space of grits for the whole wheel [11]. The grinding wheel then is assumed to be discretized along the axial direction into thin disks which are named as the elements. Recognizing that some of the abrasive grits do not participate in the chip formation action, the active grits are identified with the geometric-kinematic model by analyzing the trajectories of the individual grits as the grinding wheel is turned over the workpiece virtually. The geometric-kinematic model

allows calculation of the active number of grits, instantaneous chip thickness and the surface roughness of the workpiece. The chip thickness calculation allows the prediction of the grinding force and two methods namely mechanistic and thermo-mechanical force model are applied in order to verify the models and to compare the performance of both. The thermo-mechanical force model's performance surpasses the other model by being applicable to wider range and not relying calibration methods for different grinding conditions. The results for the number of the active grits conclude that the number depends on the specifications of the wheel and the process parameters such as the radial depth of cut and the feed rate. The surface roughness of the workpiece surface along the perpendicular to cutting direction is observed that it is not affected by the process parameters as the wheel prints the topography and of its surface onto the surface of the workpiece.

## **4 DYNAMIC FORCE MODEL FOR ABRASIVE PROCESSES**

The dynamics of grinding operations have always been an obstacle for abrasive operations since the main goal of the abrasive processes is to finalize the workpiece geometry and the surface roughness given the fact that the instability will hinder the part quality in a considerable way. One of the first stability models for grinding was developed by Inasaki [60] where the problem was defined as a one-degree-of-freedom model and the whole grinding geometry was constructed as a single point representation. This representation resembles a turning operation as the dynamics are constructed as one-degree-of-freedom and the varying chip thickness is calculated along the radial depth of cut of the system. One may say that considering this representation turns grinding chatter into macro level phenomenon. As described in the literature survey of this thesis, the following literature consists of either the analytical solutions to the problem for the mentioned simplifications, or numerical solutions such as time domain simulations where the problem is enhanced in terms of complexity. On the other hand, by utilizing the advantages of the geometric-kinematic model, the micro-level representation of the grinding process is possible. In this thesis, a dynamic model for surface grinding is developed. Applying the milling analogy and the geometrical random distribution of the grits on the grinding wheel, the simulation can predict the dynamic forces and vibrations. A geometric-kinematic model is developed in order to predict the grit trajectories during the grinding process. The active grits are calculated and the chip thickness per active grit is computed with the trajectory simulation of the wheel. The dynamic model is created with the inclusion of the regenerative effect of the workpiece surface. The aim of this model is to model the dynamic behavior of the surface grinding and predict the region of grinding parameters which cause instability in the closed loop time domain system.

### **4.1 Dynamic Chip thickness and Dynamic Forces**

As a reminder, the geometric and kinematic simulation, the model inherently obtains the undeformed chip thickness by the trajectories of the grits and their intersections. Once the active grit number is calculated the passive grits are disregarded and the

problem transforms into a milling cutter analogy around the discretized element of the wheel surface. The active grits have different heights which make them have different radial distance from the center of the wheel. This similar to a milling cutter with runout. Thus, the chip thickness is calculated as the chip thickness in a milling cutter with a runout with some modifications [61]. The equation is given:

$$h_{i,j} = R_n - R_m + (n - m) \cdot f_t \sin(\theta_{i,j}) \quad 0 < \theta_{i,j} < \theta_{exit,i,j} \quad (18)$$

where  $h$  is the undeformed chip thickness per grit, with the indices  $i$  and  $j$  mean the  $i$ 'th active grit on the  $j$ 'th element. Indices  $n$  and  $m$  represent the consecutive positions of the active grits along with the circumference of the wheel. Angle  $\theta$  represents immersion angle of the current grit. Also,  $f_t$  indicates the feedrate. In the dynamic model, the calculation of the grinding force is a straightforward multiplication of the calculated undeformed chip area with the cutting force coefficients.

$$F_{n_{i,j}} = K_{nc} \cdot w \cdot h_{i,j} \quad (19)$$

$$F_{t_{i,j}} = K_{tc} \cdot w \cdot h_{i,j} \quad (20)$$

where  $F_n$  and  $F_t$  represent the forces in normal and tangential directions respectively.  $K_{nc}$  and  $K_{tc}$  are the experimentally defined cutting force coefficients in the respective directions. The edge forces are also experimentally identified with linear regression method and added to the overall force values after the cutting forces are calculated.  $w$  is the average width for a grit. The forces are then projected into the machine coordinates. The summation of individual grit and the elemental forces yield to the total forces:

$$\begin{bmatrix} F_x \\ F_y \end{bmatrix} = \sum_{i,j} \left( \begin{bmatrix} -\cos\theta_{i,j} & -\sin\theta_{i,j} \\ \sin\theta_{i,j} & -\cos\theta_{i,j} \end{bmatrix} \times \begin{bmatrix} F_{t_{i,j}} \\ F_{n_{i,j}} \end{bmatrix} \right) \quad (21)$$

Calculating the dynamic undeformed chip thickness is the crucial part when simulating the grinding dynamics in the time domain. Applying milling cutter analogy in grinding allows the use of the dynamic milling equations presented in [3,4]. After the calculation of active grit number per one element of the wheel, the active grits can be assumed to be distributed with their respective pitch angles along the circumference of the wheel. This way the wheel is discretized into thin disk-shaped  $n$  number of milling tools each having different number of teeth. The problem here is that the constructed structure does not have any predefined from. The grit distributions are totally random, and this will create random delays within the elements. For this reason, the regeneration of the

chip thickness is studied element by element as all the elements are treated as a separate disk shape milling tool. The axial discretization is also formulated in [58]; however in the case of a standard milling tool the number of cutting edges and the pitch angle are fixed. The introduction of helix angle can also be coped with analytical relations between the discretized elements along the axis of the tool. But in the case of grinding, the pitch angle will not be a constant number as the cutting edges are placed on any arbitrary positions on the circumference of the wheel. The pitch angles and the number of grits will be different for each element.

In turning operations, the chip thickness is a constant value over the surface. In milling analogy, the chip thickness is an immersion angle dependent value under the circular tooth path assumption. If the tool is subjected to the vibrations in x and y coordinates as a result of the grinding forces, the equation of chip thickness should be modified.

The initial step of these equations to transform the vibrations into machine coordinates to the surface normal (associated with the  $i$ 'th number of grit in the  $j$ 'th number of the element) of the current grits according to the instantaneous immersion angle.

$$n_{i,j} = -x\sin(\theta_{i,j}) - y\cos(\theta_{i,j}) \quad (22)$$

where x and y are the global vibrations of the wheel in the respective directions which affect each element. The instantaneous chip thickness H for tooth i in element j becomes:

$$H_{i,j} = (h_{i,j} + n_{i-1,j} - n_{i,j}) \times g(\theta_{i,j}) \quad (23)$$

where  $n_{i-1,j}$  indicates the vibration of the previous active grit on the same element. The change in the surface normal creates a dynamic chip thickness, thus creating a dynamic force in normal and tangential directions. The projected dynamic forces create the vibrations due to the frequency response functions in which the modal parameters are obtained by hammer tests. The switching function  $g(\theta_{i,j})$  is equal to 1 if the current active grit in the current element is in between its respective start and exit angles:

$$g(\theta_{i,j}) = \begin{cases} 1, & \text{when } \theta_{s_{i,j}} \leq \theta_{i,j} \leq \theta_{e_{i,j}} \\ 0, & \text{when } \theta_{i,j} < \theta_{s_{i,j}}, \theta_{i,j} > \theta_{e_{i,j}} \end{cases} \quad (24)$$

where  $\theta_{s_{i,j}}$  and  $\theta_{e_{i,j}}$  are the start and exit angles of the current active grit of the current element, respectively. The vibration on the surface normal is included in the chip

thickness formula. The chip thickness formula in terms of x and y directions can be calculated as shown in equation (25). The static chip thickness may be removed if the equation is going to be used for calculating the stability only. For the calculation of the dynamic forces and the real values of the vibration amplitudes, the static chip thickness should also be added:

$$H_{i,j} = [R_n - R_m + (n - m) \cdot f_t \sin(\theta_{i,j}) - x_{j-1} \sin(\theta_{i,j}) - y_{j-1} \cos(\theta_{i,j}) - (x_j \sin(\theta_{i,j}) - y_j \cos(\theta_{i,j}))] \times g(\theta_{i,j}) \quad (25)$$

Introducing the conventions;

$$x_j - x_{j-1} = dx \quad \& \quad y_j - y_{j-1} = dy \quad (26)$$

Equation (25) can be rewritten as:

$$H_{i,j} = [R_n - R_m + (n - m) \cdot f_t \sin(\theta_{i,j}) + dx \sin(\theta_{i,j}) + dy \cos(\theta_{i,j})] \times g(\theta_{i,j}) \quad (27)$$

And if the stability will be investigated in equation (27) the static chip thickness can be removed:

$$H_{i,j} = [dx \sin(\theta_{i,j}) + dy \cos(\theta_{i,j})] \times g(\theta_{i,j}) \quad (28)$$

By using the equations (19) and (20) the dynamic forces in the x and y directions can be written as shown in equation (29).

$$\begin{bmatrix} Fx \\ Fy \end{bmatrix} = \sum_{i,j} \left( \begin{bmatrix} -\cos\theta_{i,j} & -\sin\theta_{i,j} \\ \sin\theta_{i,j} & -\cos\theta_{i,j} \end{bmatrix} \times \begin{bmatrix} K_{tc} \cdot w \cdot [dx \sin(\theta_{i,j}) + dy \cos(\theta_{i,j})] \times g(\theta_{i,j}) \\ K_{nc} \cdot w \cdot [dx \sin(\theta_{i,j}) + dy \cos(\theta_{i,j})] \times g(\theta_{i,j}) \end{bmatrix} \right) \quad (29)$$

The total force acting on the wheel disturbs the system though the equations of motions in 2 directions.

$$\begin{bmatrix} Fx \\ Fy \end{bmatrix} = \begin{bmatrix} m_x \ddot{x} + c_x \dot{x} + k_x x \\ m_y \ddot{y} + c_y \dot{y} + k_y y \end{bmatrix} \quad (30)$$

where  $m_x$  and  $m_y$  are the modal mass,  $c_x$  and  $c_y$  are the modal damping and  $k_x$  and  $k_y$  are the modal stiffness of the grinding system in the respective directions of x and y.

## 4.2 Vibration and surface roughness in the cutting direction

The surface roughness of the workpiece holds quite an importance in grinding. The surface roughness in perpendicular to the cutting direction was shown in the previous chapter to be the imprint of the topography of the grinding wheel onto the workpiece. The surface roughness in perpendicular to the cutting direction can be calculated and predicted with a sufficient accuracy by using the geometric-kinematic model. However, the geometric-kinematic model is unsatisfactory for predicting the surface roughness in the cutting direction as the model predict only the feed marks of the active grits on the workpiece surface. The real surface roughness in the cutting direction is shown to be larger and it is the result of the dynamic behavior of the process. The roughness that is created by the vibrations of the grinding wheel is more dominant compared to the other process effects.

In the dynamic model that is proposed in this thesis the vibrations of the grinding wheel in both directions, namely x and y, are considered. The calculated vibrations are stored in an array and then the grit path profiles are printed with the geometric kinematic model, such as shown in Figure 37. The path profiles are updated in each step.

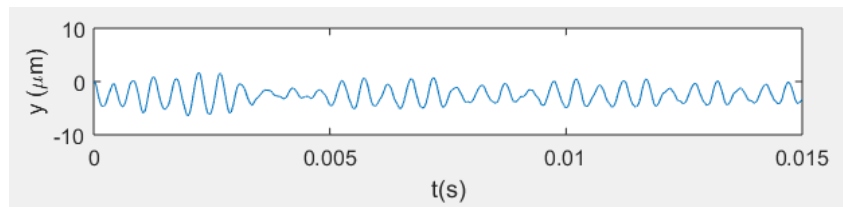


Figure 37: Y path profile

The surface roughness of the workpiece is calculated using the stored position values in the model. The average roughness value  $R_a$  is calculated as shown in equation (31)

$$R_a = \frac{1}{n} \sum_{i=1}^n |y_i| \quad (31)$$

where n is the number of samples and y is the displacement values of the tool from the surface of the workpiece.

### 4.3 Time domain Simulation

In the time domain simulation of the grinding process, the time is discretized into a small number of steps determined with the consideration of the interested frequencies. The time step should yield enough frequency content for the natural frequency of the tool. Each step number  $k$  represents an angular step  $d\theta$  and a time step  $dt$ . The angular position of the wheel can be found as follows,

$$\theta_w = k \times d\theta \quad (32)$$

The instantaneous angular immersion angles of the active grits per each element can be found by angular incrementation of each grit considering the angular position of the wheel and the pitch angle corresponding to the current element. The algorithm consists of three loops in sequence  $k$ ,  $j$  and  $i$  namely the loops for angular increment, elemental increment, and the grit number increment respectively.

In the grit loop, the kinematic-geometric model is applied. All grits along the current element's circumference are spanned. With the trajectory and the intersection calculation, the active grit number is identified, and thus the pitch angles are found. The forces are calculated with the beforementioned formulae (considering the undeformed chip thickness and the dynamic chip thickness) at that angular position of the wheel if the corresponding grit is between the corresponding contact angles with the workpiece. The forces are accumulated at the end of this loop. The element loop provides that the calculations are done for each element of the wheel. At the end of the elemental loop, the accumulated forces are summed and transformed into the  $x$  and  $y$  direction vibrations for the specific angular position of the wheel. The outermost loop provides every calculation is repeated for each angular position of the loop.

It is worth to mention that this work's difference from the milling cutter problem is that each element acts as a disk-shaped milling tool with a different number of teeth as a result of the stochastic nature of the grinding process. The elements are lumped and the relative vibration between them is neglected. The total forces from each grit from each element are accumulated and then the vibrations are created, affecting each element of the wheel. This allows a continuous and simultaneous calculation of the dynamic grinding.

The overall flowchart for the operation is shown in Figure 38.

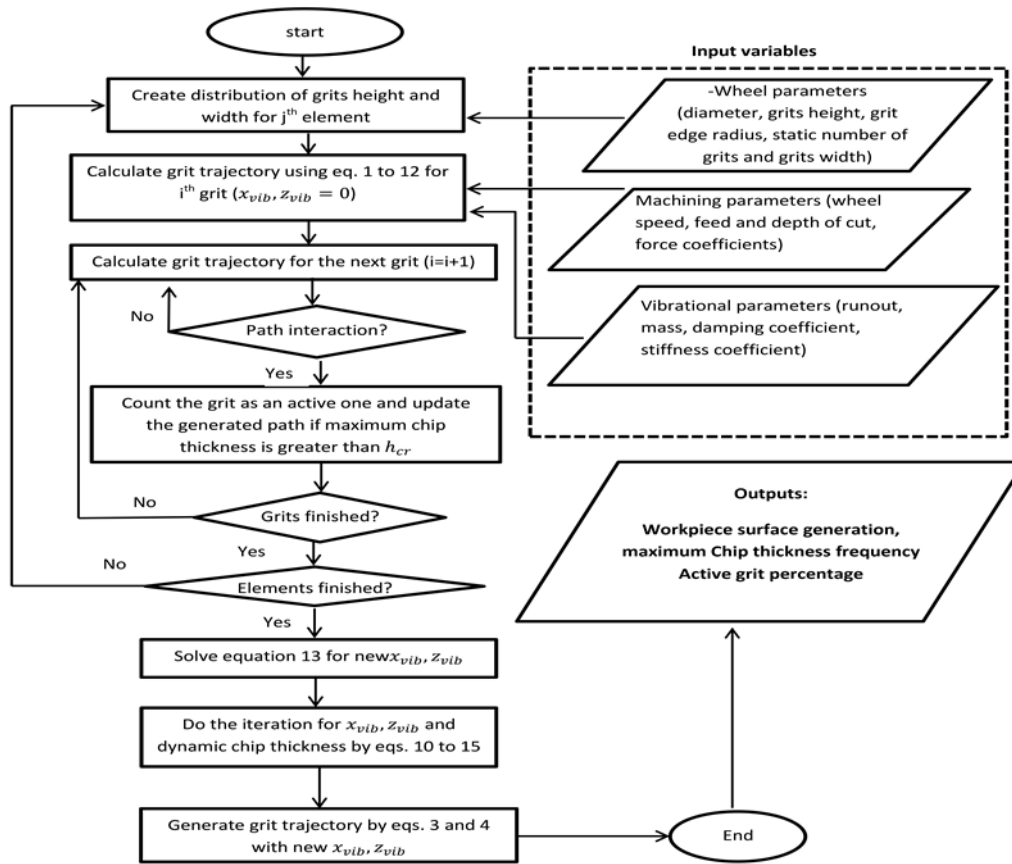


Figure 38: The dynamic grinding flowchart

The governing delayed differential equation of the system is given in block diagram in Figure 39 where  $x$  and  $x(t-\tau)$  are the dynamic and delayed displacements of the tool tip in the  $x$  direction respectively. Similarly,  $y$  and  $y(t-\tau)$  are the dynamic and delayed displacements of the tool tip in the  $z$  direction respectively.  $h$  and delay amount are the instantaneous chip thickness and delay term respectively that is calculated from the kinematic model.  $K_t$  and  $K_n$  are the cutting force coefficients in the tangential and normal directions, respectively. In “thickness to force” block equations 10, 11 and 12 are applied where the forces in  $x$  and  $z$  are obtained. The dynamic model can be used to calculate the stability of the system and it is also used to predict the accurate dynamic force and displacement values in order to predict the surface roughness in the cutting direction. The delayed differential equation is solved through Runge – Kutta method ODE solver provided by Simulink application. The delayed feedback system is developed after the calculated force values are transferred to displacements in  $x$  and  $z$

directions and the delayed displacements are fed back to the block where the force calculations are done.

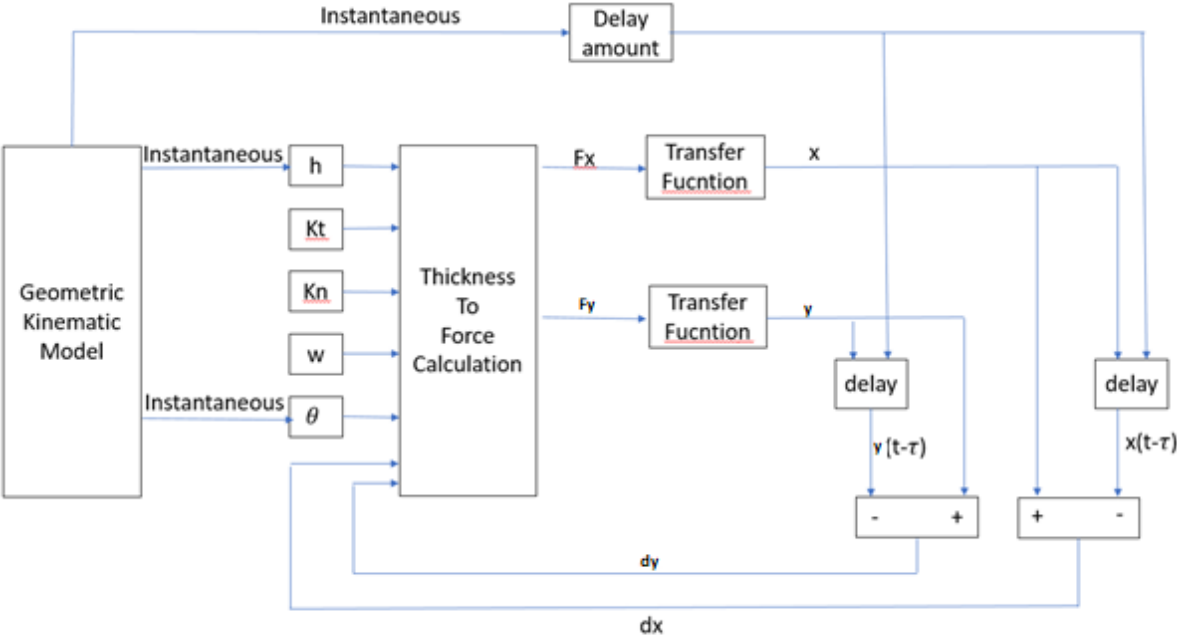


Figure 39: The block diagram

It is necessary to note that within this model two algorithms are running simultaneously. This is a requirement of the stochastic nature of the grinding process as it contains a number of non-linearities that are not in common sense when studying milling and turning problems. The main problem in grinding is that if the geometric-kinematic model is applied and the grinding wheel is discretized into elements, all active grits will be placed on the periphery of the elements in a random fashion. There will be no pre-defined rules to create the wheel after the grits have been measured. This results in random delays for the delayed-differential system.

The way that the random delays are handled is a straightforward method. Remember that initially the wheel element is created with all grits (active or passive) before the active grit calculation as shown in Figure 40. Let us assume that there are n number of grits on the periphery of this element and they all have index values. These elements

will be created with equal spacing and thus will produce a fixed amount of delay if all of the grits are active.

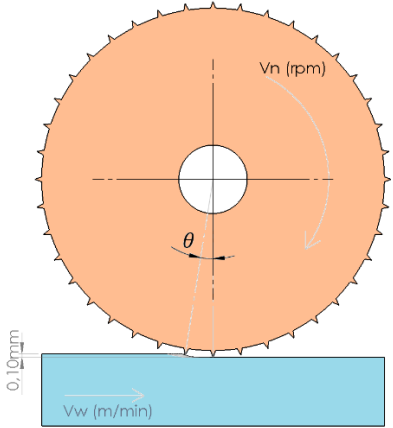


Figure 40: The discretized wheel element

Of course, this is not the case, thus some of the grits will be active as shown in Figure 41. The active grits are shown as bold particles.

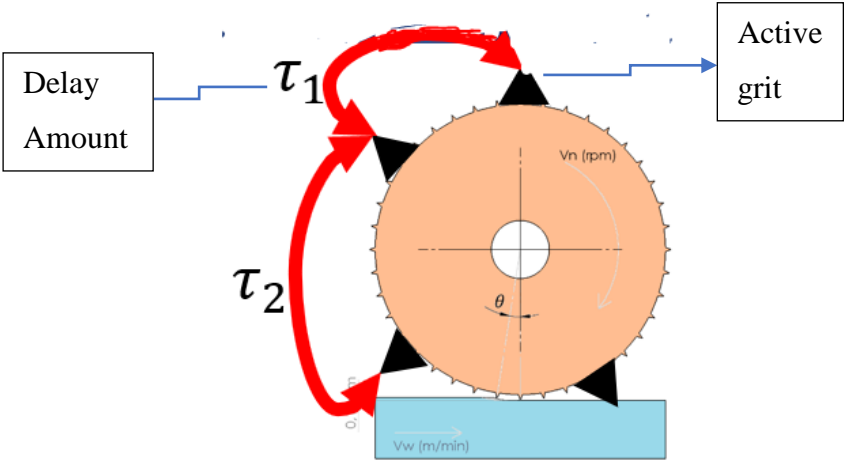


Figure 41: The active grits and delays

The active grits will have their respective index values. For example, let's say that out of n number of grits on the elements, the 1<sup>st</sup>, 50<sup>th</sup> and the 10<sup>0th</sup> grits are active. Then the

delay between the consecutive active grits will have the delay amount calculated for every passive grit, times the number of passive grits that are missed until the next active grit. In our example, the delay between the first and the second active grit will be 49 times the delay amount per all passive grits.

The other non-linearity that is covered in the model is the change of the number of the active grits during the vibration of the grinding tool. In grinding operations, the depths of cut are selected in the range of microns and some cutting edges can easily go out of the cut due the tool vibrations. This phenomenon is handled through a modification in the model. In the dynamics part of the model after a single step is executed, the geometric-kinematic model is run through a shadow (or a copy) of the element. In the shadow element a full rotation is simulated, and the active grits are calculated. This means a full rotation of a shadow element is always executed after each step is calculated. This is shown in Figure 42.

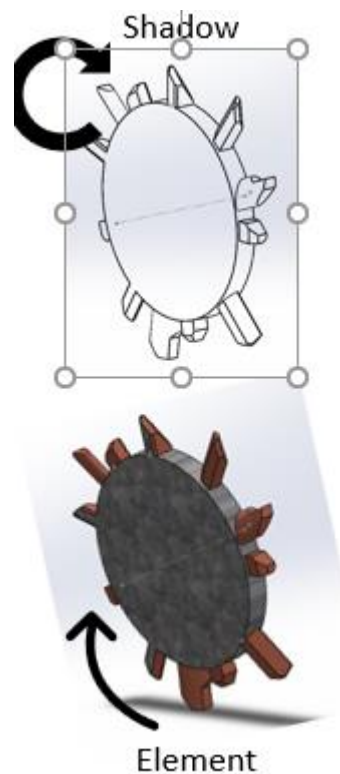


Figure 42: The shadow-element method visualization

#### 4.4 Experimental Procedure

For the proposed dynamic model, the modal parameters of the grinding tools are measured by the hammer tests. The hammer used in the tests is PCB model number 086C01 and the accelerometer is Kistler model number 8728A500. The data is collected through National Instruments USB Carrier model number NI USB-9162. The FRF of the tool and the modal parameters are calculated with the software CutPro. The measurement setup is given in Figure 43. This is Wheel 1 from Figure 16 which is a 10mm EP CBN B126 fresh wheel as shown in Figure 44.

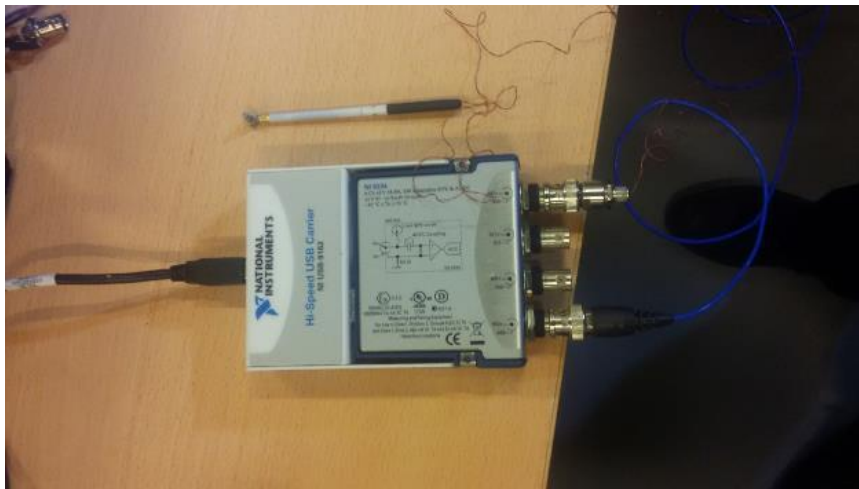


Figure 43: The hammer test setup

The modal parameters for the x and y directions obtained from the program analyzing the information transmitted to the data acquisition board by the accelerometer are given in Table 6.

Direction	Frequency (Hz)	Damping Ratio (%)	Modal Stiffness (N/mm)
X	2100	3,9	3124287
Y	2023	2,3	1326700

Table 6: Modal parameters of the wheel

The main aim of this work is the dynamic force investigation of the CBN wheels on hardened alloys. In this manner, experiments are carried out on the Chevalier Smart H/B 818III CNC surface grinding machine with the combination of Pferd BZY-N 20x10/6 B126 CBN wheel and 7mmx90mm 50HRC hardened AISI1050 carbon steel. Force measurements are gathered via Kistler 9129AA table type 3-axis dynamometer with 5kHz external signal amplifier due to the magnetic chuck limitations. Keyence LK-G5000 series laser displacement sensor has been installed which has 50kHz sampling rate onto the wheel shaft to detect vibration of the tool. A simple microphone is used to measure sound data to detect if there is instability during the grinding process. All devices are connected to Labview program via NI USB-6251 BNC with 50kHz sampling rate for each channel. The experimental setup is illustrated in Figure 44 with the described devices.

In the test matrix, workpiece velocity is scanned from 100mm/min to 20m/min with the consecutive radial depth of cut from 10 to 50 $\mu$ m for constant spindle speed of 40000 rpm. The axial depth is selected as 7mm. In each data set, spark-out operations have been performed to supply a consistency of actual depth of cut. Stability is investigated through different feed rate and depth of cut since higher spindle speed resulted in higher vibration amplitude of the wheel. The grinding wheel is selected as a 20mm diameter electroplated CBN with concentration B126.

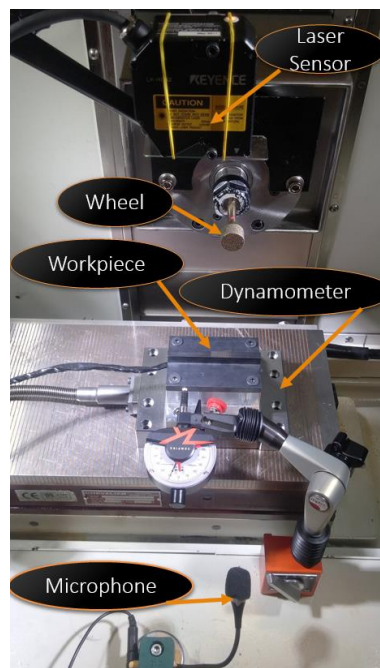


Figure 44: The experiment setup

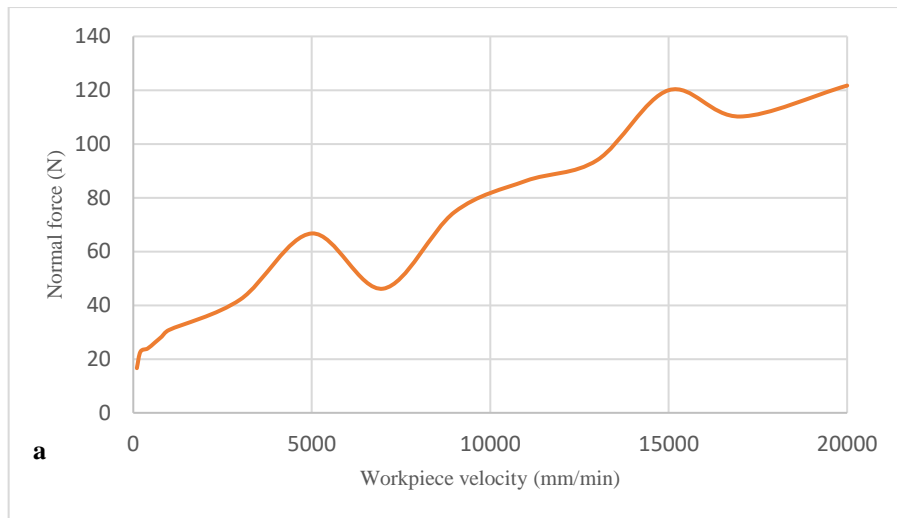


Figure 45: The measured forces of 40µm radial depth for varying feed rate

The measurement of dynamic forces is not feasible with this setup. The dynamic forces detection using the dynamometer may be insufficient as the force measurements will lack the sufficient frequency. The dynamometer used in this research has the natural frequency of 2.3kHz; however, when workpiece is clamped on it due to its mass its bandwidth reduces. The wheel natural frequency is measured to be 2.1kHz.

Another significant note here is that the laser sensor was initially intended to measure the vibrations of the grinding wheel. The laser sensor (Keyence) act as a photoreceptor and measures the distance as of the reflected light from the target. The reflected light's brightness determines the distance to the sensor. For this setup, the orientation of the laser sensor was a significant problem as the wheel arbor is thin and cylindrical which will cause reflection errors to the sensor. Another problem is about the fixture of the laser sensor. A fixture was designed and manufactured for this laser sensor to measure the wheel while the machine is in operation. The operation conditions would easily disturb the sensor orientation just enough to lose the reflection orientation. Hence, the sensor was used only for the detection of the true rpm of the machine.

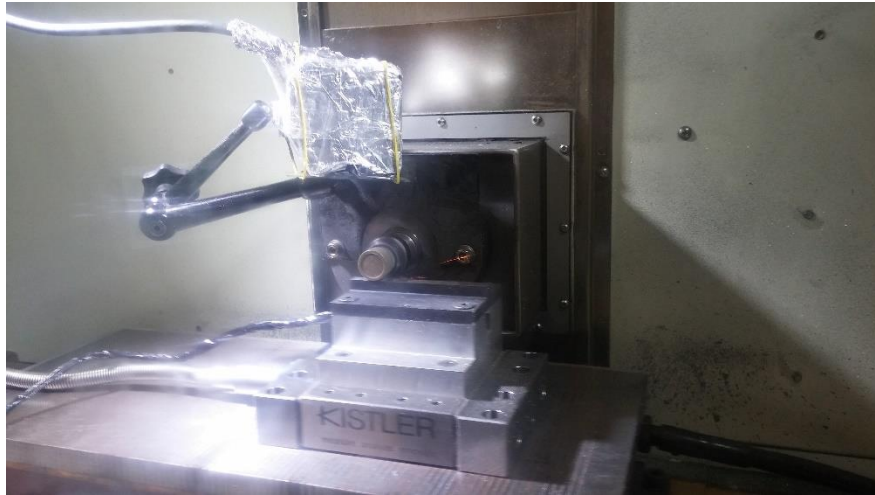


Figure 46: The laser sensor mounting

As these measurement methods could not be utilized, an indirect method to verify the dynamic force model is established.

The measured force in the test is given in Figure 45. The increase in the force in the normal direction along with the increasing feed rate almost follows a linear pattern. It is observed that trend is broken at the feed rates of 5000 and 15000mm/min. The measurements were repeated several times and the same profile is measured. This force profile is a result of the stochastic nature of the grinding process. It is known from the geometric-kinematic model that, as the feed rate increases so does the number of active grits. The increased number of active grits together with the decrease of the cutting force coefficients may have an effect on the dynamics of the system. This phenomenon is further investigated in the results section of this chapter.

#### **4.5 Dynamic Force Results**

It is assumed that there are no wheel vibrations in the geometric-kinematic model mentioned in the previous chapter. This is not very accurate because, unlike other cutting operations, low radial depths are used for surface grinding and the effect of the vibrations on the process variables will be significant. For example, a 10-micron deflection in a conventional milling operation may not significantly affect the process

result, but in an abrasive process it can make the wheel come out of the contact with the workpiece.

As described in the previous chapters, the dynamic grinding formulation was developed using the milling analogy. The dynamic chip thickness is calculated by using particle orientations, and thus the dynamic forces are obtained. The modal parameters found for the small CBN wheel (B126 20mm) are used in the time domain simulations.

An output of the dynamic model is presented in Figure 47.

In the dynamic force model, the mechanistic force model is used, and the force coefficients are identified using the maximum force output obtained from the dynamometers.

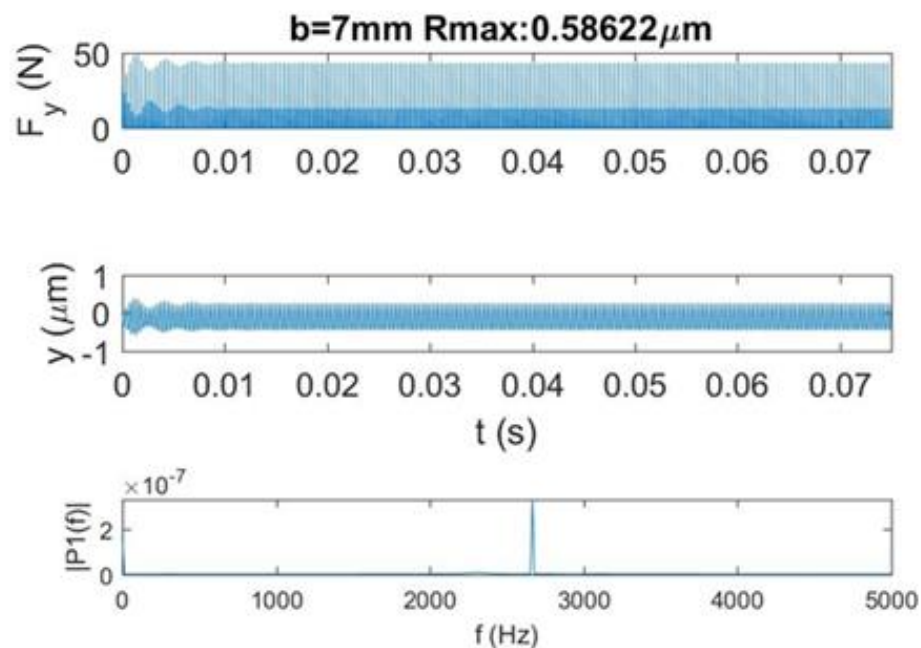


Figure 47: Dynamic forces and vibrations, 40000rpm, 0.125 mm/rev, 40 $\mu\text{m}$  radial depth  
(a) forces (b) vibration (c) vibration frequency

The process parameters given in Figure 47 are:

Rpm: 40000 / min

Feed: 0.125 mm / rev

Radial depth: 40  $\mu\text{m}$

Axial depth: 7mm

In the figure, dynamic cutting forces in the y direction and Fourier transformation spectrum of the y direction vibration are given, respectively.

The forces are obtained after the cutting coefficients are determined. When the active grit detection algorithm is used, the number of particles falling on an element is 8, depending on the process parameters given in Figure 47. Therefore, the feed per tooth is approximately 0.015 mm. Please consider that the tooth number 8 is only for one element. Considering the diameter of the tool (20mm) and the axial depth of cut (7mm) the element number is nearly 150. So, on the contact surface, the number of active grits are nearly 1200. A closer look to the force predictions are given in Figure 48.

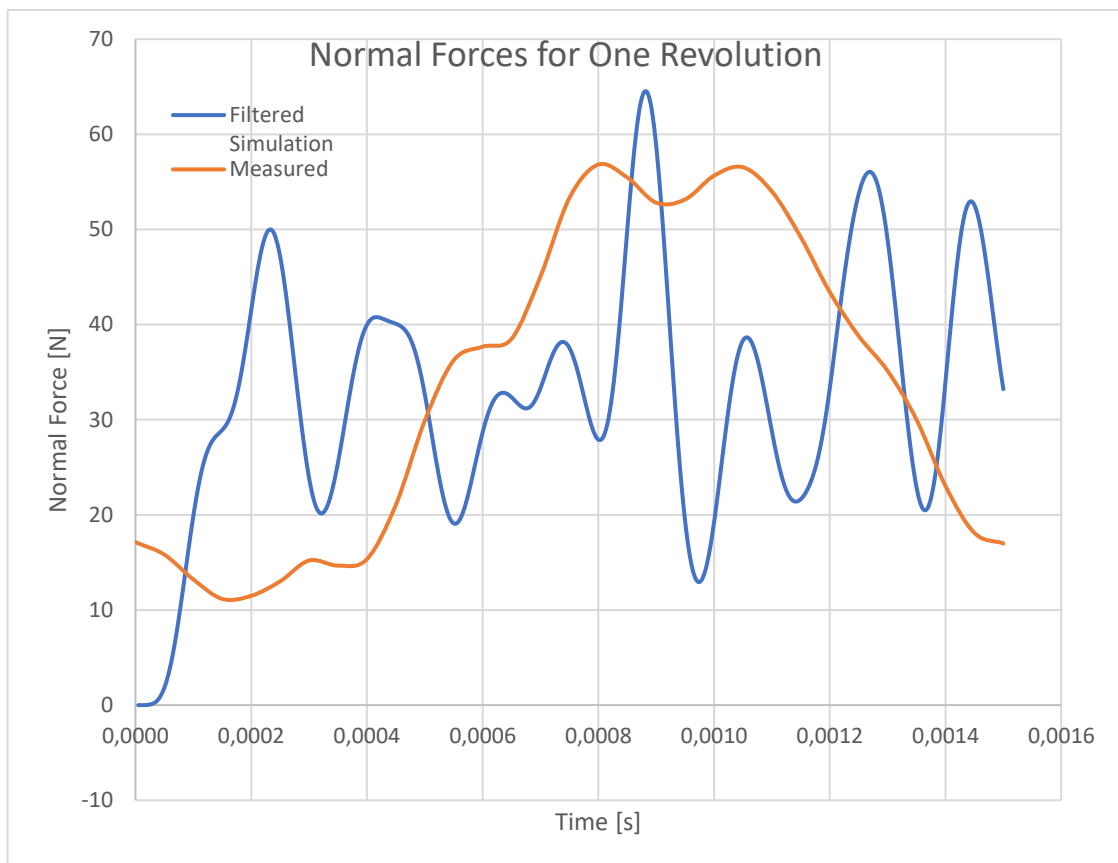


Figure 48: Comparison of the experimental force data. Wheel speed 40m/s, radial depth of cut 40 $\mu\text{m}$ , table speed: 5000mm/min

The maximum and minimum values of both simulated and measured forces are in a good order. There is no significant change in the average values of the simulated force. So, the max., min. and the average force values can be predicted. The differences at the peak points is due to the insufficiency of the dynamometer for catching the high frequency output.

The observation about the discrepancy of the linear increasing trend during the experiments was studied with the dynamic model. The comparisons of the measured and predicted force values for both models (geometric-kinematic and dynamic) are given in Figure 49 and Figure 50. The geometric kinematic model behaves as predicted such as in the previous chapter but has lower performance predicting the force at feedrates of 5000 and 15000 mm/min. The model cannot predict the unusual increase in the force at those feedrates. However, the dynamic model is able to predict the forces at feedrates of 5000 and 15000 mm/min with higher accuracy as can be seen in Figure 49 and Figure 50.

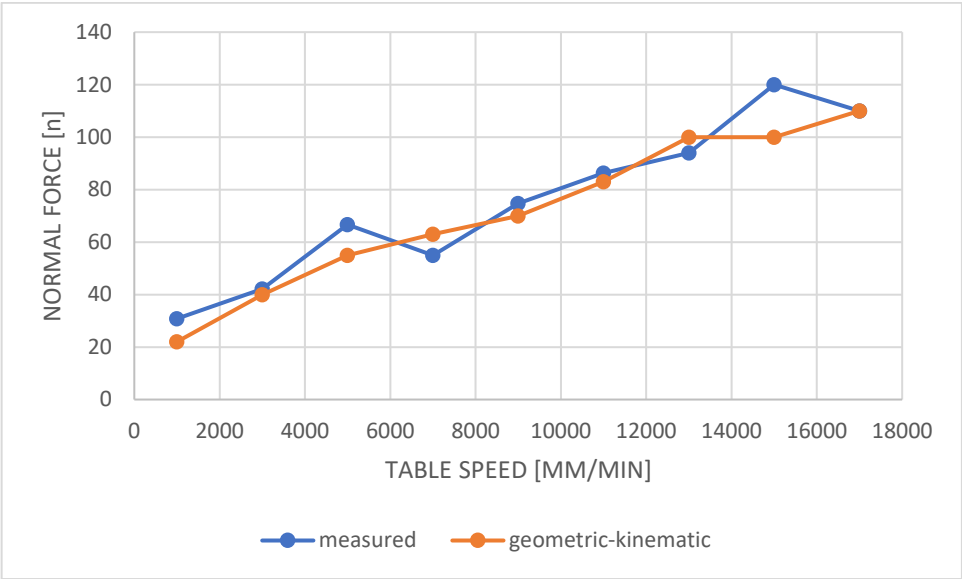


Figure 49: Comparison of measured and predicted force (Geometric-kinematic model) data for varying feed rate, wheel speed 40m/s, radial depth of cut 40 $\mu$ m

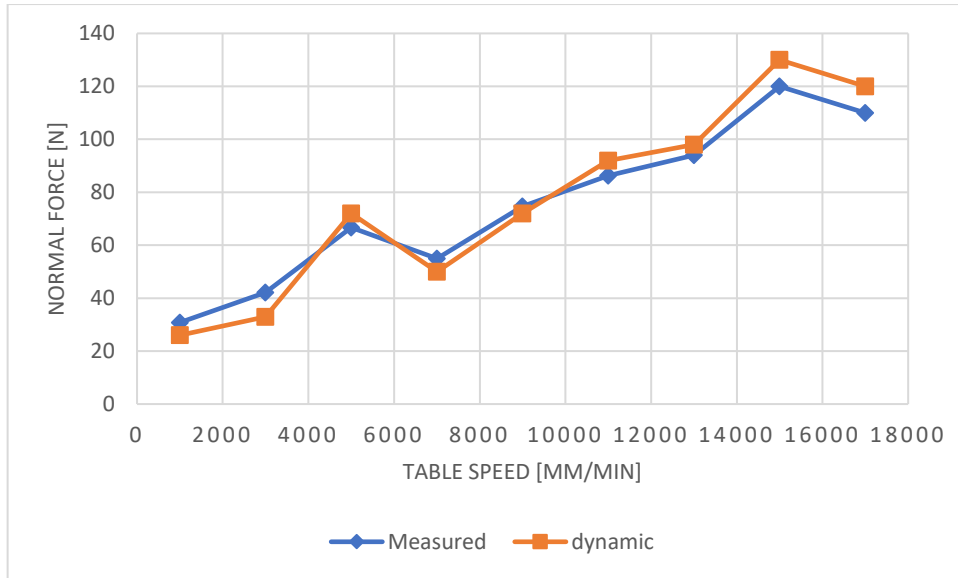


Figure 50: Comparison of measured and predicted force (Dynamic model) data for varying feed rate, wheel speed 40m/s, radial depth of cut 40 $\mu$ m

Three different test cases, simulated above, are considered. The active particle counts are as follows.

Test 1: Feed 3000 mm / min, number of active particles: 6, Kn: 5.4 GPa

Test 2: Feed 5000 mm / min, number of active particles: 8, Kn: 3.5 GPa

Test 3: Feed 7000mm / min, number of active particles: 9, Kn: 3.1 GPa

where Kn is the force coefficient in the normal direction which was determined experimentally.

The frequency of the process forces coming into the system depends on the number of active grits. In grinding, the increase in feed rate affects the number of active grits and the cutting force coefficient itself. It will be seen clearly in the next chapter from the stability charts that the condition of Test 2 is much closer to the stability limit than Test 1 and Test 3. This is the reason for the unusual increased forces at the feed rates of 5000mm/min and 15000mm/min. The dynamic forces are closely investigated at the feed rates of 5000 mm/min and 7000 mm/min and shown in Figure 51 and Figure 52. It is shown that in the case of 5000 mm/min feed rate, the vibration amplitudes are higher and the system is less stable. When the feed rate is increased to 7000mm/min the forces

become more stable. The detailed discussion with stability will be given in the next chapter.

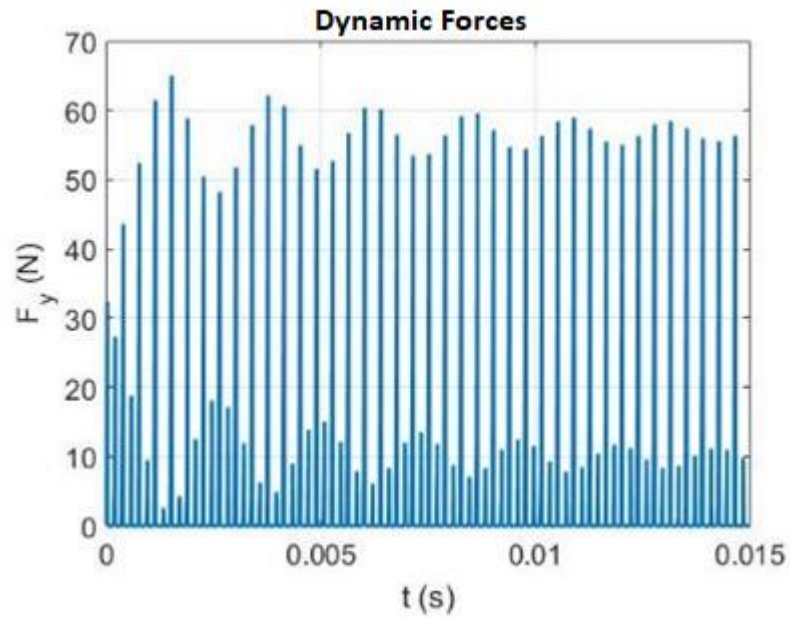


Figure 51: Dynamic forces when feedrate is 5000mm/min

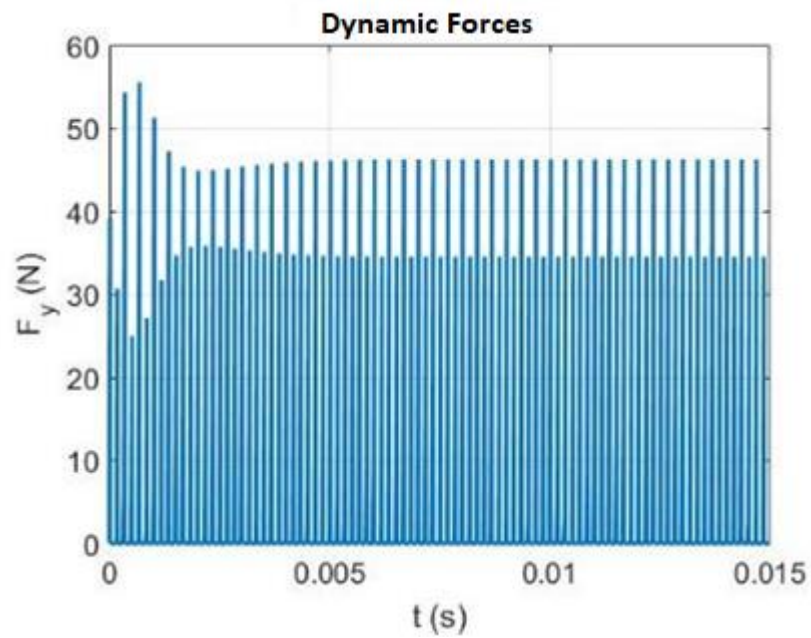


Figure 52: Dynamic forces when feedrate is 7000mm/min

## 4.6 Surface Roughness Results

A series of experiments were conducted to verify the surface roughness prediction with the dynamic model. Thin-walled Inconel 718 (2 mm thick) test piece was selected to minimize the force and wheel vibration. The experiments were planned to eliminate the elastic deflection of the wheel to assure that certain radial depth of cut is removed. Hence, the wheels were mounted with a minimum over-hang to minimize the static deflection. The experimental setup is shown in Figure 53. The surface roughness of the workpiece is measured with the Talysurf surface tracer as well as the 3D  $\mu$ surf Nanofocus microscope. Two wheels were tested: Wheel 1 and Wheel 2 as presented in Figure 8, which are the 10mm EP CBN B126 and B64, respectively. Experiments were carried out at different feed rates: 0.01 mm/rev, 0.03 mm/rev, 0.05 mm/rev and 0.1 mm/rev. The radial depth of cut was 40  $\mu$ m and the wheel speed was 40m/s. The surface roughness results are shown in Figure 54 Figure 54 and Figure 55.

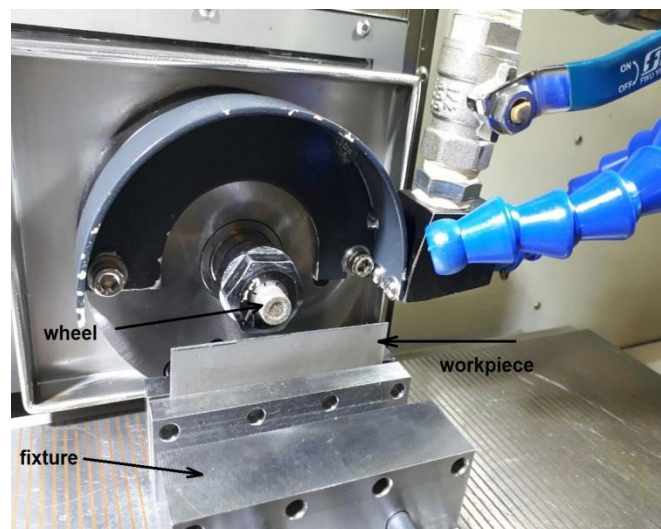


Figure 53: The experimental setup

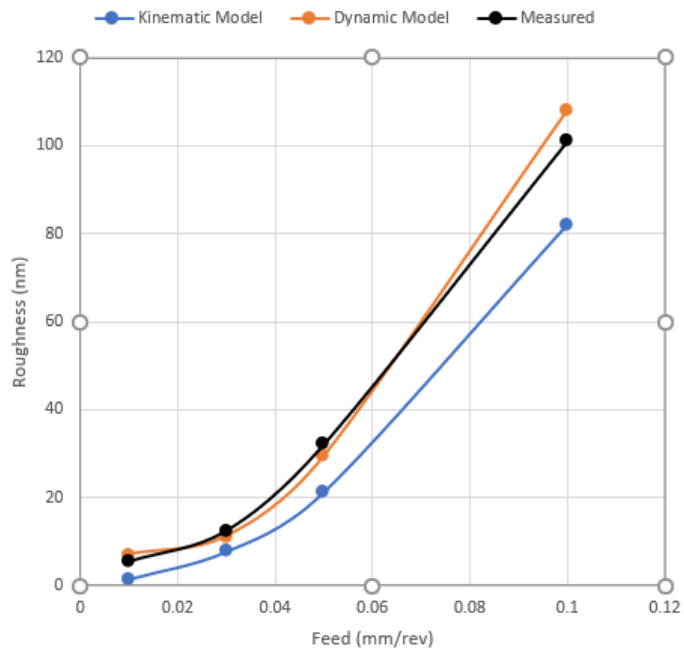


Figure 54: Model and experimental results of the surface roughness for wheel 1 at different feed rates.

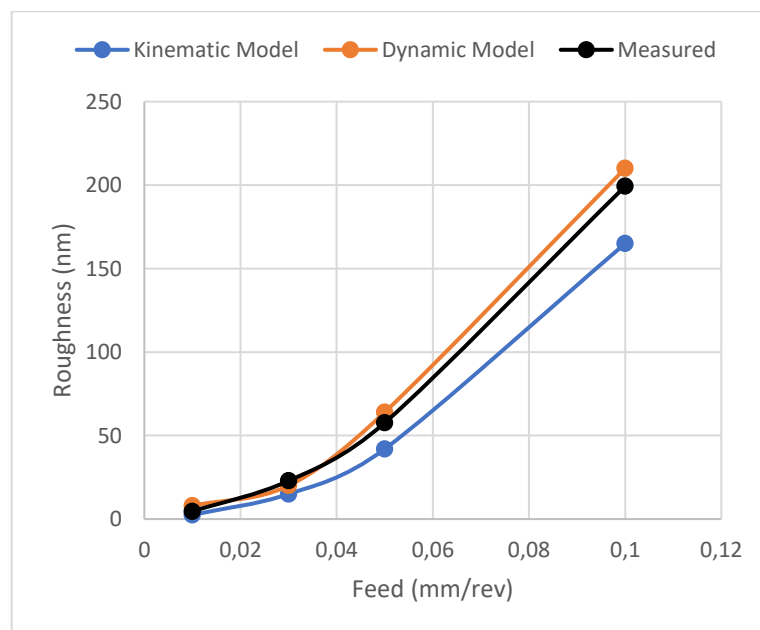


Figure 55: Model and experimental results of the surface roughness for wheel 2 at different feed rates.

As it can be seen from the figures the performance of the geometric – kinematic model on predicting the surface roughness in cutting direction is lower than the proposed dynamic model. The reason for this is the fact that the geometric- kinematic model does not account for the dynamics of the grinding process and represents only the feed marks on the surface of the workpiece whereas the dynamic model is able to predict the vibrations of the grinding wheel and their imprints on the surface. The surface roughness of the workpiece along the feed direction is higher when ground with Wheel 2. There are two reasons for that. The first one is the active grit number on Wheel 2. As shown in Figure 33, the active number of grits is higher on Wheel 2 which will experience higher grinding forces due to ploughing. The resultant dynamic forces may result in higher amount of vibrations which will produce lower surface quality. The other reason is that the modal stiffness of Wheel 2 is lower as compared to Wheel 1. The lower modal stiffness also leads to higher amplitude of vibrations of the grinding wheel.

#### **4.7 Summary**

In this chapter a dynamic force model is developed for surface grinding operations. The dynamic model was needed in order to predict the grinding forces in some cases also to predict the surface roughness in the cutting direction. The geometric-kinematic model had shortcomings to describe the process in terms of the grinding force and the surface roughness in the cutting direction.

Applying the milling analogy and the geometrical random distribution of the grits on the grinding wheel, the simulation can predict the dynamic forces and vibrations. In order to simulate the geometry of the grinding process, the geometric-kinematic model is used and integrated with the dynamic model. The active grits are calculated and the chip thickness per active grit is computed with the trajectory simulation of the wheel. The dynamic model is created with the inclusion of the regenerative effect of the workpiece surface. An algorithm is developed to simultaneously use the dynamic and the geometric-kinematic model in order to represent some of the non-linearities of the grinding process such as the change of active grit number during the wheel vibration and the random delays of the active grits. The dynamic model is used with the time

domain simulations in order to predict forces and the surface roughness is cutting direction. The model and the experiment results show a good correlation and the dynamic model has better performance than that of the geometric-kinematic model.

## 5 CHATTER STABILITY OF ABRASIVE PROCESSES

Generating the final surface and geometry is often critical in grinding operations, as they are after other machining operations. If conventional material removal methods are used, hard to machine materials may cause a higher cost. The low speed cutting will decrease the producibility while the high-speed milling will decrease the tool life dramatically when machining hard-to-cut materials. The super abrasives however, can be used in high-speed machining applications that will result in increased productivity. When high material removal rate is set as a goal, the cutting depths must be increased for high productivity. Elevated cutting depths will play an important role on the stability of the machining process. The stability is very important issue as the surface roughness of the workpiece is crucial on the finishing operations and the vibrations caused by chatter would diminish the surface. When the aim is to increase the productivity, the stability regions must be taken into account.

In literature, the stability of the abrasive processes has mostly been investigated for cylindrical grinding which most likely to face chatter. In cylindrical grinding, the workpiece is usually slender and long and susceptible to vibrations as the rigidity is low. Surface grinding has not been much of focus in the grinding chatter literature as in the surface grinding conditions the workpiece and the tool is usually rigid and high depth of cuts are not required. The most usual abrasive process conditions for the surface grinding is to have low depths of cut, relatively high feed rate and high diameter grinding tools (around 200 mm and higher). However, in the scope of this thesis, the grinding the stability model is developed for small tools (around 10-20 mm) as the measurement of the smaller tools are more useful with the microscope. When mounted on the grinding machine the small tools can be used in high-speed grinding conditions as a sufficient grinding speed is required in abrasive operations.

The time domain dynamic model proposed in the previous chapter is used to determine the stability regions of the abrasive processes which will also be studied with the frequency domain solution as well.

## 5.1 Frequency domain solution

During the studies [1,11,40], the grinding operation was modeled analogous to a micro-milling operation. According to this assumption, each grit on the grinding wheel behaves almost like a micro milling tooth. In this case, to model the dynamic of the grinding wheel, the force coefficients representing the relationship between the forces and the dynamic chip thickness must be determined. The first step is to calculate the dynamic chip thickness and cutting forces. Then an eigenvalue problem of multidimensional dynamic equations will be solved, and the stability limits will be calculated.

The frequency domain solution of the grinding operation is based on the model of multi – teeth milling problem presented in [51,52]. The grinding wheel is modeled as a milling tool with many teeth. In the analytical solution, the wheel is treated as a milling tool with an average active grit number that is distributed over the grinding wheel with average pitch angles. The averaging method is shown to be feasible in [11] as the normal distribution method leads to larger number of values around the mean value. The average pitch angles would also mean that an average delay is performed. The zero-order application may not provide very accurate results as the low radial depth of cut creates impulse-like force which will excite a larger spectrum of frequency and higher frequencies may be included to the solution.

The grinding wheel vibrates under dynamic forces leaves vibration marks on the surface. The abrasive grit that follows it also travels on the wavy surface left by previous grit. If, in any way, the process is evolving to self-oscillating waves, that is, if the amplitude of a current grit's vibration is more than or equal to the amplitude of the previous grit, then this process becomes unstable and chatter occurs. This process is called regeneration. In the developed model [11], the workpiece is assumed to be a rigid and the dynamic characteristics are not considered. By using the zero-order approach, relationship between the spindle speed and the limiting depth of cut for the instability can be calculated using the analytical equations below [51,52].

$$a_{lim} = \frac{2\pi \times A_R}{N \times K_t} (1 + \kappa^2) \quad (33)$$

$$\kappa = \frac{A_{Im}}{A_{Re}} = \frac{T \times \sin \omega_c}{1 - T \times \cos \omega_c} \quad (34)$$

$$T = \frac{\epsilon + 2k\pi}{\omega_c} \quad (35)$$

$$n = \frac{60}{N \times T} \quad (36)$$

$$\epsilon = \pi - 2\psi \quad (37)$$

$$\psi = \tan^{-1} \kappa \quad (38)$$

In these equations (33-38)  $T$  is the tooth passing period.  $\kappa$  is the ratio of the imaginary and real parts of the dynamic transfer function of the wheel end point.  $N$  is the number of grits,  $Kt$  is the predetermined cutting force coefficient, and  $k$  is the stability lobe number.  $n$  is the spindle speed.

The algorithm that is used for the zero-order application is as follows [51,52]:

- The dominant mode of the system is determined.
- The algorithm starts around a chatter frequency that is close to the dominant mode.
- The limiting depth of cut and the corresponding spindle speed is calculated. This procedure is continued for the consecutive lobe numbers ( $k=1, 2, 3, \dots$ )
- The frequency range of 1.01 times to 1.5 times of the natural frequency of the wheel is spanned and the stability lobes are created.

The frequency response model is adopted and presented along with the time domain solution. The algorithm is provided with this thesis but the theory and the detailed calculation of the zero-order application and the Fourier series approach to the frequency domain solution to the chatter problem is provided in [51,52].

## 5.2 Time domain solution

For the stability limit calculation, the time domain solution that is provided in the previous chapter is used. The chatter can be predicted by the observation of the growing vibrations of the tool from the vibration outputs and the frequency spectrum of those vibrations. If the vibrations are in a growing manner and the frequency of the vibrations are at the chatter frequency (slightly higher than the natural frequency), the process is

identified as chatter. This may be a tiresome approach, but the dynamic model proposed in this thesis can handle some nonlinearities that will enhance the prediction. The dynamic model is run for different cases and the stability regions are determined. The method is described with sample outputs.

Figure 56 shows an example of an output.

The modal parameters identified for the small CBN wheel (B126 20mm) are used in the algorithm (given in Table 6).

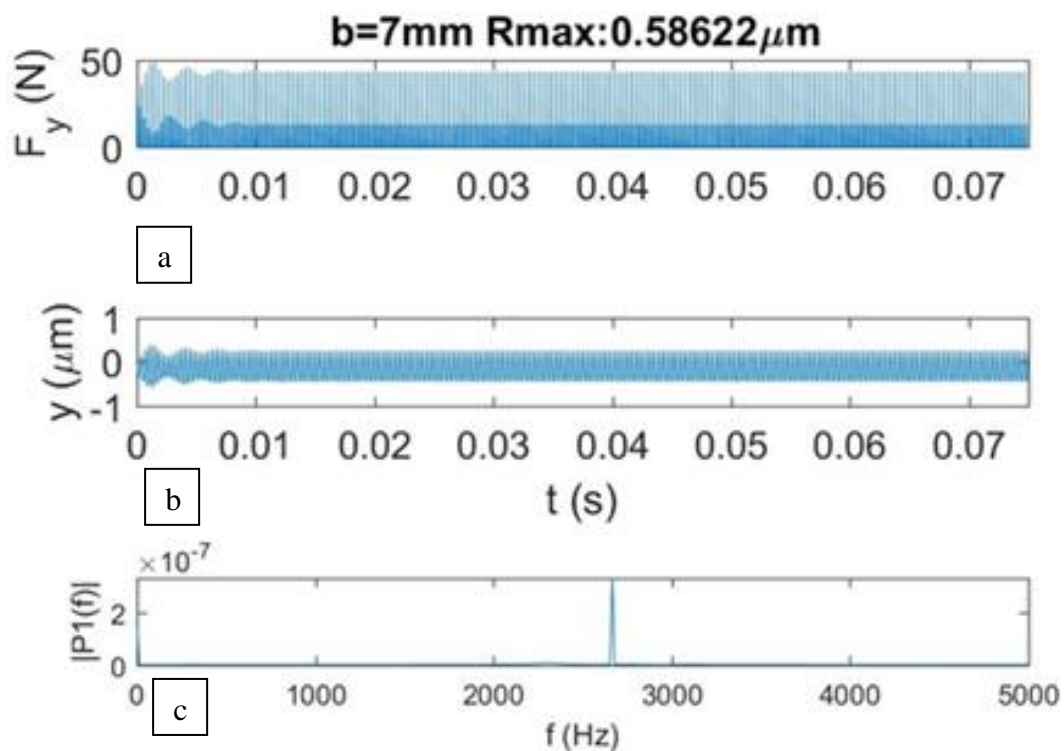


Figure 56: A sample dynamic grinding output (a) force (b) tool tip vibration (c) vibration spectrum

The process parameters given in Figure 56 are:

Rpm: 40000 / min

Feed: 0.125 mm / rev

Radial depth: 40 μm

Axial depth: 7mm

In Figure 56, dynamic cutting forces in the y direction and Fourier transformation spectrum of the y direction vibration and tool tip vibration are given, R max shows the maximum roughness in order to indicate the vibration amplitude.

In time domain simulations, the axial depth is scanned in a range of 0 to 20 mm with 0.1 mm steps. Then for all spindle speeds between 30000 and 40000rpm, (with an increasing step of a thousand rpm) the different axial depths are scanned. When the chatter is observed the current values are captured and noted.

Figure 57 shows example of time simulation output for 40000 cycles of stable grinding at a speed of 5000 mm / min.

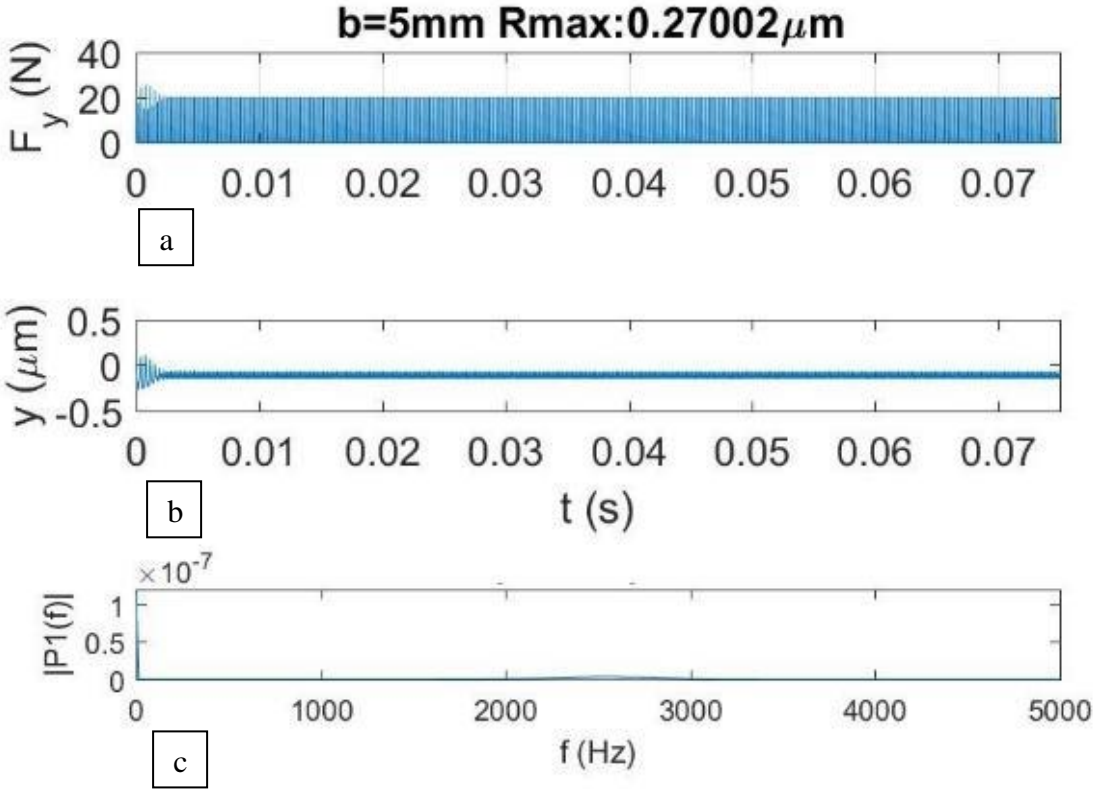


Figure 57: 40000 rpm, 5 mm depth, 5000 mm feed (a) force (b) tool tip vibration (c) vibration spectrum

Figure 57 shows a stable grinding example. For these conditions 5mm depth is stable. Vibrations and dynamic forces continue to diminish whereas there is no distinct vibration frequency in the spectrum.

No instability was seen when the depth was increased to 7 mm (Figure 58). When the vibrations were somewhat in the initial stage, they damped off later and settled on a stable profile. The frequency of the vibration is 2600 Hz. It is a harmonic of the spindle speed. (spindle speed 40000 rpm = 666 Hz).

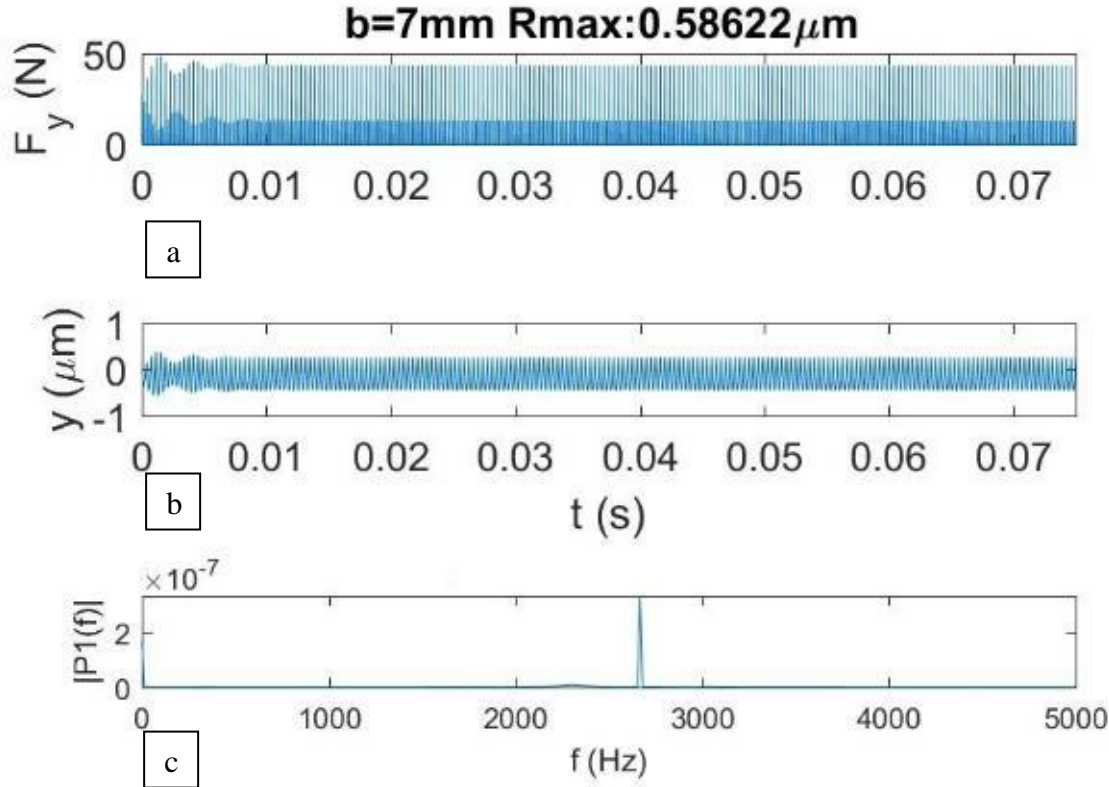


Figure 58: 40000 rpm, 7 mm depth, 5000 mm feed (a) force (b) tool tip vibration (c) vibration frequency

A marginally stable process is illustrated in Figure 59. The axial depth is increased to 7.7 mm. The frequency graph shows a small peak at 2300 Hz showing the sign of chatter. It is related to the natural frequency of the system (the measurements show there is one mode). The vibrations are settled a little bit later comparing to the previous case.

Figure 60 shows a time domain simulation of an unstable process where the axial depth is at 10mm. As can be seen, the dynamic forces and vibrations are in a state of great oscillation. The difference between the peak and the average forces and tool tip

vibrations increased dramatically. The frequency of the vibration was found to be 2300 Hz, that is, the frequency of the chatter.

This procedure is repeated for the remaining spindle speeds and the stability limit corresponding to each spindle speed is found. By combining these limits, a stability diagram is obtained.

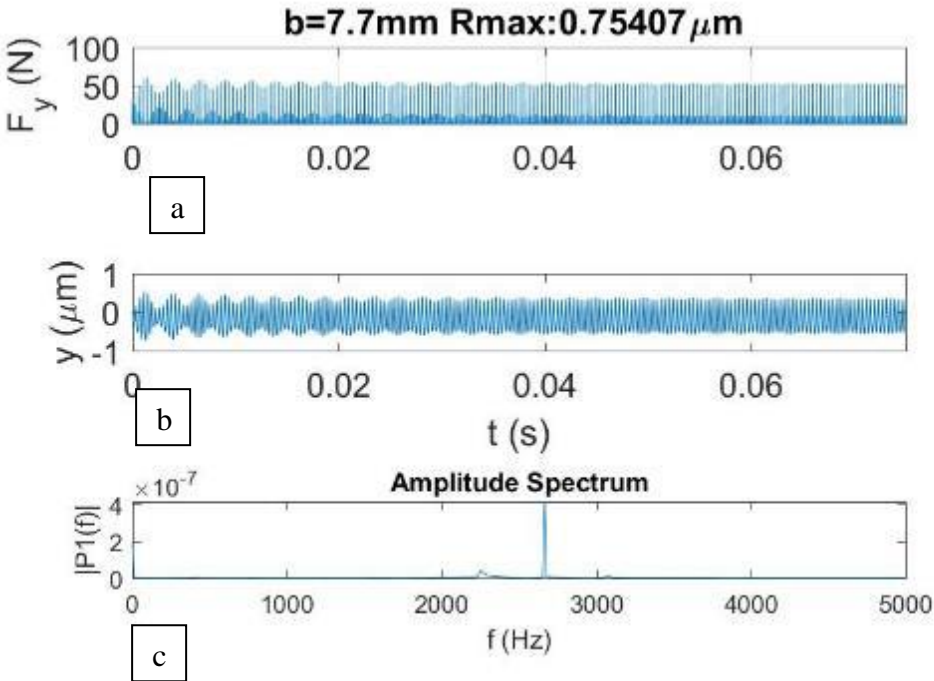


Figure 59: 40000 rpm, 7.7 mm depth, 5000 mm feed (a) force (b) tool tip vibration (c) vibration spectrum.

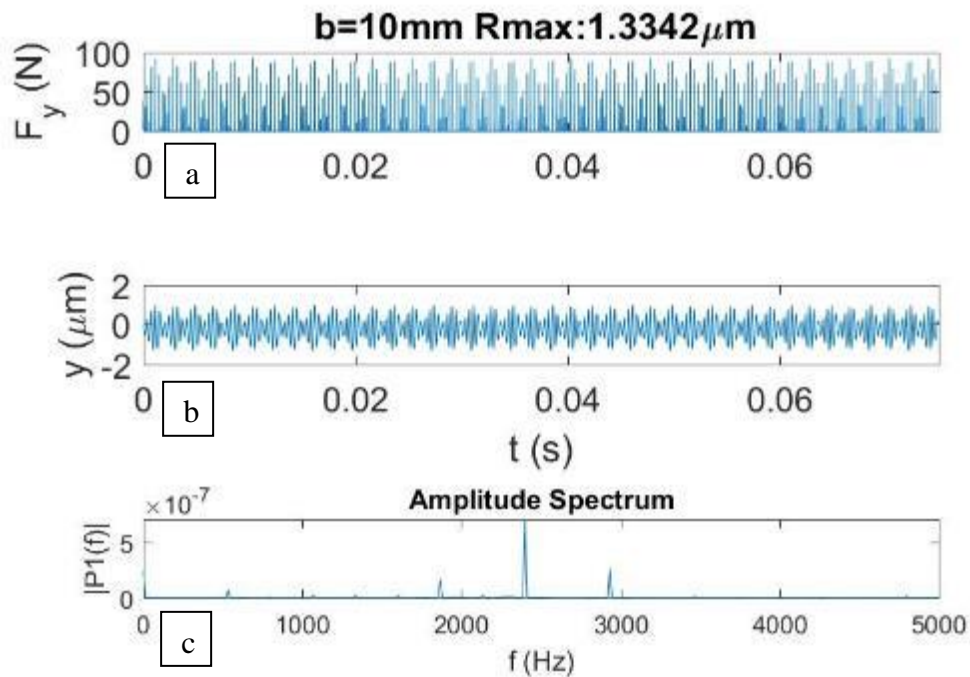


Figure 60: 40000 rpm, 10 mm depth, 5000 mm feed (a) force (b) tool tip vibration (c) vibration spectrum.

There are a few things to be careful about when determining if the process is unstable. To understand that a process is stable or unstable, the simulations should be taken at specific depths and the vibrations should be visually inspected. The distinction between stable and unstable vibrations must be detected with naked eye. The implications of the chatter reside in the repetition of the vibration “pulses” in the state of unstable case where the frequency spectrum also provides the clue. In this point an algorithm can be developed to detect the chatter automatically as the chatter occurs at most times in shapes of pulses but the pattern of the pulses may change from case to case. Therefore, a more “brute force” method is applied here. The simulations presented above cover the time including 50 rotational cycles of the grinding wheel. To be examined more closely, the following figures can be obtained in 5-cycle simulations. Figure 61 shows a stable grinding simulation at 40 000 rpm and axial depth of 5mm.

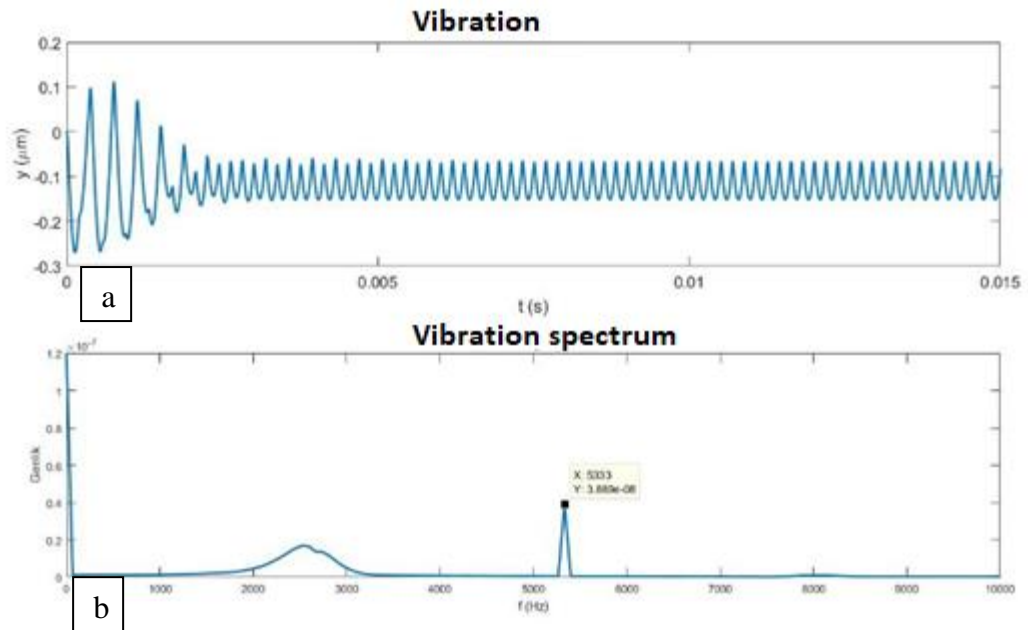


Figure 61: 40000 rpm, 5 mm depth, 5000 mm feed (a) tool tip vibration (b) vibration spectrum

Since the radial depths of cut for the grinding operations are comparably lower than other machining operations (40 microns in the example), two things come into importance. The first is the contact and the contact length of the workpiece is minimal. Therefore, the contact of the abrasive particles with the workpiece won't be a long lasting one, resulting in discrete forces rather than continuous ones. The dynamic forces are shown in Figure 62. The natural frequency of the wheel is also excited as the forces are in the form of impulses. Thus, when the grinding process is started, in the first few cycles, the wheel vibrates at higher amplitude, but then these vibrations are damped and remain under forced vibrations in a stable fashion. The frequency of the forced vibrations is the spindle speed frequency, which corresponds to 5333 Hz (666Hz spindle speed x 8 active grits).

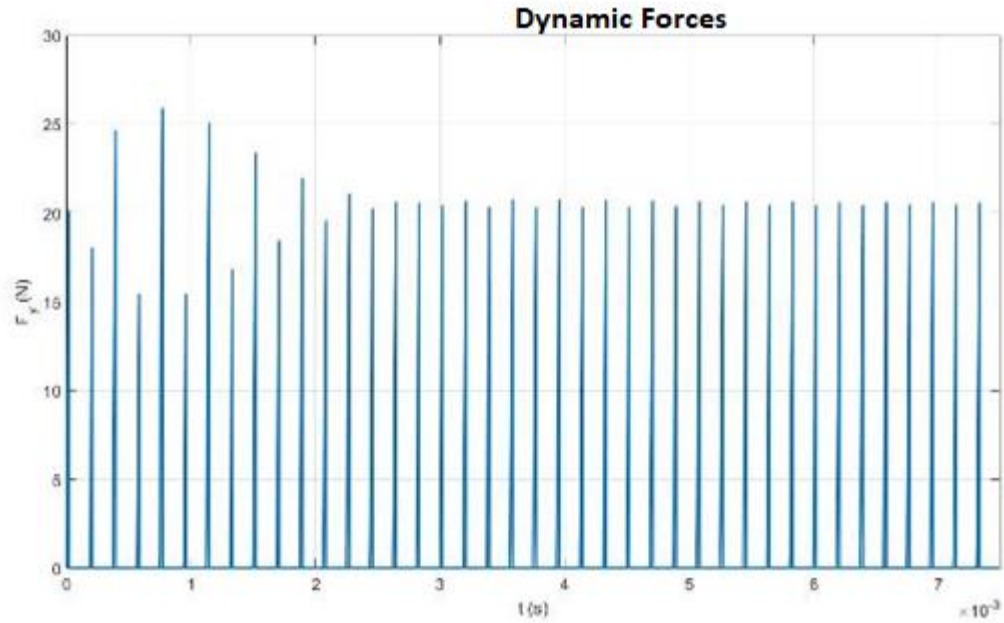


Figure 62: Stable dynamic forces, depth: 5mm, speed: 40000 rpm

The second problem caused by the low radial depth of cut in grinding is that the uncut chip thickness is very low (this can be observed by the forces that are shown in Figure 62). The process is sensitive to vibrations precisely because the difference between start angle of the grit and the exit angle of the grit is very small (can be approximated around 5 degrees). The slightest vibration can interrupt the contact of the grit with the workpiece due to the low depth, and momentarily the force is reduced to zero. Such non-linear properties are reflected in the solution of the system.

An unstable process vibration is given below (Figure 63 and Figure 64). If the spindle speed is set to 35000 rpm in the given condition, the system becomes unstable (Where the depth is 5mm and spindle speed is 35000rpm). First, a great increase in vibration amplitude is observed. This increase is much more than the average amplitude of the forces comparing to the stable case. The pulse-like pattern can be seen. The frequency of these oscillations coincides with the frequency of chatter (2333 Hz) which should locate around the natural frequency.

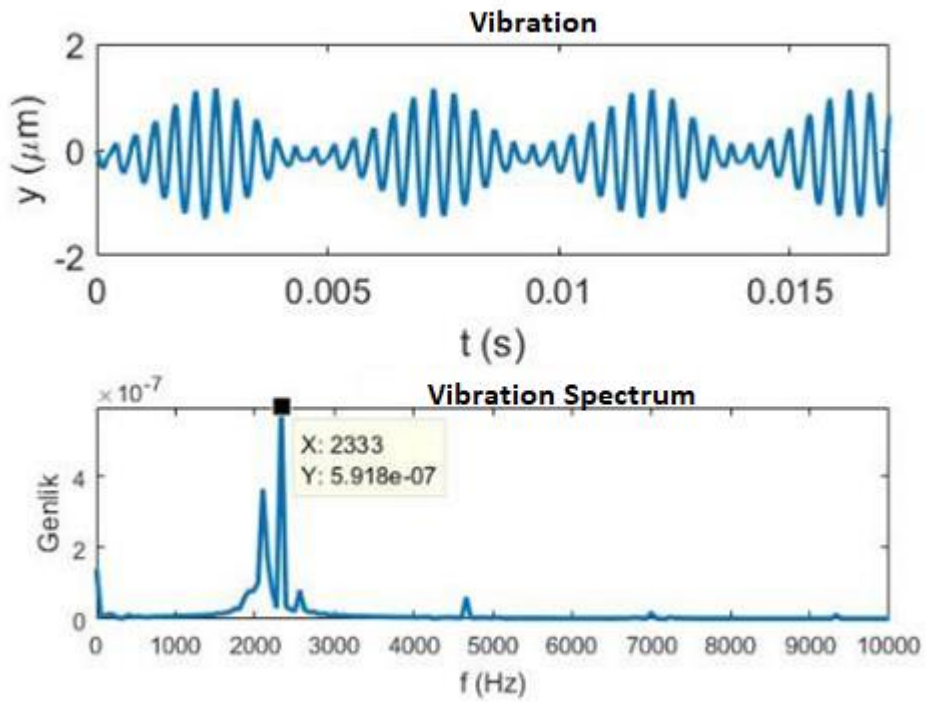


Figure 63: Unstable grinding. Depth: 5mm, Spindle speed: 35000rpm (a) tool tip vibration (b) vibration spectrum

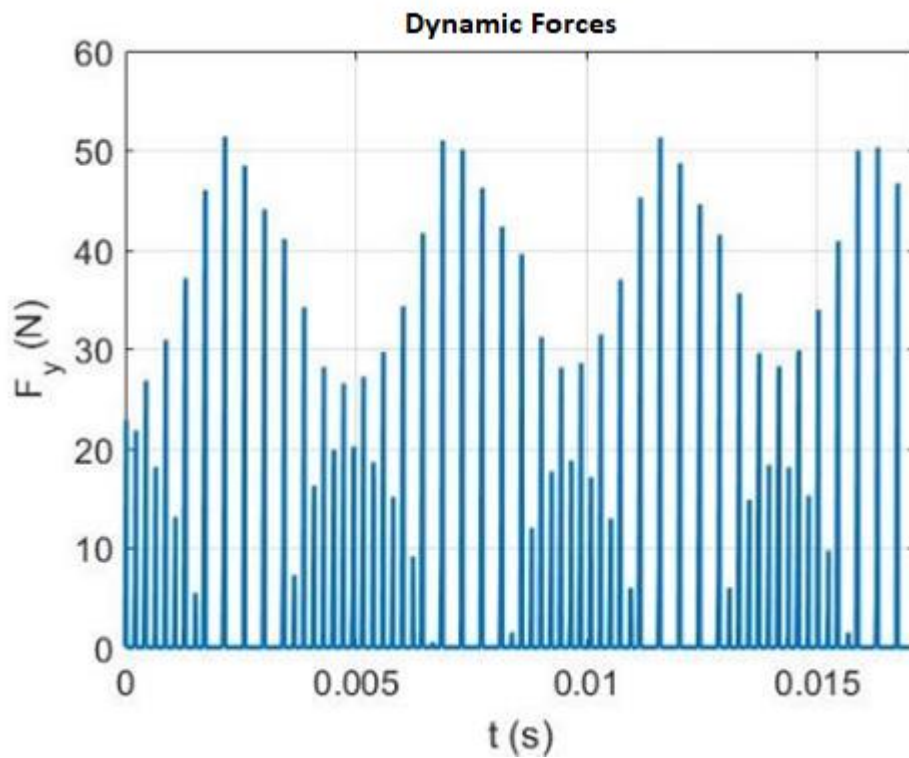


Figure 64: Unstable grinding forces. Depth: 5mm. Spindle Speed: 35000 rpm.

### 5.3 Stability diagrams

The stability charts are obtained from the time domain model simulations. A series of simulations are conducted in order to identify the limits of chatter. A sample stability chart is given in Figure 65.

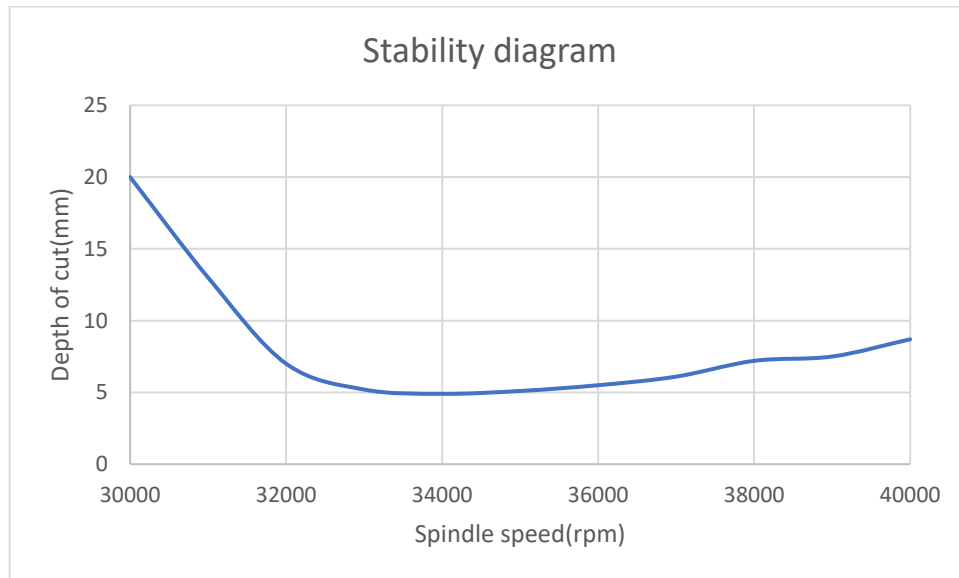


Figure 65: Stability diagram for 5000mm/min feed rate

In Figure 65, the given stability graph is for the small CBN wheel (B126 20mm), radial depth of 40  $\mu\text{m}$  and feed rate of 5000 mm/min. The average active grit number residing in one element is 8 in this example. The area above the curve is the unstable region and the area under the curve is stable region. The stability graph resembles the ones for milling operations. The range for spindle speed is selected to be between 30000 and 40000 rpm as this range is the reasonable speed for grinding for this machine and tools setup in this research.

The stability diagrams do not usually change with feed rate for turning and milling operations. But in grinding operations, the stability diagrams alter because with a change in the feed rate, the active number of grits per element changes which affects cutting coefficients as well. The diagrams for different feed rates is given in Figure 66.

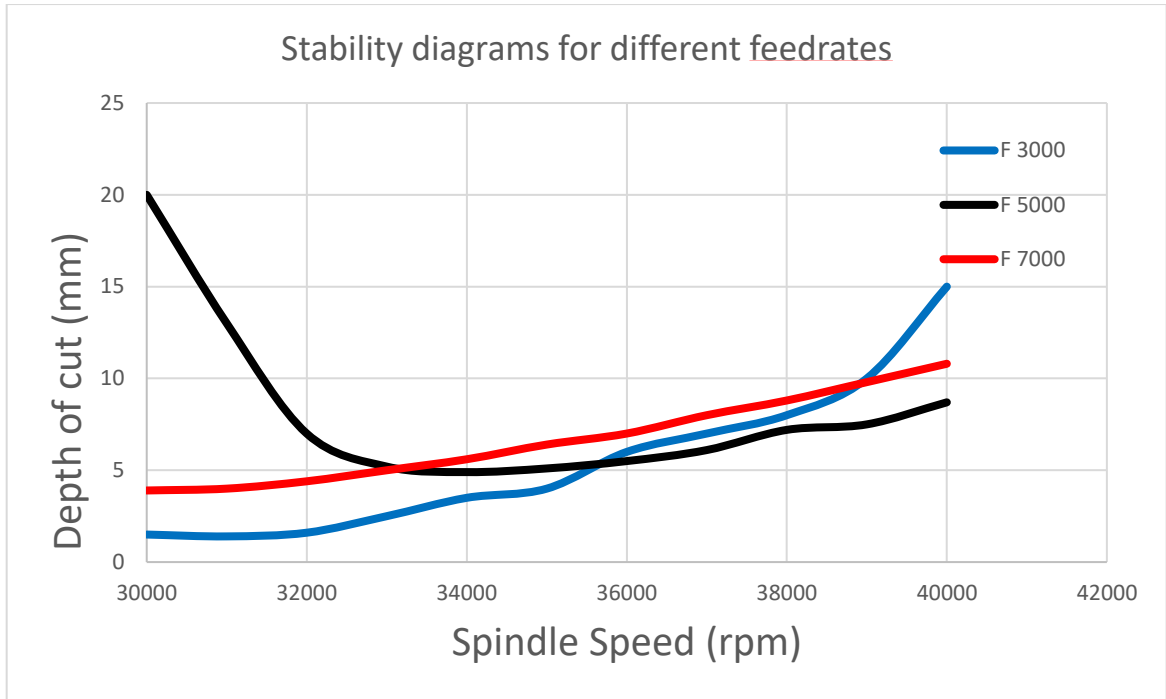


Figure 66: Stability diagrams for different feedrates

As seen from Figure 66, the stability diagrams with the CBN 20mm wheel and for the radial depth of 40  $\mu\text{m}$ , could have a different profile for feed rates of 3000, 5000 and 7000 mm/ min. The respective cutting coefficients per grit and the active grit number per single element are given in Table 7. The feed rate has an indirect effect on the process stability as it can inherently change the cutting force coefficients and the number of active grits. The table shows that the increase in feed rate has an effect on increase in the active grit number. The force coefficients have respective decreases.

Feed rate (mm/min)	Cutting Coefficient (GPa)	Active grit number per element
3000	5.4	6
5000	3.5	8
7000	3.1	9

Table 7: Process parameters for different feed rate conditions

The feed rates are chosen because of the non-linear increase in the force observed during some experiments explained in the previous chapter (Section 4.4 and Figure 45). The measured force at feed 5000 mm/min has a larger value than that of the feed rates of 3000 mm/min and 7000 mm/min. Further in the chapter, the dynamic forces of feed rates of 5000mm/min and 7000 mm/min are also compared, and it is shown that the cutting condition at the feed 5000 mm/min has a marginally stable profile( Figure 51). The results obtained in the previous chapter are compatible with the stability diagrams in Figure 66. The experiments are done with the same tool and the same radial depth, at 40000 rpm. The instability is easier to see with 5000 mm/min feed case comparing to the other feed rates at the spindle speed of 40000rpm. The limits of stability are around 7, 11 and 15 millimeters for the feed rates of 5000, 7000 and 3000 mm/min respectively. This is explained by why different force profiles are seen in these feed rates. The case with 5000mm/min in section 4.4 was marginally stable with 7mm depth of cut both for dynamic force simulations and experiments and this is also predicted with the stability graph given in Figure 66. Further investigation will be presented in the experimental results.

The effect of C numbers on different tools have also great impact on process parameters as they change the active grit number and cutting force coefficients. Two wheels are compared in terms of C numbers and different feed rates for stability diagrams. The results are given in Figure 67, with respect to the radial depth of cut limit.

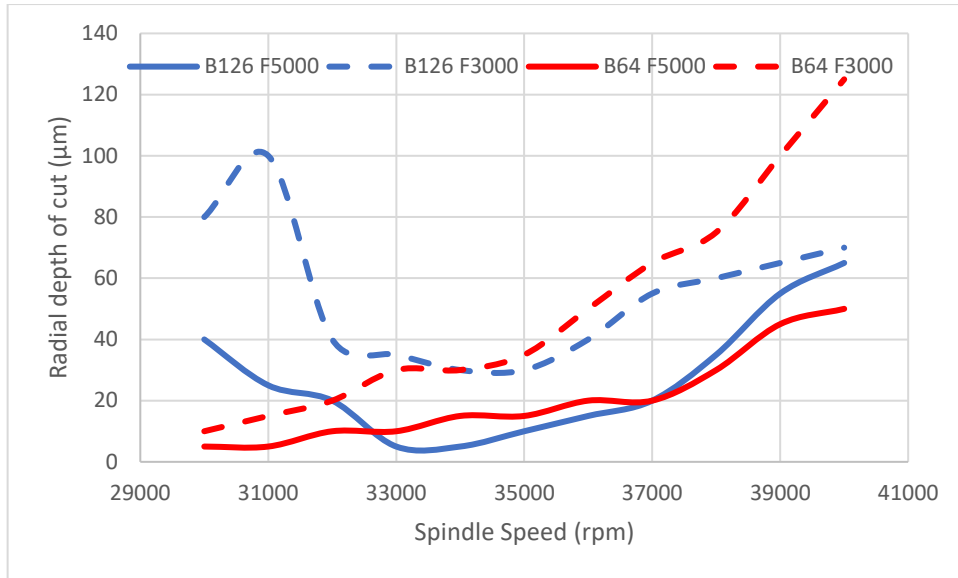


Figure 67: Stability charts with respect to radial depth of cut for different tools and feeds.

Wheel type	Feed rate (mm/min)	Cutting Coefficient (GPa)	Active grit number per element
B126	3000	5.4	6
	5000	3.5	8
B64	3000	5	12
	5000	3.2	15

Table 8: Process parameters for different feed rate and wheel conditions

In Figure 66, the blue curves represent the B126 Electroplated CBN wheel named Wheel 1 in Figure 8 and Table 2. The axial depth of cut is fixed at 7mm. The red curve represents the B64 Electroplated CBN wheel named Wheel 2 in the same figure and the table. As it can be observed, the stability curves differ greatly just like the process parameters could change with the varying grit density (number of abrasive particles and the grinding force coefficients). The feeds of 5000mm/min offer worse stability condition as the limit is lower with the similar case of axial depth of cut limits given in Figure 66. The curves may be advantageous or disadvantageous over each other depending on the selection of the spindle speed. It seems like if the second tool is selected with 3000 mm/min feed and 40000 rpm, the radial depth of cut limit can reach

up to 120  $\mu\text{m}$  which has the highest limit in the graph. Whereas if the spindle speed is chosen around 31000rpm, now it seems more advantageous to use the first wheel with feed rate of 3000mm/min in which the stability limit can reach up to 100  $\mu\text{m}$  in terms of radial depth of cut.

The process parameters for the two wheels and two feed rates are given in Table 8. The cutting force coefficient in the normal direction is reduced when the feed rate is increased for both wheels. The change in cutting force coefficient and the number of active grits is the key factor to determine the stability limits.

#### **5.4 Experimental results**

A series of experiments were conducted to detect chatter in the tests. The same test setup in Figure 44 was used for the detection of chatter. The stability investigation was decided to be necessary because of the following reason. A large number of experiments were conducted with a variety of different process parameters and wheels in order to investigate abrasive processes. The occurrence of chatter was noted when using conventional wheels at regular speeds occasionally, but in the case of high speed grinding with small CBN tools, the occurrence of chatter was seen in a few cases. To identify the regions of instability, the following process parameters were spanned with the maximum spindle speed of 40m/s (with 20mm diameter wheel). As in the literature it is generally describe that one of the main observations on chatter was the increase in workpiece velocity [42,44,48] (workpiece velocity in cylindrical grinding corresponds to feed rate in surface grinding) the feed rates of 100 to 20000 mm/min is spanned with the radial depth of cut is varied between 10  $\mu\text{m}$  to 50  $\mu\text{m}$ . The workpiece width is selected to be 7mm which is the axial depth of cut. The force measurements of the tests are given in Figure 68.

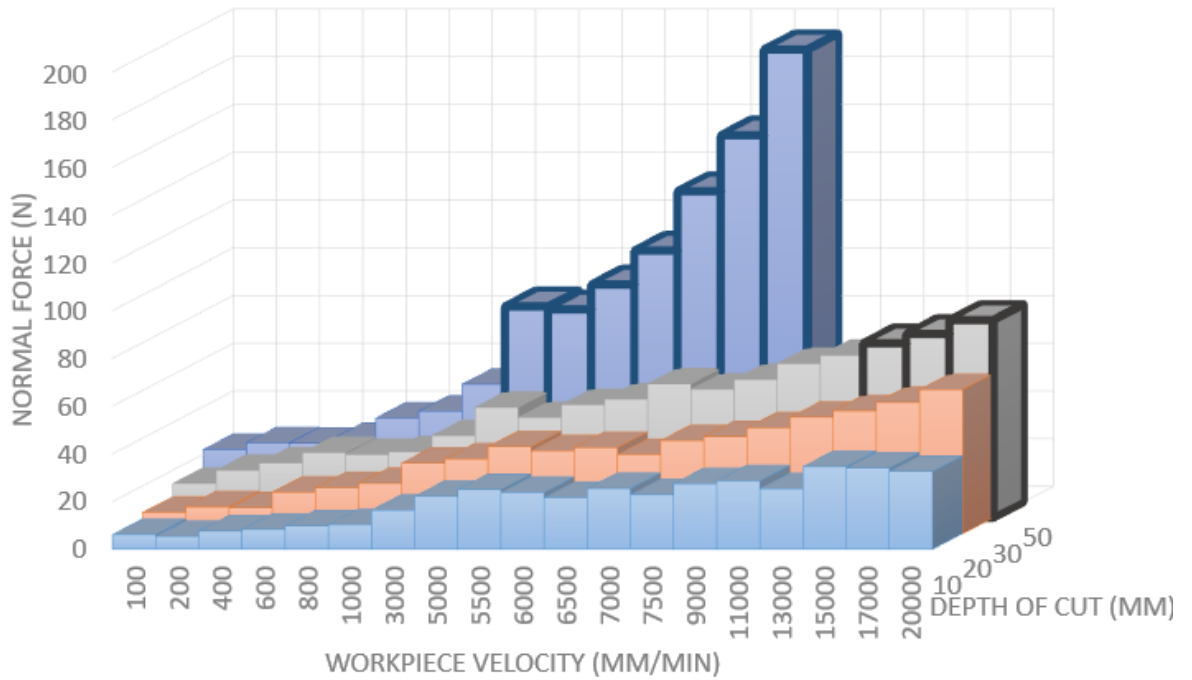


Figure 68: Force measurements of chatter investigation test

As seen from Figure 68 as the feed rate increases at some tests the force values are shown with bold figures (for example the last 3 tests of 30  $\mu\text{m}$  depth of cut). These bold figures are marked because of their likelihood of being unstable. Those tests resulted in increasing force values in the dynamometer as well as a decrease in spindle speed during the grinding. The cases shown with bold figures are studied also because some frequencies other than the rotational frequency (between 1000-1500 Hz) of the spindle in the sound data were observed. This led to an idea that these cases of instability may be a sign of chatter. The force measurements of a stable and supposedly unstable cases are given in Figure 69. The shown forces are in Newton and in the normal direction. In Figure 69b, the force measurements have an increasing profile throughout the grinding process. The sound measurements of the stable and supposedly unstable cases are also shown in Figure 70.



Figure 69: Comparison of the force measurement of the stable (a) and unstable (b) case

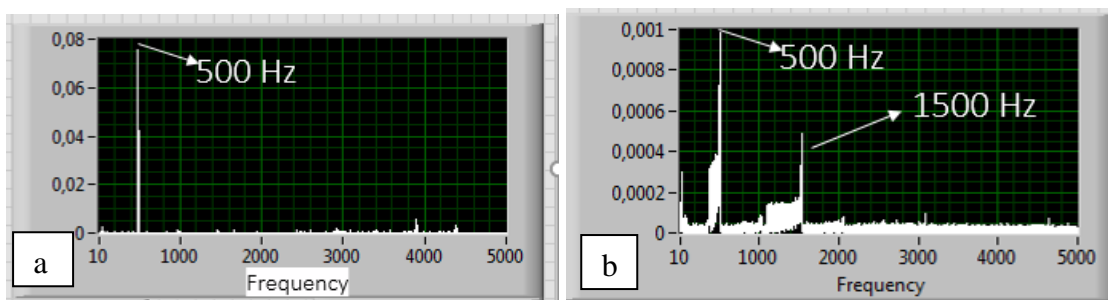


Figure 70: Comparison of the sound measurement of the stable (a) and unstable (b) case

The surface of the workpiece is shown for both cases in Figure 71. There are some marks seen on the surface and the quality has decreased dramatically in the cutting direction.



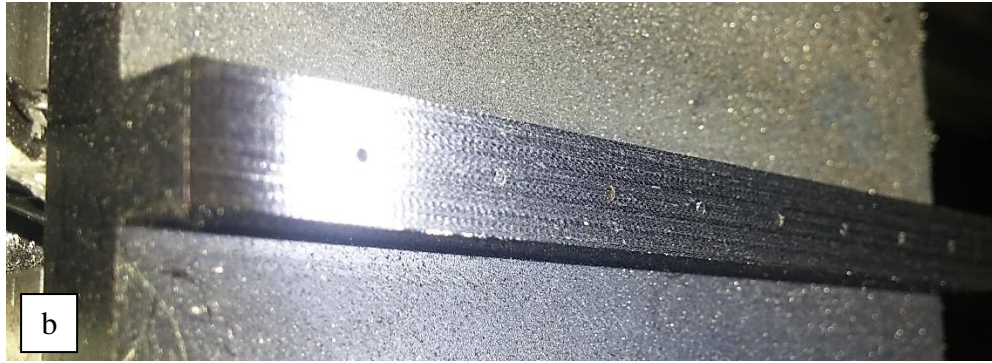


Figure 71: Comparison of surface of the workpiece of the stable (a) and unstable (b) case

The sound measurements on the unstable case show a frequency around 1500 Hz. Recall from Table 6 that the wheel used in these experiments has a natural frequency of 1900 Hz. It is known that the chatter occurs with a higher frequency than the natural frequency of the system. The output of 1500 Hz is a natural harmonic of the spindle speed frequency. Yet, a drop in the spindle speed can be easily observed in Figure 70b during the process which is a indication of insufficient power of the spindle.

To be sure, a surface roughness measurement was done on the surface of the workpiece as shown in Figure 72. The device MarSurf M400 Mobile Surface Measuring Instrument was used for the measurements. The comparison of the surfaces of the supposedly unstable and stable grinding cases is given in Figure 73.



Figure 72: Surface roughness measurement of the workpiece

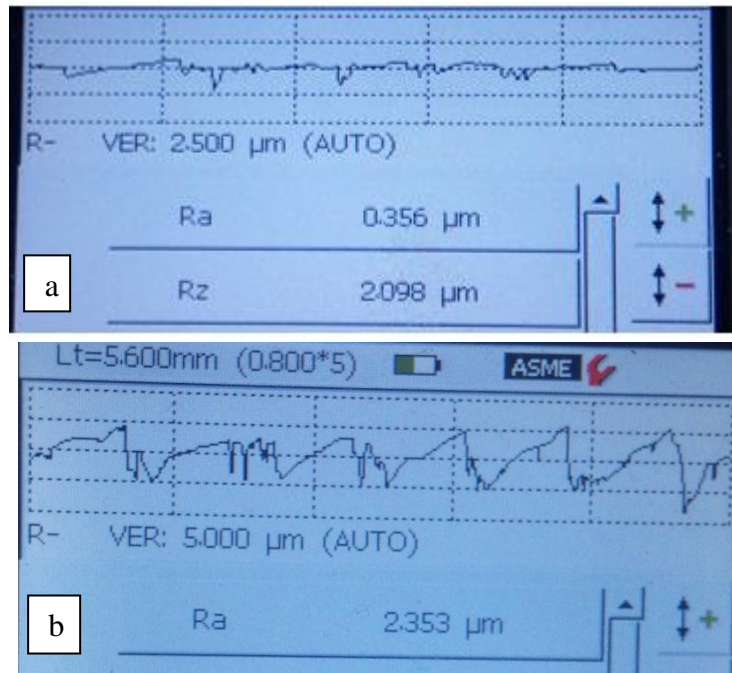


Figure 73: Comparison of surface profile of the workpiece of the stable (a) and unstable (b) case

In Figure 73, the difference between both cases can easily be observed. There are marks on the ground surface of the second case and the marks on the surface of the first case are not that visible. The surface roughness of first case is 0.356 μm and the second case is 2.353 μm (Average roughness Ra).

These signs were carefully studied in order to detect chatter during the experiments, but it is concluded that the supposedly unstable cases are not the case of chatter. A quick calculation of the wave length and the frequency of the marks in Figure 73b, show that they are just feed marks left on the surface. The amplitude of the vibrations may have increased significantly but it doesn't necessarily mean that this is a case of chatter. Therefore, it is decided that these cases are not chatter but an overloading case of the spindle.

The high-speed spindle installed on this grinding machine has the power limit of 2.5 kW at full speed. At full speed (40000rpm) with a 20mm wheel (corresponds to 40m/s), the power limit suggests that maximum power loading can be around 60 N force in the tangential direction which corresponds to around 150 N force or more in the normal direction (depends on the process parameters and the workpiece material). So, this

amount of process forces will lead to a disturbance in the spindle that will change the spindle speed during grinding. In some cases, spindle nearly stopped especially at the last stages of the 50  $\mu\text{m}$  depth of cut test set. At the feed rate of 7000mm/min the spindle came to a full stop and the tool was damaged. Bunks of grit pull-out was observed on the tool after the last operation, please see Figure 74.



Figure 74: Condition of the wheel after the last operation

In the light of the experimental procedure described above, it is concluded that the chatter could not be observed under the general grinding conditions that can be selected from the literature (high feed rate, low depth of cut) in this setup. The torque and power requirements of the process could not be sufficed by the high-speed spindle at full speed. The power curve of the spindle drops even more when the spindle speed is decreased. The advice of the company that provided the spindle was not to reduce the spindle speed lower than 30000 rpm. Therefore, the lower spindle speed tests also led to spindle stoppage. A possible solution to this situation is to change the spindle of the grinding machine to its regular spindle which has a normal speed and higher power capability.

Moreover, one may think that in order to see chatter, the stiffness and the damping ratio of the system can be lowered. This is possible by increasing the overhang length of the grinding wheel. For the above experimental sets, the overhang length of the wheel was selected as 5mm as it was the suggested value from the wheel manufacturer. If the overhang length is increased, apart from the amplified effect of the eccentricity of the

wheel, the spark-out phenomenon emerges. The need for spark-out is observed when the grinding wheel could not remove the intended (nominal) radial depth of cut. The elastic deformation of the wheel towards the normal direction changes the real depth of cut during the process. Therefore, many spark-out passes may be necessary after the first grinding pass. The spark-out increases as the overhang increases, as well as with increased feed rate as shown experimentally in [12]. An increased spark-out would hinder the predictive modeling in grinding because the radial depths of cut in abrasive operations are already low compared to milling operations and the difference between the nominal and real depth of cut would be significant in terms of percentage.

Hence, feed rate should be kept low in order to cope with the spark-out effect introduced by the increased overhang length and to compensate the power requirement that will be increased by higher depth of cut. A case of chatter is observed when the spindle speed is reduced from 40000 to 35000 rpm with a feed rate of 300 mm/min, radial depth of cut of 100  $\mu\text{m}$ , axial depth of cut of 9mm and overhang distance of 21mm. The modal parameters of the new mounting of the wheel are given in Table 9.

Frequency (Hz)	Damping Ratio (%)	Modal Stiffness (N/m)	Mass (kg)
1129	0.534	$1.62 \times 10^6$	0.032

Table 9: Modal parameters of the 21mm overhang tool

The chatter was observed in accordance with the model predictions, both time domain and frequency domain. The comparison of the model and experiment results is given in Figure 75. The curves represent the stability limits calculated with both methods. The circles represent the experiments.

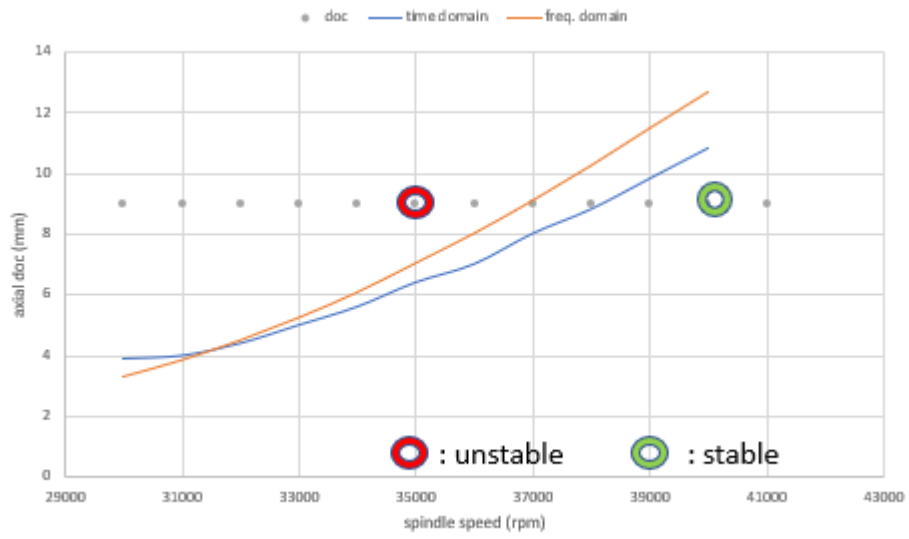


Figure 75: Model and experiment comparison



Figure 76: The chatter marks on the workpiece

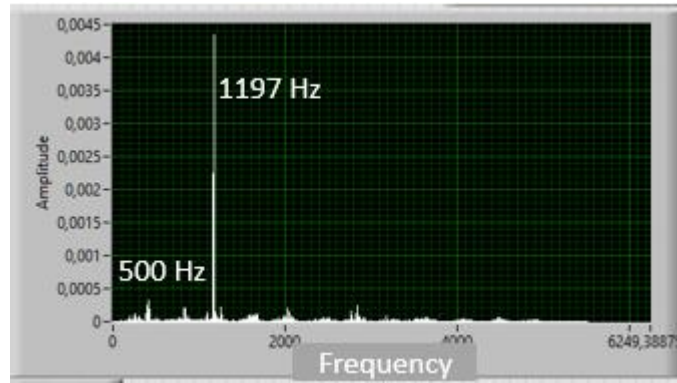


Figure 77: Detection of chatter sound

In Figure 76, the surface of the workpiece is shown. The chatter occurs at some parts of the workpiece along the cutting direction. During the experiments it was visually observed that the tool starts its unstable vibrations and then stops and become stable again. Later along the workpiece this phenomenon occurs one more time. This may be due to the process related damping factors that occur in the grinding operation. The process damping itself may have little effect, even though the spindle speed is high. Furthermore, it can be due to the fact that the active grit number constantly changes during the vibrations and where chatter occurs indicating so called active grit damping affect during the onset of chatter. In Figure 77, the sound measurement of the test is shown. The chatter vibration creates the sound frequency of 1197 Hz, which is slightly above the natural frequency of the wheel. The force measurements are shown in Figure 78. The forces are increased at the point of the chatter marks that are shown on workpiece.

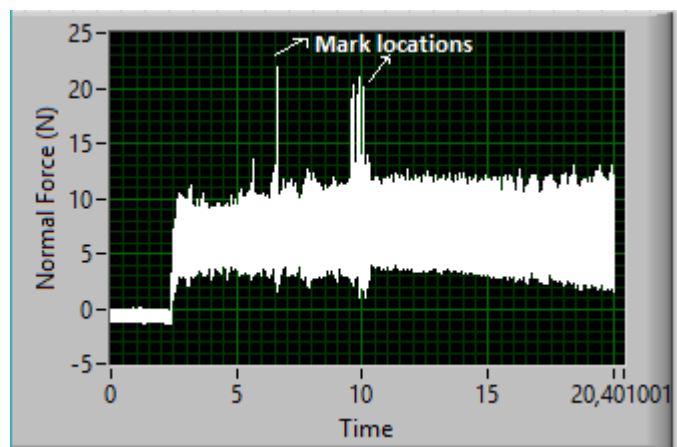


Figure 78: The force measurements of chatter case

## 5.5 Summary

Chatter phenomena in grinding operations are investigated with the proposed dynamic-kinematic model. Two chatter methods are used, the frequency and the time domain solution models. The frequency domain solution model is an adaptation of the model that is proposed in [11] to the mounted point electroplated CBN wheels which is an adaptation of milling stability model to abrasive operations. The time domain model offers a closer perspective to grinding. Taking the stochastic nature of the process into account, the model is capable of predicting the active grit number which is dependent on the process parameters and the random delays that is produced by the random distribution of the grits on the wheel surface. The stability diagrams are obtained by calculating a series of time domain solutions. The unstable cases are detected by taking the Fast Fourier Transform of the vibrations of the tool and checking if the vibrations have the frequency of the chatter frequency that is generally slightly higher than the natural frequency of the tool. The simulations state an interesting point. In milling operations, the stability diagrams would not change if the feed rate is varied but it is not the case in grinding. It is shown that the diagrams would shift if the feed rate is changed in grinding operations as the active grit number and the cutting force coefficients are affected significantly. It was observed that the effect of feed rate can create differences in the stability conditions of the process. A series of experiments are conducted in order to scan the conventional process parameters for the grinding operations to see where the chatter would happen. But using electroplated mounted point (small) wheels and applying it to the high-speed surface grinding operation it was seen that chatter could not be observed due to the spindle power of high speed spindle and the spark-out effect within the conventional process parameter range. Instead, a creep feed grinding (CFG) process condition is observed in separate set of experiments and chatter could be observed with an increased overhang distance of the wheel (CFG conditions are generally low feed high depth of cut parameters). The chatter case could be predicted by the models.

## 6 SUGGESTIONS FOR THE FUTURE RESEARCH

A set of suggestions for the future studies are proposed below in the light of this research:

- The wheel modelling in grinding is crucial. If the wheel is modelled in an enhanced way, the process modelling will be more accurate. The wheel modelling is done by optical measurements however measurement of all the grits is not possible. Thus, a 3D scan measurement method can be developed to truly represent the wheel topography
- The high negative rake angle results in a dead zone during chip forming which leads to material to material contact. This has been observed during the SEM measurements of the wheel. The kinematics of the grinding operation can be enhanced by modelling the third deformation zones during grinding.
- The active grit calculation is validated through indirect methods in this thesis (with force and surface roughness prediction). A direct method to validate the active grit number can be developed.
- The time domain solution to the grinding stability problem is a versatile algorithm and involves several non-linearities that are existent in abrasive operations such as random delay and active grit number change during vibrations. The solution can be enhanced if the wear mechanisms can be integrated.
- The frequency domain solution to chatter problem is developed by using an averaging method in which the wheel is treated as a complete milling tool. The frequency domain solution can be enhanced by offering a random delay solution.
- The developed models can be implemented on cylindrical grinding operations where the chatter is studied more often in the literature.

## 7 DISCUSSIONS AND CONCLUSIONS

In this thesis, analytical methods including kinematic and dynamic models which represent the mechanical, kinematic and the dynamic behavior of the abrasive processes are presented. The developed models and algorithms are tested with experimental data. The identification of the wheel and grinding parameters such as the geometric properties of the abrasive grits, the grinding force coefficients and the modal parameters of the wheel are presented by proposing measurement and calibration methods. The wheel modelling is done by the grit-wise optical measurements, identifying the process related parameters of the grits and applying them to the geometric-kinematic model which makes the normal distribution of the grits on the wheel surface possible. The models are shown to be accurate to simulate the grinding operations. Specific contributions that are presented in this thesis are listed as:

- A method for grinding wheel measurement and modelling is presented. A necessity of modelling grinding wheel is crucial as a result of the stochastic nature of the grinding processes. The basic process parameters of the grinding wheel are not provided by the manufacturers and this makes modelling difficult or prone to over simplified methods. Instead, the abrasive operations are modeled with milling analogy and the abrasive grits are virtually put on the periphery of the wheel under certain assumptions.
- After the milling analogy is applied, the analogous process parameters such as number of cutting teeth (grit concentration), grit dimensions and process related angles are found by optic measurements using a light scatter microscope. 2D and 3D measurements enable identification of key parameters that will be used in the process modelling. For more accurate edge radius measurements of the CBN wheels, electron microscopy (SEM) is used.
- For the representation of the whole wheel individual grit measurements cannot be repeated for all of the grits on the wheel surface as there are tens of thousands of grits on the wheel. Instead, a normal distribution method is

applied on a smaller set of samples to create a virtual wheel to mimic the real wheel. This way, the properties of all of the grits can be stored in an array for modelling purposes.

- It is known in the literature that not all of the grits on the wheel surface participate in grinding process. Because of the stochastic nature of the process, some of the grits are active and some or not because during the chip removal process the active grits became dominant over the passive grits. This is mainly due to the height difference that exists among the abrasive grains. In this thesis, a simulation method for determining the number of active grits is developed namely the geometric-kinematic model.
- The geometric-kinematic model works after the individual grits are put on the periphery of the wheel. The virtual wheel is turned over the workpiece and the interactions of the workpiece and the individual grits are analyzed. The kinematic trajectories of the individual grits are printed over the trajectories of each other. The intersections of the trajectories are well studied in order to determine which grits are active or not. The grits that produce a chip thickness that is larger than the minimum chip thickness are flagged as active. The virtual wheel is then recreated with the passive grits are omitted.
- The prediction of the surface roughness of the workpiece is a highly valuable prediction as the abrasive processes are usually applied for finishing operations. The surface roughness prediction can inherently be done with the developed geometric-kinematic model as the trajectories have the last surface data intersected with the workpiece. The last surfaces obtained from the trajectories will be printed for each element. Each last surface of each element along the axial direction of the wheel is 3D projected over each other. The result of the projection is the surface roughness of the workpiece surface along perpendicular to the cutting direction.

- The force prediction using the geometric-kinematic model is based on the chip thickness calculation. Using the analogy to the milling tool run-out mechanism, radial differences between the trajectories of consecutive active grits will provide the chip thickness. This way, the chip thickness will be identified by analytic measures instead of empirical models.
  
- In this thesis, two methods for predicting the grinding force is presented. Once the chip thickness can be identified through the geometric-kinematic model either mechanistic or analytic force model can be applied on the chip thickness to calculate the grinding force. Mechanistic model need calibration methods with a series of experiments whereas the analytic models are more applicable to wider range as the analytical relations between the process inputs and outputs can be established.
  
- The geometric-kinematic model is enhanced by a dynamic model to build the time-domain solution to the dynamics of the grinding processes. The milling analogy is also deployed for this model. The time domain solution is able tackle with the some linearities of the grinding process such as the random delay caused by the random placements of the grits over the wheel and the change in the number of active grits due to the vibrations.
  
- The stability diagrams are proposed by using the time-domain kinematic solution to the grinding problem and it is compared with both analytical averaging solutions and the experiments.
  
- The case of chatter was reported within the prediction boundaries. The chatter for surface grinding with mounted point wheels observed to happen different from the cases in milling or turning. The chatter may occur in cycles where it may start and stop several times. This is the reason of the stochastic nature of the process. A process damping effect is applied on the vibratory tool as the number of engaged grits will change if the chatter is propagated. This way, the chatter may be damped and then start again.

## 8 REFERENCES

- [1] M. Kocaefe, “Temperature and Force Modeling On Grinding”, MSc. Thesis, Sabanci University, 2017.
- [2] S. Malkin and C. Guo, *Grinding technology: theory and application of machining with abrasives*. Industrial Press Inc., 2008.
- [3] M. C. Shaw, *Principles of abrasive processing*, no. 13. Oxford University Press on Demand, 1996.
- [4] W. B. Rowe, *Principles of modern grinding technology*. William Andrew, 2013.
- [5] S. Sun, M. Brandt, and M. S. Dargusch, “Thermally enhanced machining of hard-to-machine materials—a review,” *Int. J. Mach. Tools Manuf.*, vol. 50, no. 8, pp. 663–680, 2010.
- [6] I. Inasaki, “Grinding of Hard and Brittle Materials,” *CIRP Ann.*, vol. 36, no. 2, pp. 463–471, Jan. 1987.
- [7] C. F. Yao, Q. C. Jin, X. C. Huang, D. X. Wu, J. X. Ren, and D. H. Zhang, “Research on surface integrity of grinding Inconel718,” *Int. J. Adv. Manuf. Technol.*, pp. 1–12, 2013.
- [8] E. O. Ezugwu, Z. M. Wang, and A. R. Machado, “The machinability of nickel-based alloys: a review,” *J. Mater. Process. Technol.*, vol. 86, no. 1, pp. 1–16, 1999.
- [9] E. Brinksmeier *et al.*, “Advances in modeling and simulation of grinding processes,” *CIRP Ann. - Manuf. Technol.*, vol. 55, no. 2, pp. 667–696, 2006.
- [10] J. O. Outwater, “Surface temperatures in grinding,” *Trans. Asme*, p. 73, 1952.
- [11] D. Aslan, “Modeling Of Grinding Process Mechanics,” MSc. Thesis, Sabanci University, 2014.
- [12] B. Yastikci, “Investigation of Tool Wear in Grinding Processes”, MSc. Thesis, Sabanci University, 2016.
- [13] H. K. Tönshoff, J. Peters, I. Inasaki, and T. Paul, “Modelling and simulation of grinding processes,” *CIRP Ann. Technol.*, vol. 41, no. 2, pp. 677–688, 1992.

- [14] H. K. Tönshoff, T. Friemuth, and J. C. Becker, "Process monitoring in grinding," *CIRP Ann. Technol.*, vol. 51, no. 2, pp. 551–571, 2002.
- [15] U. Rosenberger and G. Warnecke, "Assessment of tool and process condition in grinding of advanced ceramics," *Trans. North Am. Manuf. Res. Inst. SME 1994.*, vol. 22, pp. 179–185, 1994.
- [16] H. Buchholz, "Aufbau und Erprobung eines Messwertaufnehmers für den radialen Schleifkörperverschleiss," *Maschinenbautechnik*, vol. 25, no. 8, pp. 364–365, 1976.
- [17] J. D. Gomes de Oliveira, "Dimensional Characterization of Grinding Wheel Surface through Acoustic Emission," *CIRP Ann.*, vol. 43, no. 1, pp. 291–294, Jan. 1994.
- [18] J. Peklenik, "Contribution to the correlation theory for the grinding process," *ASME J. Eng. Ind.*, vol. 86, pp. 85–99, 1964.
- [19] R. Piegert, "Optoelektrischer Sensor zur Inprocess-Messung des Schleiskörperverschleisses," *Maschinenbautechnik*, vol. 31, no. 3, pp. 105–108, 1982.
- [20] I. Inasaki, "Grinding Process Simulation Based on the Wheel Topography Measurement," *CIRP Ann. - Manuf. Technol.*, vol. 45, no. 1, pp. 347–350, 1996.
- [21] I. Inasaki, "Application of the Simulation Technologies for grinding operations," *VDI. Ber.*, vol. 1276, pp. 197–211, 1996.
- [22] P. Koshy, L. K. Ives, and S. Jahanmir, "Simulation of diamond-ground surfaces," *Int. J. Mach. Tools Manuf.*, vol. 39, no. 9, pp. 1451–1470, 1999.
- [23] W. L. Cooper and A. S. Lavine, "Grinding Process Size Effect and," vol. 122, no. February 2000, pp. 59–69, 2001.
- [24] G. Warnecke and U. Zitt, "Kinematic simulation for analyzing and predicting high-performance grinding processes," *CIRP Ann. Technol.*, vol. 47, no. 1, pp. 265–270, 1998.
- [25] X. Chen and W. B. Rowe, "Analysis and simulation of the grinding process. Part I: Generation of the grinding wheel surface," *Int. J. Mach. Tools Manuf.*, vol. 36, no. 8, pp. 871–882, 1996.
- [26] X. Chen and W. B. Rowe, "Analysis and simulation of the grinding process. Part II: Mechanics of grinding," *Int. J. Mach. Tools Manuf.*, vol. 36, no. 8, pp. 883–896, 1996.

- [27] X. Chen, W. B. Rowe, B. Mills, and D. R. Allanson, "Analysis and simulation of the grinding process. Part III: Comparison with experiment," *Int. J. Mach. Tools Manuf.*, vol. 36, no. 8, pp. 897–906, 1996.
- [28] X. Chen, W. B. Rowe, B. Mills, and D. R. Allanson, "Analysis and simulation of the grinding process. Part IV: Effects of wheel wear," *Int. J. Mach. Tools Manuf.*, vol. 38, no. 1–2, pp. 41–49, 1998.
- [29] A. McDonald, A. O. Mohamed, A. Warkentin, and R. J. Bauer, "Kinematic simulation of the uncut chip thickness and surface finish using a reduced set of 3D grinding wheel measurements," *Precis. Eng.*, vol. 49, pp. 169–178, 2017.
- [30] D. Barrenetxea, J. Alvarez, J. I. Marquinez, and J. A. Sanchez, "Grinding with controlled kinematics and chip removal," *CIRP Ann. - Manuf. Technol.*, vol. 65, no. 1, pp. 341–344, 2016.
- [31] M. Kuffa, S. Züger, F. Kuster, and K. Wegener, "A Kinematic Process Model and Investigation of Surface Roughness for High Efficiency Dry Grinding," vol. 46, pp. 636–639, 2016.
- [32] E. Uhlmann, S. Koprowski, W. L. Weingaertner, and D. A. Rolon, "Modelling and simulation of grinding processes with mounted points : Part II of II - Fast modelling method for workpiece surface prediction," vol. 46, pp. 603–606, 2016.
- [33] S. K. Khare and S. Agarwal, "Predictive modeling of surface roughness in grinding," *Procedia CIRP*, vol. 31, pp. 375–380, 2015.
- [34] W. Liu, Z. Deng, Y. Shang, and L. Wan, "Effects of grinding parameters on surface quality in silicon nitride grinding," *Ceram. Int.*, vol. 43, no. 1, pp. 1571–1577, 2017.
- [35] L. Ma, Y. Gong, and X. Chen, "Study on surface roughness model and surface forming mechanism of ceramics in quick point grinding," *Int. J. Mach. Tools Manuf.*, vol. 77, pp. 82–92, 2014.
- [36] G. Werner, "Influence of work material on grinding forces," *Ann. CIRP*, vol. 27, no. 1, pp. 243–248, 1978.
- [37] L. Lichun, F. Jizai, and J. Peklenik, "A study of grinding force mathematical model," *CIRP Ann. Technol.*, vol. 29, no. 1, pp. 245–249, 1980.

- [38] S. Malkin and T. W. Hwang, "Grinding Mechanisms for Ceramics," *CIRP Ann. - Manuf. Technol.*, vol. 45, no. 2, pp. 569–580, 1996.
- [39] D. Anderson, A. Warkentin, and R. Bauer, "Experimental and numerical investigations of single abrasive-grain cutting," *Int. J. Mach. Tools Manuf.*, vol. 51, no. 12, pp. 898–910, 2011.
- [40] D. Aslan and E. Budak, "Surface roughness and thermo-mechanical force modeling for grinding operations with regular and circumferentially grooved wheels," *J. Mater. Process. Technol.*, vol. 223, pp. 75–90, 2015.
- [41] S. Malkin and C. Guo, *Grinding Technology: Theory and Application of Machining with Abrasives*, 2. New York: Industrial Press, 2008.
- [42] I. Inasaki, B. Karpuschewski, and H.-S. Lee, "Grinding Chatter – Origin and Suppression," *CIRP Ann. - Manuf. Technol.*, vol. 50, no. 2, pp. 515–534, 2001.
- [43] M. Leonesio, P. Parenti, A. Cassinari, G. Bianchi, and M. Monno, "A time-domain surface grinding model for dynamic simulation," *Procedia CIRP*, vol. 4, pp. 166–171, 2012.
- [44] H. Li and Y. C. Shin, "A time-domain dynamic model for chatter prediction of cylindrical plunge grinding processes," *J. Manuf. Sci. Eng.*, vol. 128, no. 2, pp. 404–415, 2006.
- [45] J. Biera, J. Viñolas, and F. J. Nieto, "Time-domain dynamic modelling of the external plunge grinding process," *Int. J. Mach. Tools Manuf.*, vol. 37, no. 11, pp. 1555–1572, 1997.
- [46] E. Ozlu, A. Molinari, and E. Budak, "TWO-ZONE ANALYTICAL CONTACT MODEL APPLIED TO ORTHOGONAL CUTTING," *Mach. Sci. Technol.*, vol. 14, no. 3, pp. 323–343, Nov. 2010.
- [47] R. D. Entwistle and B. J. Stone, "The effect of workpiece torsional flexibility on chatter performance in cylindrical grinding," in *Proceedings of the fifth international congress on sound and vibration, University of Adelaide, South Australia*, 1997, pp. 15–18.
- [48] Y. Altintas and M. Weck, "Chatter Stability of Metal Cutting and Grinding," *CIRP Ann. - Manuf. Technol.*, vol. 53, no. 2, pp. 619–642, 2004.

- [49] Z. Liu and G. Payre, “Stability analysis of doubly regenerative cylindrical grinding process,” *J. Sound Vib.*, vol. 301, no. 3–5, pp. 950–962, 2007.
- [50] Y. Yan, J. Xu, and M. Wiercigroch, “Chatter in a transverse grinding process,” *J. Sound Vib.*, vol. 333, no. 3, pp. 937–953, 2014.
- [51] E. Budak and Y. Altintas, “Analytical prediction of chatter stability in milling—part I: general formulation,” *J. Dyn. Syst. Meas. Control*, vol. 120, no. 1, pp. 22–30, 1998.
- [52] E. Budak and Y. Altintas, “Analytical prediction of chatter stability in milling - Part II: Application of the general formulation to common milling systems,” *J. Dyn. Syst. Meas. Control. Asme*, vol. 120, no. 1, pp. 31–36, 1998.
- [53] D. Aslan and E. Budak, “Semi-analytical force model for grinding operations,” *Procedia CIRP*, vol. 14, pp. 7–12, 2014.
- [54] H. C. Chang and J. J. J. Wang, “A stochastic grinding force model considering random grit distribution,” *Int. J. Mach. Tools Manuf.*, vol. 48, no. 12–13, pp. 1335–1344, 2008.
- [55] H. Jamshidi, B. Yastıkcı, M. Gürtan, and E. Budak, “Grinding force model for Inconel 718 with CBN and conventional wheels,” 2017.
- [56] R. Transchel, C. Leinenbach, and K. Wegener, “Cutting and ploughing forces for small clearance angles of hexa-octahedron shaped diamond grains,” *CIRP Ann. Technol.*, vol. 63, no. 1, pp. 325–328, 2014.
- [57] E. Budak, E. Ozlu, H. Bakioglu, and Z. Barzegar, “Thermo-mechanical modeling of the third deformation zone in machining for prediction of cutting forces,” *CIRP Ann. Technol.*, vol. 65, no. 1, pp. 121–124, 2016.
- [58] Y. Altintas, *Manufacturing automation: metal cutting mechanics, machine tool vibrations, and CNC design*. Cambridge university press, 2000.
- [59] F. Klocke, D. Lung, and S. Buchkremer, “Inverse identification of the constitutive equation of Inconel 718 and AISI 1045 from FE machining simulations,” *Procedia CIRP*, vol. 8, pp. 212–217, 2013.
- [60] I. INASAKI, K. TONOU, and S. YONETSU, “Regenerative chatter in cylindrical plunge grinding,” *Bull. JSME*, vol. 20, no. 150, pp. 1648–1654, 1977.
- [61] W. A. Kline and R. E. DeVor, “The effect of runout on cutting geometry and forces in

end milling,” *Int. J. Mach. Tool Des. Res.*, vol. 23, no. 2–3, pp. 123–140, 1983.